Proximity-Based Mass Spectrometry:

Direct Detection and Characterization of Biomolecules

BY

MELISSA MARIE GALEY

B.S., Rose-Hulman Institute of Technology, 2012

THESIS

Submitted as partial fulfillment of the requirements for the degree of Master of Science in

Pharmacognosy in the Graduate College of the University of Illinois at Chicago, 2019

Chicago, IL

Defense Committee:

     Laura M. Sanchez, Chair and Advisor

     Joanna E. Burdette

     Douglas D. Thomas

DEDICATION

I would like to dedicate to Matt Moore, my husband. He has been my unwavering support system

through this entire journey and I could not have completed it without him.

ACKNOWLEDGMENTS

I am extremely grateful for all of the support I have received in graduate school, whether it be related to my research or personal life. I am thankful for the impact that each of the people mentioned below have made in my life and they have all shaped me into the person I am today in different, yet wonderful ways.

I would like to start by thanking Dr. Laura Sanchez for being such a fantastic advisor and mentor. She made me truly feel welcome in graduate school and provided me with so much motivation and support throughout my career. She created such a caring and wonderful research environment at UIC and I look forward to seeing what great science the lab will accomplish in years to come. She is the best advisor I could have asked for and I owe her the world for all of her mentorship and support.

I would also like to thank my lab mates for making my tenure in graduate school extremely gratifying and for making me love coming to work. They are always there to celebrate the good times, talk about science and commiserate with when experiments aren't always going the way you'd expect. Alanna Condren has been a welcoming presence in the lab through the start and is someone I am truly grateful to know. She has been such a great friend, fantastic listener, shoulder to cry on, fellow baker and so much more. I cannot imagine having gone through this journey without her. Jessica Little has helped me so much in becoming a better scientist. She's always available to help with troubleshooting and is so handy - she can fix just about every instrument in the lab. We've also gotten to bond over our love for our dogs, Stella & Caye, as well as good wine and cheese! Katherine Zink is a such a wonderful person and a great scientist. She is so willing to share her research insights and has been instrumentally helpful for my ovarian cancer project. We have a shared love for travel, both having grown up overseas, and it's been great to have someone with the same travel bug that I have! Valya Petukhova has been instrumental in helping

me get started with my research in lab and I will be eternally grateful. I would also like to acknowledge the newest members of the Sanchez lab, Cynthia Grim and Gordon Luu. I'm so glad that they will be carrying on our lab's traditions and continuing the good fight after we all graduate - I wish both of them the best.

I would also like to thank Leslie Martinez, a fabulous undergraduate student, who I was fortunate enough to mentor over the last year. She is such a fast learner and so excited about science. She was my first mentee and has been so patient with me as this was a learning process for both of us. She has been extremely helpful towards the work in this dissertation and a true pleasure to mentor. I am so proud of all she has accomplished in the past year and I can't wait to see what she does next!

I would also like to thank my thesis committee members, Drs. Joanna Burdette and Doug Thomas, as well as my additional members, Drs. Stephanie Cologna and Larisa Nonn, from my preliminary examination committee. They have been extremely supportive during my academic career and provided invaluable feedback and advice. Each committee member has been a great member, both as a group and individually, and I can't thank them enough for helping me accomplish my scientific goals and complete my degree.

I would also like to thank Dr. Mark Brandt who supported and encouraged my transition from industry to graduate school. He was my thesis advisor at Rose-Hulman and was always looking out for what was best for me. He gave me the opportunity to do university-level research for the first time and truly help spark my interest into further my education past a bachelor's degree. Even though I graduated seven years ago, we still catch up at least once a year and I will always be grateful for all the support he has provided me. He truly made a marked difference in my life and will always be one of my favorite professors.

I would also like to thank Dr. Chris Nicholas who has been extremely supportive in my journey towards higher education. He has been a great mentor during my time at Honeywell and has always been available for advice and scientific conversations. He is a great friend and an even greater advocate. I have been fortunate to have been able to work with him on UZM-55, my favorite zeolite, even after I left industry and continue to have an impact on the catalysis world. I am extremely grateful to have met him and am so thankful for all of his wise words and support.

I would also like to thank my friends for helping me maintain my work-life balance and making the past few years an absolute joy. Christine Adams, Derek Archer and Gretchen West have been my best friends since Rose-Hulman and I can't imagine life without them. They have listened to my struggles, celebrated in my accomplishments and provided lots of love and laughter to my life. A big thank you to Rachel Knopp, Cutler Lewandowski and Carlo Rosales for our weekly Tuesday night trivia and for being a part of "Somehow We Manage". They all kept me sane during the week and gave me something fun to look forward every Tuesday. I'd also like to thank Laura Cooper and Audra Lemley for all their support and friendship throughout graduate school. We all found each other in my second year and have been great friends ever since - I couldn't have gotten through until the end without them both.

I would also like to thank my family, Sheila, Loran and Madeline, for all their love, support and encouragement throughout this process. They have been instrumental to my success and I can't thank them enough for everything. I would also like to sincerely thank the Moore family, Ellen, Doug and Brendan, for all of their support during my time at UIC.

Finally, I would like to thank Matt Moore and Caye. I don't know if this adventure was what Matt expected when we got married five years ago but he went on it with no hesitation. He has been

my rock, my lifesaver and my greatest comfort over the last three years and I thank him for everything. Caye has been my support system in a completely different way. We adopted her right before I started at UIC and she has been with me every step of the way. She is my joy at the end of every day and has helped me cope with stress in a way that no one else can. I can't imagine going on this journey without both of them and can't wait to see where this next path leads us as a family.

CONTRIBUTION OF AUTHORS

Chapter 1 is partially adapted from a published manuscript (Galey, M.M, and Sanchez, L.M., *mSystems* 2018 3:e00148-17, DOI: 10.1128/mSystems.00148-17) of which Melissa M. Galey is the primary author.

Chapter 2 is adapted from a published preprint (Galey, M.M. *et. al*, bioRxiv 2019) of which Melissa M. Galey is the primary author and primary driver of the research. This manuscript is currently in submission at the Journal of Proteome Research. My co-authors contributed to this work in the following ways: Alexandria Young was involved with the collection of IVIS imaging data. Valentina Petukhova was involved in a portion of the MALDI-TOF analysis. Amrita Salvi and Angela Russo were involved in the FACS cell counting study. Mingxun Wang and Jian Wang were instrumental in the statistical analysis. Laura Sanchez and Joanna Burdette are my co-mentors for this project and provided helpful discussion and contributed to writing the manuscript.

Chapter 3 represents my own unpublished work and will be continued after I leave the lab in the hopes of being incorporated into a manuscript.

TABLE OF CONTENTS

LIST OF TABLES

LIST OF FIGURES

Chapter 3

LIST OF FIGURES (CONTINUED)

LIST OF ABBREVIATIONS

ACN	Acetonitrile
AMR	Antimicrobial Resistance
BHI	Brain Heart Infusion
CA-125	Cancer Antigen 125
CCA	Cheese Curd Agar
CDC	Center for Disease Control
COSY	Correlated Spectroscopy
Cryo-EM	Cryo-Electron Microscopy
CVF	Cervico-Vaginal Fluid
DDA	Data Dependent Acquisition
DESI	Desorption Electrospray Ionization
ESI	Electrospray Ionization
FACS	Fluorescence-Activated Cell Sorting
GC	Gas Chromatography
HGSOC	High Grade Serous Ovarian Cancer
HMBC	Heteronuclear Multiple Bond Correlation Spectroscopy
HPLC	High Performance Liquid Chromatography
HSQC	Heteronuclear Single Quantum Coherence Spectroscopy
HygR	Hygromycin
IMS	Imaging Mass Spectrometry
IP	Intraperitoneal
LC	Liquid Chromatography
LC-MS/MS	Liquid Chromatography - Tandem Mass Spectrometry
LTQ	Linear Trap Quadrupole

LIST OF ABBREVIATIONS (CONTINUED)

MALDI   Matrix-Assisted Laser Desorption/Ionization

MicroED   Microcrystal Electron Diffraction

MS   Mass Spectrometry

m/z   Mass to Charge Ratio

NASH   Non-Alcoholic Steatohepatitis

NMR   Nuclear Magnetic Resonance

PCAMS   Plate Count Agar Supplemented with 0.1% Milk and 1% Salt

PCR   Polymerase Chain Reaction

PE   Phycoerythrin

qTOF   Quadrupole Time-of-Flight

REIMS   Rapid Evaporative Desorption Mass Spectrometry

RCF   Relative Centrifugal Force

RFP   Red Fluorescent Protein

RPM   Revolutions Per Minute

RT   Room Temperature

SM   Specialized Metabolite

SNR   Signal-to-Noise Ratio

SPE   Solid-Phase Extraction

SSC   Side Scatter

TSB   Tryptone Soya Broth

TOF   Time-of-Flight

SUMMARY

Mass spectrometry (MS) is a powerful analytical tool that can be applied to the identification and characterization of biomolecules, ranging from specialized metabolites to proteins. In Chapter 1, recent developments have further expanded its use to include proximal detection, in which biomolecules can be directly detected from their local microenvironment with minimal sample manipulation. The work embodied in the following chapters focuses on two distinct projects that investigate outstanding biological questions using a combination of proximity-based MS and biology.

Chapter 2 focuses on the direct detection of ovarian cancer, a severe gynecological disease, using matrix-assisted laser desorption/ionization time-of-flight MALDI-TOF MS analysis of vaginal lavage samples. In an effort to improve detection of ovarian cancer and patient prognosis, a murine xenograft model was used in which mice were given weekly vaginal lavages - sourcing cells from a local microenvironment of reproductive organs for MALDI-TOF MS analysis. This proximal technique allowed for the detection of small proteins that were longitudinally significantly up- and downregulated and work is currently being done to determine their identification and function.

Chapter 3 focuses on the cheese rind microbiome and the ability of its microbial population to produce antimicrobials. A series of three bacterial-fungal interactions are investigated for the production of antifungal or antibacterial metabolites using a combination of bioactivity assays and analytical tools, such as MS and nuclear magnetic spectroscopy (NMR). Following the observation of promising bioactivity, the isolation and/or elucidation of metabolites from each interaction are currently in progress.

Chapter 1

Proximity-Based Mass Spectrometry:

The Importance of Specialized Metabolites

1.1. Introduction to Specialized Metabolites

The importance of understanding the chemical communication that takes place between cells, whether it be in host-tumor, bacterial, fungal, or host-microbe interactions, has shown that these multifaceted exchanges have the ability to significantly influence the overall health of a system. Specialized metabolites (SMs) are natural products produced by microorganisms, plants and animals that are not necessary for survival but serve a variety of other purposes *in vivo*, such as enabling pathogenic or symbiotic relationships.[1,2] The impact that SMs can have on the health of a biological system suggests continued investigation is needed to provide a better understanding of how system-specific interactions and their associated molecular mechanisms can be related to health or disease states.

The study of these *in vitro* or *in vivo* cellular interactions has led to the discovery of a wide range of SMs with varying complexity and biological functions (**Figure 1.1**). Spinosad (**1A**) is an insecticide produced by *Saccharopolyspora spinosa*, a soil bacterium, was originally isolated in 1992 and had observed activity against mosquito larvae.[3] It is now commonly used as both a crop pesticide and a treatment for head lice, with low toxicity towards mammals, birds and beneficial insects such as honeybees and beetles.[4,5] Lovastatin (**1B**), taxol (**1C**) and penicillin (**1E**) are all fungal-based SMs that are used to treat high cholesterol, breast cancer and bacterial infections, respectively, and represent a wide spectrum of biological function within metabolites of fungal origin.[6–8] Norepinephrine (**1D**), a SM found in humans, was recently found to stimulate the invasion of fallopian tube cells with a p53 mutation, which may play a contributing factor to high grade serous ovarian cancer (HGSOC) primary metastasis.[9] The implication of norepinephrine in this process was observed using imaging mass spectrometry (IMS), which allowed for the spatial visualization of communication between a murine ovary and mutated HGSOC cell lines.[9] These compounds, along with many others, have a direct impact on multiple areas of human health, including dietary health and treatment of diseases such as breast and ovarian cancer. *In vitro*

and *in vivo* cellular interactions have the ability to specifically influence the chemistry within a biological system and through the mechanism of chemical communication, the health of the SM-producing organisms and/or their proximal surroundings.
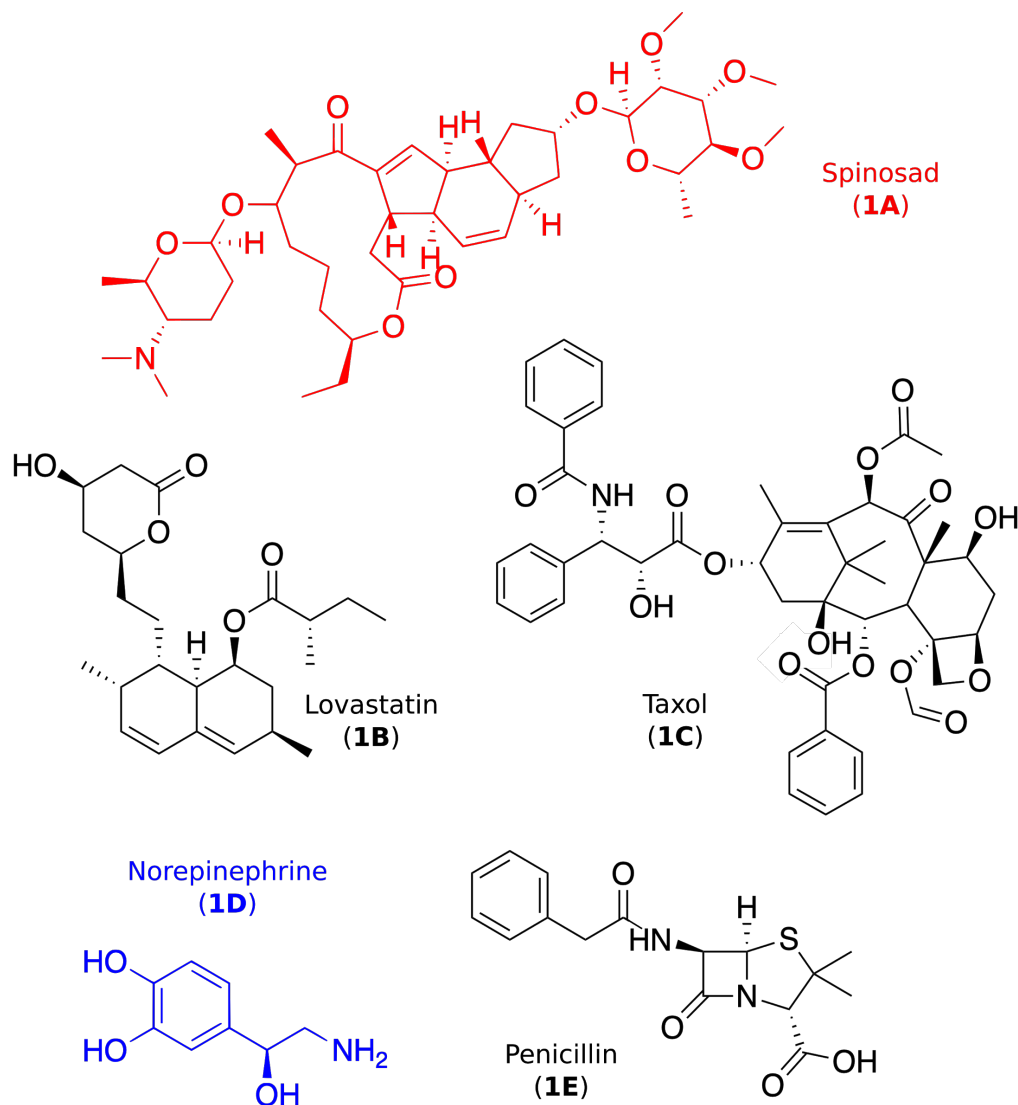
Figure 1.1. Representative SMs produced by bacteria (red), fungi (black) and mammalian cells (blue) that are found to impact human health

Studies focused on microbial interactions have revealed that, within a community of microbes, the presence of certain species directly correlates to the production of specific metabolites from discrete locations through the use of tandem mass spectrometry (MS), which assigns compound

identities based on fragmentation patterns, and molecular networking, a tool that aids in the visualization of chemical space based on fragmentation data.[10,11] While these studies investigate the presence of microbes in or on a host and the use of MS aids in clarifying known versus unknown SMs within a system, they do not explicitly elucidate the molecular mechanisms and SMs produced by the microbes that may influence a host organism's health. To move forward in our knowledge of the impact that these communities have on host health, it is imperative that model systems and tools be developed to better study this chemical communication *in situ.* Therefore, it is increasingly important to work towards building a comprehensive inventory of the SMs that are utilized for survival, communication and migration within a host to test and design better treatments for disease.

Previous studies have focused on the introduction of specific microbial species or whole communities to gnotobiotic animal models in order to determine the full effect that these microorganisms have on their hosts, whether it be influencing a disease state or the overall microbiome of the host.[12,13] While these types of animal studies have proven to be enlightening in terms of establishing the influence of *specific* microbe(s) or whole communities have on host organisms, it can fail to take into account the interactions found between native microbial species normally found within the host. A multitude of processes within a gnotobiotic host would not be observed, such as bile acid recycling in the enterohepatic system, due to the fact that specific microbial community members may not be present.[14] This leads to an incomplete understanding of the chemical communication involved in host-microbe interactions as the microbial origins of SMs being produced are still unknown.

In addition to using gnotobiotic animal models to study microbe-host interactions, researchers have also taken an interest in the interactions between host tissue and its inherent microbiota. In a recent paper by Ismail *et. al*, a unique relationship was observed between mammalian epithelial

cells and enteric quorum-sensing bacteria, where *Vibrio harveyi* was used as the model bacterial species.[15] The research findings point to the existence of a quorum-sensing mimic produced by mammalian cells which aids in communication between the host and its bacterial partners. While this finding has exciting potential for deciphering this type of chemical communication, the underlying chemistry remains elusive and that has limited further studies or an expansion to other systems. In order to better study these interactions along with the functional role of microbial species or other instigators in host health and disease, it is necessary to establish analytical methodologies and tools to fully explain the interchange of SMs within these interactions.

The structures or molecular mechanisms implicated in the biological health of a system often represent a knowledge gap as the extent of chemical communication *in situ* is still an active area of research. In order to close this gap, a combinatorial approach pulling from microbiology and analytical chemistry can be pursued to further investigate these interactions to gain a better understanding of the chemistry being produced. Therefore, it is necessary to develop tools that directly allow for the study of this local chemistry *in situ* to elucidate chemical dialogue and how it can impact disease states within a system.

1.2. Use of Proximity-Based Mass Spectrometry for the Direct Detection of Biomolecules

While the concept of using MS as an analytical tool to identify and characterize biomolecules is not novel, its applicability has expanded to include measurements that depend on proximity within a system or on a surface. Ionization techniques, such as rapid evaporative ionization (REIMS), desorption electrospray ionization (DESI) and matrix-assisted laser desorption/ionization (MALDI), have been instrumental in proximal detection as SMs can be directly detected with minimal sample preparation and results in sensitive and specific measurements. These three unique ionization techniques have each carved out their own niche in the world of direct detection

and are used to answer a wide variety of biological questions ranging from human disease and

food safety (**Figure 1.2**).

REI (Rapid Evaporative Ionization) MS

N₂ ... Analyzer ... Detector

Electrode

Ions

Sample is burned upon contact with the electrode.

Aerosolized ions are transferred to the mass spectrometer.
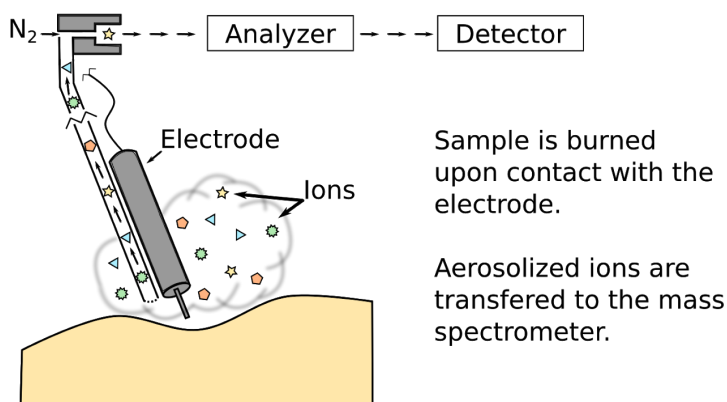
Advantages
- Provides real-time feedback
- No sample preparation
- Solvent free technique

Disadvantages
- Destructive to sample
- Poor spatial resolultion
- Dependant on aerosolization of sample

DESI (Desorption Electrospray Ionization)

Solvent

High Voltage

Nebulizing Gas

Detector

Analyzer

Ionization occurs via an charged mist sprayed on the sample surface.

Charged droplets are transferred to the mass spectrometer.
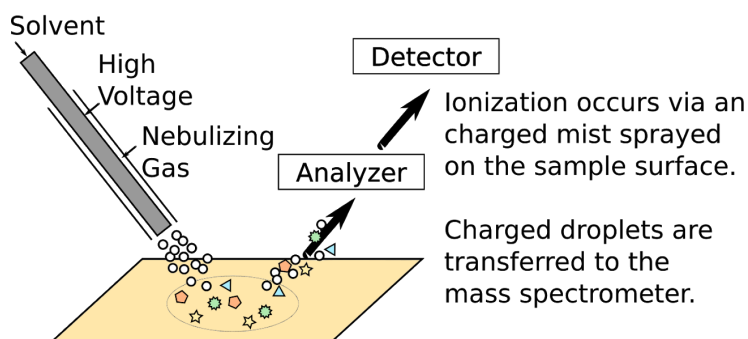
Advantages
- Provides real-time feedback
- No sample preparation
- Minimally destructive

Disadvantages
- Spectral complexity due to multiply charged ions
- Analysis dependant on analyte solubility

MALDI (Matrix-Assisted Laser Desorption/ Ionization)

Laser

Detector

Analyzer

Sample and matrix are ablated by the laser and ions are transferred to the mass spectrometer
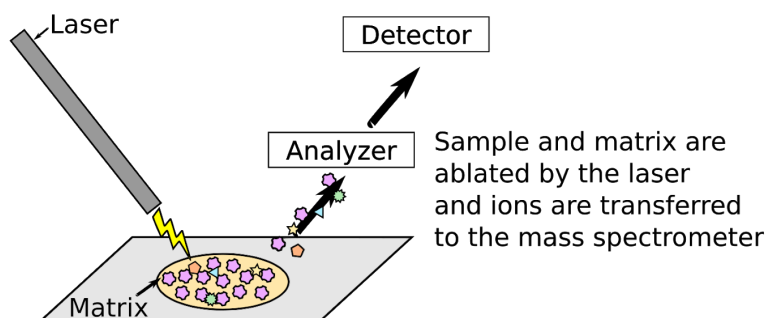
Matrix

Advantages
- Highly sensitive
- Large dynamic range
- Solvent free technique

Disadvantages
- Sample preparation
- Matrix background
- Offline technique

Figure 1.2. Overview of REIMS, DESI and MALDI ionization techniques with their respective advantages and disadvantages

For example, REIMS, an ionization technique published in 2009 by Schafer *et. al*, has been applied to the detection of SMs to a wide variety of samples including biological tissues and food matrices.[16,17] Due to the ability of REIMS to provide real-time feedback, it has recently been utilized to determine tumor margins during resection surgery.[18] However, despite its ease in use, this ionization technique is destructive to the tissue as it is burned upon contact with the electrode. DESI, an ambient ionization technique, has also grown in popularity due to its ability to detect SMs, such as explosive volatiles or lipids, from a wide variety of matrices such fingerprints, gunshot residues and tissue samples.[19–21] DESI, like REIMS, is advantageous due to the fact that there is no necessary sample preparation and real-time feedback is possible. However, its ability to detect multiply charged ions can lead to overly complex spectra and it can have lower a spatial resolution than comparable ionization techniques. MALDI, published by Karas *et. al* in 1985, is an ionization technique that is solvent-free with a large dynamic range, when paired with a time-of-flight (TOF) analyzer. It is commonly used for a variety of applications including microbial biotyping, the identification of bacteria based on their protein spectral fingerprint, in the clinic and IMS, which allows for the introduction of a two dimensional spatial component to study the distribution of SMs within a system.[22–24] The increase in popularity for analytical techniques that can directly detect and characterize biomolecules from local environment has led to further technological advances such as the iKnife, MasSpec Pen and Biotyper, which are all based on the direct detection of SMs using MS.[18,25,26]

1.2.1. Disease Detection and Progression in Human Hosts

With the progression of modern medicine, it is now possible to move from treating a visibly present disease to the investigation of disease progression prior to symptoms appearing. Bioassays, such as immunoassays and polymerase chain reactions (PCR), are prevalent in the clinic but can be slow, costly and result in high incidences of false positives as was the case with (cancer antigen - 125) CA-125 biomarker detection for ovarian cancer diagnoses.[27,28] An alternative to the role of

these molecular biology-based techniques in the clinic is the emerging use of MS for diagnostics purposes.

Tandem MS for Newborn Screening Introduced

MS Applied to Molecular Diagnosis of Bloodborne Infections

Knife Guided by Real-Time MS Readout for Cancer Surgery

Rapid ID of Intact Bacteria by MS

1988 — 1990 — 1996 — 1998 — 2010 — 2013 — 2015

Guidelines for Federal Drug Testing Issued: MS Confirmation Required

Clinical Applications Shift from GC-MS to LC-MS/MS

FDA Approval for MALDI-TOF Identification of Microbes

MS Applied to Metabolomics, Proteomics & Other "Omics"

Figure 1.3. MS integration into an increasing number of clinical applications over the last three decades. *Figure adapted from Jannetto *et. al.*[29]

Clinical MS began to take off in the late 1980s, with its mandated use in drug testing by the FDA during the Reagan presidency when it was used to verify drug screens after positive immunoassay results. It has since expanded to a variety of clinical applications (**Figure 1.3**). One major shift for clinical use was in the 1990s with the transition from gas (GC) to liquid chromatography (LC) as it allowed for clinicians to identify non-volatile analytes while working with a wider array of biological matrices including blood. Another important step in the advancement of MS was the development of the iKnife in 2013, which makes use of REIMS, for use in a surgical setting.[18] This technique couples the detection of MS signatures in lipids for a real-time readout of cancerous or healthy tissue margins during surgical resection. This method has been found to be extremely useful as it can be applied to tissue without any necessary preparation or modification but also has a significant limitation in that it is destructive to the tissue

surface. A second valuable addition to the field of clinical MS is the development of the MasSpec Pen by the Eberlin lab in 2017, which incorporates DESI-based design for real-time feedback for surgeons during tumor removal.[30] This method requires no sample preparation and is non-destructive to biological tissues as water is used as the solvent to desorb lipids from tumor surfaces- which also contributes to a limitation that all detected molecules must be soluble in water for subsequent analysis. While both of these techniques are ground-breaking in their ability to distinguish between healthy and cancerous tissue margins in living organisms, they are only applicable for later stages of disease once surgery is in progress for tumor resection. As many cancer types, including ovarian cancer, are diagnosed after metastasis has occurred, surgical removal of tumors is not always sufficient as a treatment plan for patients. Therefore, being able to diagnose this disease state during its early stages, when tumors are localized to their tissue of origin, would be extremely beneficial for the medical field as it would result in improved patient outcomes.

One possible method of detecting disease states in their early stages would be the clinical use of MALDI-TOF mass spectrometers for disease diagnostics and progression. The Biotyper system, currently patented by Bruker Daltonics, is already widely used for microbial typing of clinically relevant bacterial strains isolated from infected patients, which involves the identification of genus and species based on collected spectral data.[31] While this technique is more time-consuming in terms of sample preparation, it also allows for samples taken from a patient to be obtained outside of surgery. Clinical laboratories that already take advantage of MALDI-TOF MS for microbial typing could be envisioned repurposing their instruments for the characterization of human-derived samples sourced from local microenvironment. In the coming years, it is likely that MALDI-TOF MS will become more prevalent as its use for the analysis of clinical samples increases. Expansion of the utility of MALDI-TOF MS will be further elaborated upon in the second chapter for the detection of ovarian cancer using vaginal lavage samples.

1.2.2. Microbial Interactions on Food Matrices

Going back to early civilizations, humans have made use of microbial organisms to naturally preserve food through fermentation.[32–35] This process, which consists of converting complex sugars into smaller organic molecules such as ethanol or formic acid, is still used today. Fermentation has also been repurposed to have a larger impact of the food processing industry through the addition of new textures and flavors to our diets. For example, the addition of yeast to bread to create a rising effect or *lactobacilli* to yogurt, to impart an acidic taste. Fermentation is typically carried out by bacteria and fungi, which are introduced to our food during the production stage. While we have grown accustomed to the unique olfactory and flavor characteristics this adds to our diet, little is known about the chemistry resulting from these microbial interactions that occur in and on our food.

One striking example of the use of fermentation in our daily life is the manufacturing of cheese. During the ripening process of naturally aged cheeses, rinds composed of relatively small microbial populations, in terms of diversity, form on the surface. These communities impart certain characteristics to the cheese such as *Penicillium roqueforti* and its addition of blue streaks and distinct flavor profile to many popular blue cheeses.[36] Work has been done to identify the extent of diversity that occurs within the cheese rind through the use of high-throughput sequencing as well as looking into the impact of horizontal gene transfer within the microbial community.[37–40] Based on work done by Wolfe *et. al*, an average of ten microbial species are present on any given cheese rind, which lends favorability to the study of this particular microbiota as it is a relatively simple model to study for the discovery of SMs and their *in situ* growth conditions can be easily reproduced in a laboratory setting.[38] Previous studies of the cheese rind microbiota have led to the identification of many SMs synthesized by either bacteria or fungi whose presence imparts distinct characteristics, such as pigmentation throughout the body of the cheese. In particular, a

pink pigment resulting from a bacterial-fungal interaction was recently identified by Cleary *et. al* as zinc-coproporphyrin III which is produced by *Glutamicibacter arilaitensis* (**Figure 1.4**).[41]
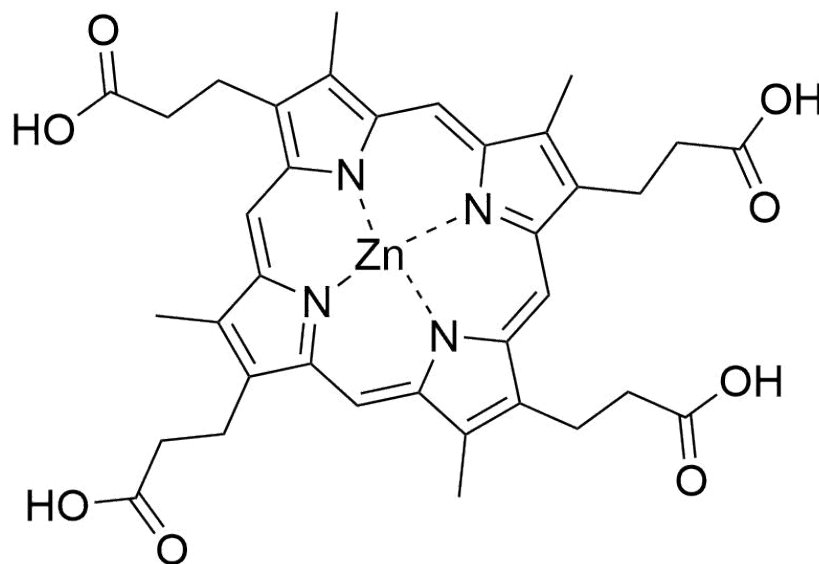
Figure 1.4. Zinc-coproporphyrin III produced by *Glutamicibacter arilaitensis* in response to co-culture with a *Penicillium* species, both of which were isolated from cheese rinds

In additional to the ability to create complex flavor and texture profiles, the microbiome that exists on our food can also lay claim to a wide range of biological interactions between microbial species; resulting in a plethora of unexplored chemistry. Bacterial and fungal species, both of which are traditionally found on fermented foods, are known to be rich sources of SMs and the characterization of their role in food has been vastly understudied. Based on community and pairwise interactions, there is evidence of antimicrobials as negative growth inhibition has been initiated by either fungi or bacteria.[42,43] This idea is further elaborated upon in the third chapter in which microbial interactions from the cheese microbiome are examined for the production of antimicrobial compounds.

1.3. Conclusions

The investigation of chemical communication between cells has shown that production and secretions of SMs can have a significant impact on the biological health of a system. There is

previous knowledge of some of the SMs that are produced by microorganisms, plants and animals and additional study has the potential to unlock an abundance of new chemistry that is waiting to be discovered. By working together across different fields, skill sets can be combined to better understand the molecules that drive both disease and symbiosis within an interaction and move forward to determining causation as opposed to remaining in a correlative stage. The majority of preliminary research into chemical communication is initiated using observable phenotypes such as growth inhibition caused by an antifungal metabolite or symbiotic colonization of a host by bacteria. However, the use of analytical techniques, including chromatography, NMR and MS, is necessary to further elucidate the chemistry that is responsible for these phenotypes. In particular, MS is well suited for the investigation of chemical communication due to its ability to carry out proximity-based measurements based on or from samples collected from the source of disease or cellular interactions that are physically adjacent.

The combination of biology and MS will allow us to better probe and identify SMs produced during disease progression and on the surfaces of fermented food that we consume. In order to better understand the chemical pathways within a system that are responsible for diseases and/or microbial phenotypes that we observe in a laboratory setting, we can combine our skill sets to investigate the molecules that drive both disease and symbiosis within a host-microbe interaction and move towards determining causation as opposed to remaining in a correlative stage. The following chapters highlight two distinct biological systems that have the ability to be investigated using similar analytical methodologies with the unifying concept of sourcing samples from their local environment, in hopes that this can be used to answer some of nature's more challenging questions.

1.4. References

1. Peleg, A. Y., Hogan, D. A. & Mylonakis, E. Medically important bacterial–fungal interactions. *Nat. Rev. Microbiol.* **8**, 340–349 (2010).

2. Cleary, J. L., Condren, A. R., Zink, K. E. & Sanchez, L. M. Calling all hosts: Bacterial communication in situ. *Chem* **2**, 334–358 (2017).

3. Kirst, H. A. *et al.* Discovery, Isolation, and Structure Elucidation of a Family of Structurally Unique, Fermentation-Derived Tetracyclic Macrolides. in *Synthesis and Chemistry of Agrochemicals III* **504**, 214–225 (American Chemical Society, 1992).

4. Thompson, G. D., Dutton, R. & Sparks, T. C. Spinosad--a case study: an example from a natural products discovery programme. *Pest Management Science: formerly Pesticide Science* **56**, 696–702 (2000).

5. Villegas, S. C. & Breitzka, R. L. Head lice and the use of spinosad. *Clin. Ther.* **34**, 14–23 (2012).

6. Alberts, A. W. *et al.* Mevinolin: a highly potent competitive inhibitor of hydroxymethylglutaryl-coenzyme A reductase and a cholesterol-lowering agent. *Proc. Natl. Acad. Sci. U. S. A.* **77**, 3957–3961 (1980).

7. Stierle, A., Strobel, G. & Stierle, D. Taxol and taxane production by Taxomyces andreanae, an endophytic fungus of Pacific yew. *Science* **260**, 214–216 (1993).

8. Kardos, N. & Demain, A. L. Penicillin: the medicine with the greatest impact on therapeutic outcomes. *Appl. Microbiol. Biotechnol.* **92**, 677–687 (2011).

9. Zink, K. E., Dean, M., Burdette, J. E. & Sanchez, L. M. Imaging Mass Spectrometry Reveals Crosstalk between the Fallopian Tube and the Ovary that Drives Primary Metastasis of Ovarian Cancer. *ACS Cent Sci* **4**, 1360–1370 (2018).

10. Garg, N. *et al.* Mass spectral similarity for untargeted metabolomics data analysis of complex mixtures. *Int. J. Mass Spectrom.* **377**, 719–717 (2015).

11. Bouslimani, A. *et al.* Molecular cartography of the human skin surface in 3D. *Proc. Natl. Acad. Sci. U. S. A.* **112**, E2120–9 (2015).

12. Kim, Y.-G. *et al.* Neonatal acquisition of Clostridia species protects against colonization by bacterial pathogens. *Science* **356**, 315–319 (2017).

13. Turnbaugh, P. J. *et al.* An obesity-associated gut microbiome with increased capacity for energy harvest. *Nature* **444**, 1027–1031 (2006).

14. Hofmann, A. F. The enterohepatic circulation of bile acids in mammals: form and functions. *Front. Biosci.* **14**, 2584–2598 (2009).

15. Ismail, A. S., Valastyan, J. S. & Bassler, B. L. A Host-Produced Autoinducer-2 Mimic Activates Bacterial Quorum Sensing. *Cell Host Microbe* **19**, 470–480 (2016).

16. Schäfer, K.-C. *et al.* In vivo, in situ tissue analysis using rapid evaporative ionization mass spectrometry. *Angew. Chem. Int. Ed Engl.* **48**, 8240–8242 (2009).

17. Balog, J. *et al.* Identification of the Species of Origin for Meat Products by Rapid Evaporative Ionization Mass Spectrometry. *J. Agric. Food Chem.* **64**, 4793–4800 (2016).

18. Balog, J. *et al.* Intraoperative tissue identification using rapid evaporative ionization mass spectrometry. *Sci. Transl. Med.* **5**, 194ra93 (2013).

19. Takáts, Z., Wiseman, J. M., Gologan, B. & Cooks, R. G. Mass spectrometry sampling under ambient conditions with desorption electrospray ionization. *Science* **306**, 471–473 (2004).

20. Morelato, M., Beavis, A., Kirkbride, P. & Roux, C. Forensic applications of desorption electrospray ionisation mass spectrometry (DESI-MS). *Forensic Sci. Int.* **226**, 10–21 (2013).

21. Banerjee, S. *et al.* Diagnosis of prostate cancer by desorption electrospray ionization mass spectrometric imaging of small metabolites and lipids. *Proc. Natl. Acad. Sci. U. S. A.* **114**, 3334–3339 (2017).

22. Karas, M., Bachmann, D. & Hillenkamp, F. Influence of the wavelength in high-irradiance ultraviolet laser desorption mass spectrometry of organic molecules. *Anal. Chem.* **57**, 2935–2939 (1985).

23. Croxatto, A., Prod'hom, G. & Greub, G. Applications of MALDI-TOF mass spectrometry in clinical diagnostic microbiology. *FEMS Microbiol. Rev.* **36**, 380–407 (2012).

24. Cornett, D. S., Reyzer, M. L., Chaurand, P. & Caprioli, R. M. MALDI imaging mass spectrometry: molecular snapshots of biochemical systems. *Nat. Methods* **4**, 828–833 (2007).

25. Zhang, J. *et al.* Nondestructive tissue analysis for ex vivo and in vivo cancer diagnosis using a handheld mass spectrometry system. *Sci. Transl. Med.* **9**, (2017).

26. Maier, T. M., Schwarz, G., Kostrzewa, M. *Application Note # MT-80: Microorganism Identification and Classification Based on MALDI-TOF MS Fingerprinting with MALDI Biotyper*. (Bruker Daltonics GmhB).

27. Borst, A., Box, A. T. A. & Fluit, A. C. False-positive results and contamination in nucleic acid amplification assays: suggestions for a prevent and destroy strategy. *Eur. J. Clin. Microbiol. Infect. Dis.* **23**, 289–299 (2004).

28. Moss, E. L., Hollingworth, J. & Reynolds, T. M. The role of CA125 in clinical practice. *J. Clin. Pathol.* **58**, 308–312 (2005).

29. Jannetto, P. J. & Fitzgerald, R. L. Effective Use of Mass Spectrometry in the Clinical Laboratory. *Clin. Chem.* **62**, 92–98 (2016).

30. Zhang, J. *et al.* Nondestructive tissue analysis for ex vivo and in vivo cancer diagnosis using a handheld mass spectrometry system. *Sci. Transl. Med.* **9**, (2017).

31. Maier, T. & Kostrzewa, M. Spectrophotometric identification of microbe subspecies. *US Patent* (2011).

32. McGovern, P. E. *et al.* Fermented beverages of pre- and proto-historic China. *Proc. Natl. Acad. Sci. U. S. A.* **101**, 17593–17598 (2004).

33. Legras, J.-L., Merdinoglu, D., Cornuet, J.-M. & Karst, F. Bread, beer and wine: Saccharomyces cerevisiae diversity reflects human history. *Mol. Ecol.* **16**, 2091–2102 (2007).

34. Sieuwerts, S., de Bok, F. A. M., Hugenholtz, J. & van Hylckama Vlieg, J. E. T. Unraveling microbial interactions in food fermentations: from classical to genomics approaches. *Appl. Environ. Microbiol.* **74**, 4997–5007 (2008).

35. Boethius, A. Something rotten in Scandinavia: The world's earliest evidence of fermentation. *J. Archaeol. Sci.* **66**, 169–180 (2016).

36. Kinsella, J. E. & Hwang, D. H. Enzymes of Penicillium roqueforti involved in the biosynthesis of cheese flavor.pdf. *CRC Crit. Rev. Food Sci. Nutr.* **8**, 191–228 (1976).

37. Button, J. E. & Dutton, R. J. Cheese microbes. *Curr. Biol.* **22**, R587–9 (2012).

38. Wolfe, B. E., Button, J. E., Santarelli, M. & Dutton, R. J. Cheese rind communities provide tractable systems for in situ and in vitro studies of microbial diversity. *Cell* **158**, 422–433 (2014).

39. Bonham, K. S., Wolfe, B. E. & Dutton, R. J. Extensive horizontal gene transfer in cheese-associated bacteria. *Elife* **6**, e22144 (2017).

40. Yeluri Jonnala, B. R., McSweeney, P. L. H., Sheehan, J. J. & Cotter, P. D. Sequencing of the Cheese Microbiome and Its Relevance to Industry. *Front. Microbiol.* **9**, 1020 (2018).

41. Cleary, J. L., Kolachina, S., Wolfe, B. E. & Sanchez, L. M. Coproporphyrin III Produced by the Bacterium Glutamicibacter arilaitensis Binds Zinc and Is Upregulated by Fungi in Cheese Rinds. *mSystems* **3**, (2018).

42. Izquierdo, E., Wagner, C., Marchioni, E., Aoude-Werner, D. & Ennahar, S. Enterocin 96, a novel class II bacteriocin produced by Enterococcus faecalis WHE 96, isolated from Munster cheese. *Appl. Environ. Microbiol.* **75**, 4273–4276 (2009).

43. Kastman, E. K. *et al.* Biotic Interactions Shape the Ecological Distributions of Staphylococcus Species. *MBio* **7**, (2016).

Chapter 2

Detection of Ovarian Cancer Using Samples Sourced from the Vaginal Microenvironment

Adapted with permission from BioRxiv, Detection of Ovarian Cancer Using Samples Sourced from the Vaginal Microenvironment. Galey, M.M., Young, A.N., Petukhova, V.Z., Wang, M., Wang, J., Salvi, A., Russo, A., Burdette, J.E., Sanchez, L.M. (2019)

2.1. Introduction

2.1.1. The Hurdles of Ovarian Cancer Diagnostics

Ovarian cancer is a severe gynecological disease that is currently the fifth leading cause of cancer deaths among women in the United States, with an estimated 22,530 newly diagnosed cases and 13,980 deaths expected in 2019.[1] This disease has a five-year survival rate of 93% if diagnosed when tumor growth is limited to reproductive organs, such as the ovaries or fallopian tubes.[2,3] However, the majority of diagnoses occur during the late stages of the disease when tumors have already metastasized, resulting in a five-year survival rate of less than 30%. Around 90% of these diagnoses are of epithelial origin, of which high-grade serous ovarian cancer (HGSOC) is the most common subtype.[3–5] These late-stage diagnoses can be attributed to the limited diagnostic methods available for implementation in routine women's health exams. Current diagnostic methods, such as transvaginal ultrasounds and CA-125 biomarker tests, are generally used only after patients present with symptoms, as they are invasive procedures. These invasive methods also suffer from inaccuracy and a lack of specificity, which limits their use in diagnosing ovarian cancer in its early stages.[6,7]

In a routine health screening, women receive a Pap smear to determine cervical health but recent data suggests that these samples may be repurposed for ovarian cancer detection.[8] This study by Kinde *et. al*, along with other studies, shows that DNA derived from ovarian cancer cells can be detected in clinical samples, such as Pap smears, which represents a concentrated sample from the local microenvironment in the female reproductive system.[8–10] This clinical evidence would suggest that cells and/or cellular fragments from ovarian tumors reside outside of the proximal environment in areas such as the cervix or vagina. Further confirmation of the Pap smear being linked to HGSOC detection was recently detailed in a case report, in which adenocarcinoma cells derived from HGSOC precursor lesions were observed in a cervical smear.[11] This case study indicates that developing a technology or method of measurement from

Pap smears or other vaginal samples may allow for the detection of HGSOC in its earlier stages at which point, patient prognosis is more promising.

2.1.2. The Rise of Clinical Mass Spectrometry for Diagnostic Purposes

While reliable early diagnostic markers for ovarian cancer have remained elusive, research has moved closer towards characterizing the proteome of a healthy female reproductive system using mass spectrometry (MS).[12] For instance, the iKnife and MasSpec Pen are both innovative devices that couple MS signatures in lipids to the detection of cancerous tissue in surgical resections.[13,14] Work has recently been done using MS to investigate Pap smears under the assumption that cells, cellular debris or secreted proteins from the female genital tract would be present.[12] Bottom-up proteomics experiments using a linear trap quadrupole (LTQ) Orbitrap mass spectrometer were performed on liquid Pap smear samples from women considered healthy to create a 'Normal' Pap Test Core Proteome.[12] Bottom-up proteomics is highly sensitive but requires significant sample preparation steps in order to obtain accurate measurements such as sample cleanup to remove salts and insoluble particulates, protein digestion, and lengthy liquid chromatography experiments leading to a significant time investment, as well as a high degree of expertise needed to operate a high mass resolution tandem mass spectrometer (LC-MS/MS). Matrix-assisted laser desorption/ionization time-of-flight (MALDI-TOF) MS is considered a versatile analytical technique used in a variety of applications ranging from the rapid characterization of microbial species to biomarker detection using protein signatures.[15–17] For example, the MALDI-TOF Biotyper system is currently FDA approved for use in clinical diagnostic laboratories for microbial typing.[18] MALDI-TOF MS has also been used to characterize mammalian cells based on spectral fingerprints, which in turn, allows for their identification.[19–21] While MALDI-TOF spectra are considered to be low resolution in comparison to LC-MS/MS where proteins can be fully identified, its use in a clinical setting is highly advantageous due to the speed in which analysis occur, since rapid diagnosis is key for patient prognosis. The direct

measurement of proteins, particularly those that change in abundance over time from a local source, may improve strategies that can be leveraged for detection, especially when combined with genome sequencing.
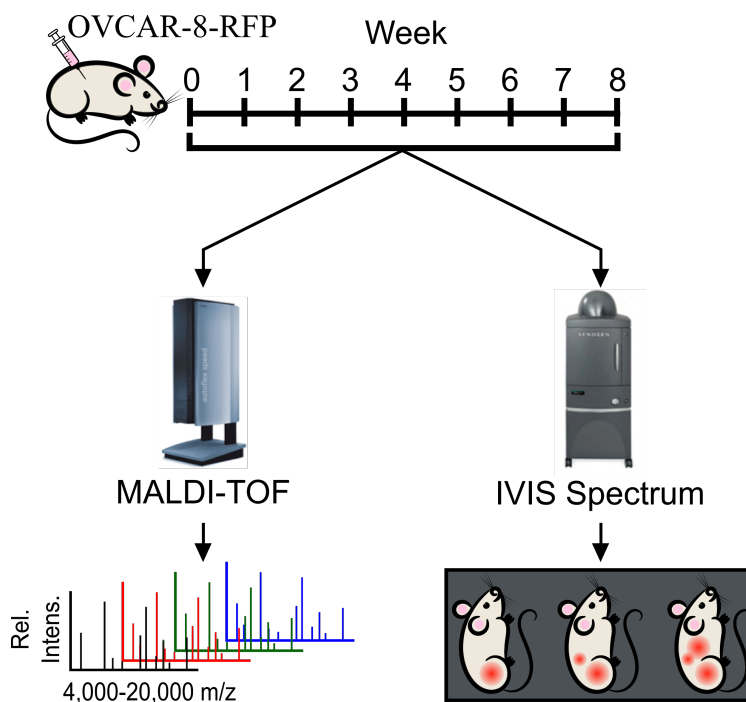
Figure 2.1. Workflow of murine xenograft study. Female athymic mice were IP injected with OVCAR-8-RFP and tumors were allowed to develop over an eight week period. Each week, mice were given vaginal lavages and were imaged using an IVIS imaging system to track tumor burden. Vaginal lavages were analyzed using MALDI-TOF MS to obtain mass spectra for statistical analyses.

As previous studies have highlighted that ovarian cancer cells and associated cellular debris have the ability to travel through the female reproductive system to the cervix, we felt it would be feasible to detect these changes to the reproductive environment using MALDI-TOF MS based on whole-cell fingerprinting with protein signatures.[8,10,21] As a proof of principle for this concept, we used a murine model of HGSOC. In this study, we used vaginal lavages (analogous to Pap smears) in a murine xenograft model to detect the increasing burden of ovarian cancer based on protein fingerprints in the 4-20 kDa mass range obtained using MALDI-TOF MS (**Figure 2.1**). Statistical analysis of the protein signatures found candidate proteins that both increase and

decrease over time as the disease progresses, highlighting the importance of sampling a local microenvironment proximal to disease origin. By sourcing cells from a local microenvironment, we hoped to achieve greater sensitivity and specificity while also exploring the ability of small proteins to lend themselves as possible biomarkers of disease progression.

2.2. Results and Discussion

2.2.1. *In Vivo* Imaging to Monitor Tumor Progression in OVCAR-8 Xenograft Model

In order to emulate the progression of HGSOC, an *in vivo* xenograft model was performed using OVCAR-8, a human-derived ovarian carcinoma cell line. OVCAR-8 has a p53 mutation, a gene that is found in up to 96% of HGSOC tumors and is responsible for increased tumorigenic and metastatic potential as evidenced in previous animal studies.[22–24] Following the intraperitoneal (IP) injection of OVCAR-8 cells tagged with red fluorescent protein (RFP), all mice were imaged every seven days and their respective fluorescence increased in intensity and tumors colonized the peritoneum over time. (**Figure 2.2**). At the conclusion of the longitudinal study, all five of the mice had significant metastatic tumor burden and four out of the five presented with ascites, a buildup of fluid in the abdominal cavity, which is a symptom present in over a third of ovarian cancer patients.[25]
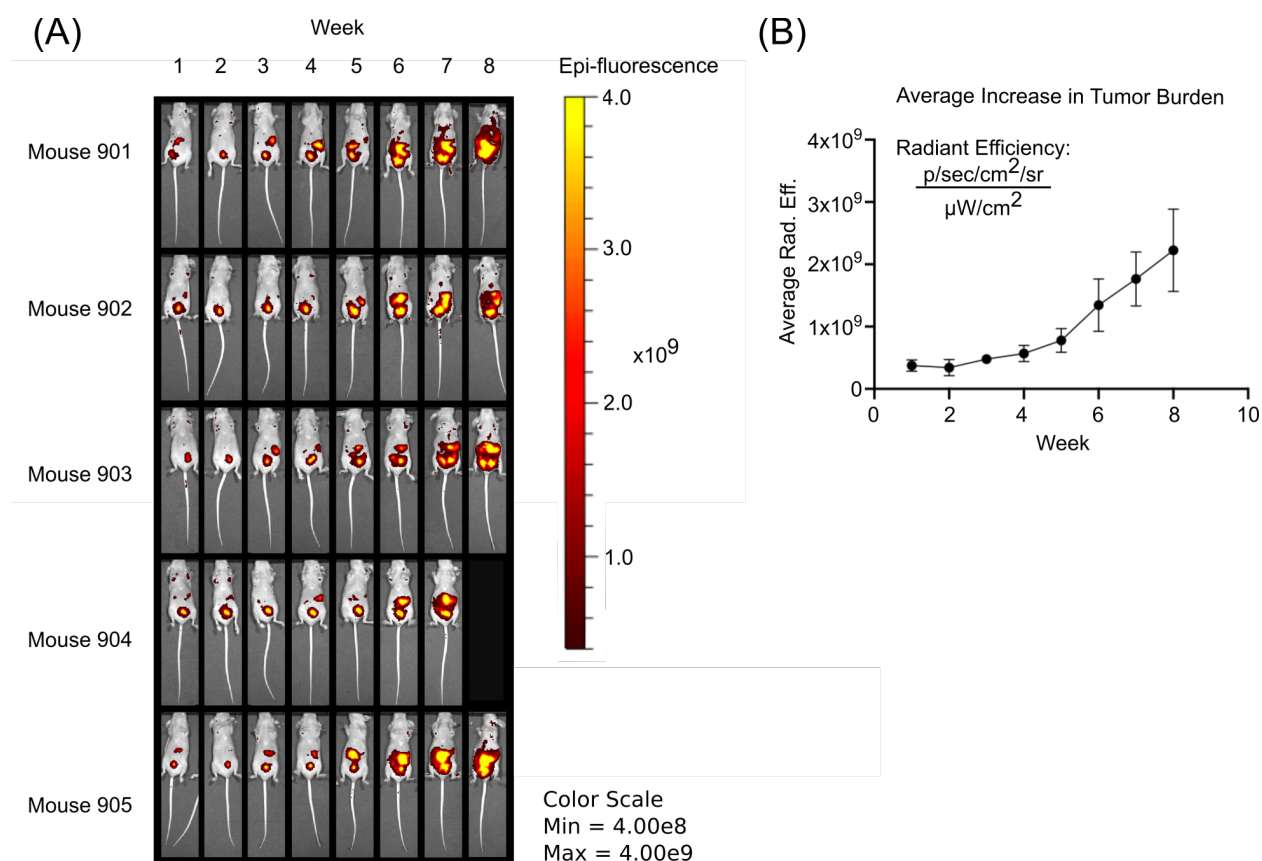
Figure 2.2. (A) *In vivo* fluorescence imaging of OVCAR-8-RFP IP tumors in athymic nude mice over an eight week period (B) Average radiant efficiency over time for all mice indicating an increase in tumor burden

2.2.2. Origin of Detected Proteins do not Appear to be Escaped Cells

Previous work in our lab by Petukhova *et. al* has demonstrated that whole-cell fingerprinting using MALDI-TOF MS is capable of detecting as low as 1% of cancer cells in an otherwise healthy heterogenous two-component mixture.[21] Given our ability to detect unique signatures using MALDI-TOF MS, the next question we sought to examine was whether we were detecting signatures from escaped cells. Deep sequencing technologies have demonstrated the ability to amplify ovarian-cancer derived cells in vaginal fluids, vide supra. As part of the study design we sought to utilize the fluorescence of the OVCAR-8 RFP cells in vaginal lavages to correlate protein signatures to escaped cell populations. However, we were not able to detect any fluorescent proteins during the lavage cell counting (**Figure 2.3**).

Cell Type	Average Cell Count (Fluorescence)	Average Cell Count (Brightfield)	Average Fluorescence (%)	Standard Deviation	Fluorescence Based on FACS (%)
100% OVCAR-8-RFP	913.167	1715.500	43.552	0.154	98.52
10% OVCAR-8-RFP 90% Lavage	17.500	1217.125	1.429	0.008	2.17
1% OVCAR-8-RFP 99% Lavage	1.375	1326.625	0.065	0.001	0.17
100% Lavage	0.000	1324.000	0.000	0.000	0.04

(B)
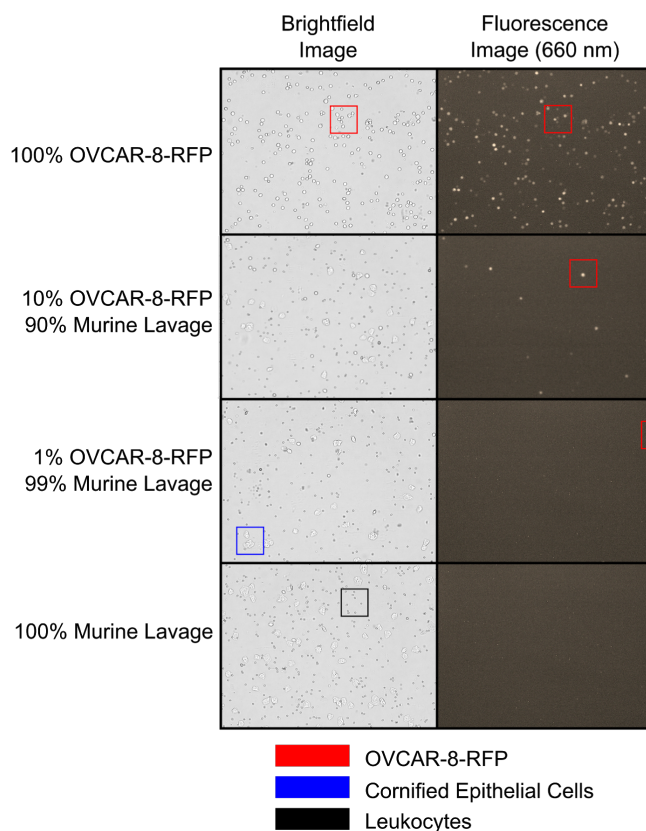
Figure 2.3. (A) Table detailing the average cell count (fluorescent and brightfield) along with average fluorescence with respective standard deviation values (n=6) and fluorescence based on flow cytometry. (B) Representative brightfield and fluorescence (600 nm) images of OVCAR-8-RFP cells, murine lavages and mixtures of the two components. Colored boxes are used to outline examples of fluorescent OVCAR-8 cells (red), cornified epithelial cells (blue) & leukocytes (black), the latter two being normally found in the murine reproductive system.

This was further confirmed using fluorescence-activated cell sorting (FACS), a technique based on flow cytometry, in a controlled spiking study that has the quantitative ability to separate a group of murine lavage cells into subpopulations according to their ability to fluoresce. Based on these

experiments, it was shown that 2.17%, 0.17%, and 0.02% of fluorescent cells spiked into healthy

lavage samples were detectable using this technique with samples comprised of 10%, 1% and

0.01% OVCAR-8-RFP cells, respectively, while it was able to detect 98.52% of a sample

comprised of 100% OVCAR-8-RFP cells (**Figure 2.4**). This is in line with our previous whole cell

MALDI-TOF MS proof of principle study in which detection of multiple distinguishing features

occurs with increasing percentages of cancer cells (5-10%) mixed with healthy cells and yields

only a limited number of unique features when 1% of cancer cells are in an otherwise healthy

heterogenous two-component mixture.[21]
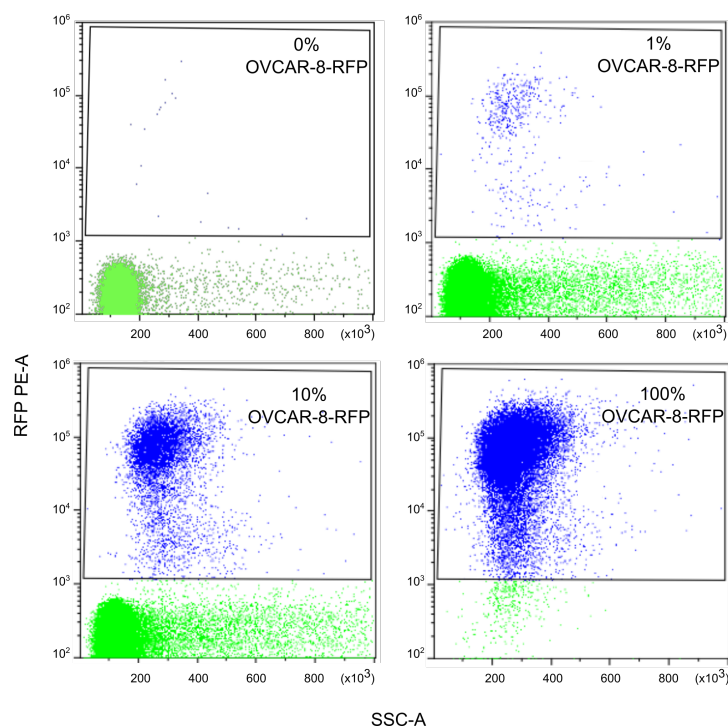
Figure 2.4. Scatter plots of phycoerythrin (PE) absorbance vs. side scatter (SSC) in our FACS analysis where the blue and green dots are representative of fluorescent and non-fluorescent cell counts, respectively, for four different conditions.

We believe that it is possible that while a small proportion of tumorigenic cells escape into the

vaginal microenvironment, it is unlikely that the signatures we are directly detecting arises from

these escaped cells. In our MALDI-TOF MS method, the detection of proteins is from all cell types

and likely some cellular debris within lavage samples, as opposed to rigorously purified whole cells, making the source of these proteins ambiguous. For instance, we cannot differentiate between cellular origination from tumor cells versus those found in the murine reproductive system. It could also be possible that we are observing the cellular response to cancer; in which case, this represents an exciting avenue for further study as these protein signatures does not rely on our ability to detect escaped cells within the lavage, as we do not have the ability to amplify our MS signals, as is done in deep sequencing studies. This could potentially provide an excellent opportunity to multiplex sequencing and amplification that comes from tumor cells with changes in the vaginal microenvironment. We have also further demonstrated that the response is unique at least to ovarian cancer as the lavages from mice with nonalcoholic steatohepatitis (NASH) resulted in murine fingerprints in aged, sexed matched mice that were distinct, which represents an entirely different peritoneal disease. The observance of statistically significant changes in feature intensity, regardless of whether the proteins are from ovarian cancer tumor cells or not, is of importance for this study as we are not focused on the appearance of tumor cells in the murine lavage but rather changes in the overall system.

2.2.3. Vaginal Lavages from a HGSOC Model Yields Distinct Differences from Other Disease Models

Based on our previous work with two-component mixtures with different cell lines, it was anticipated that a vaginal lavage taken over time could be useful for monitoring HGSOC progression.[21] In order to verify that these protein fingerprints are unique to disease state and not a result of any peritoneal disease, mice with NASH, which results in severe liver damage, were age-matched to those in our OVCAR-8 xenograft model in the seventh week and vaginal lavages were collected. Upon comparison of average spectra for each condition, it was observed that the protein signatures were distinct between the two peritoneal diseases (**Figure 2.5**). Therefore, our

MALDI-TOF MS methodology yields distinct, disease specific protein fingerprints from the vaginal microenvironment.

(A)

(B)

(C)
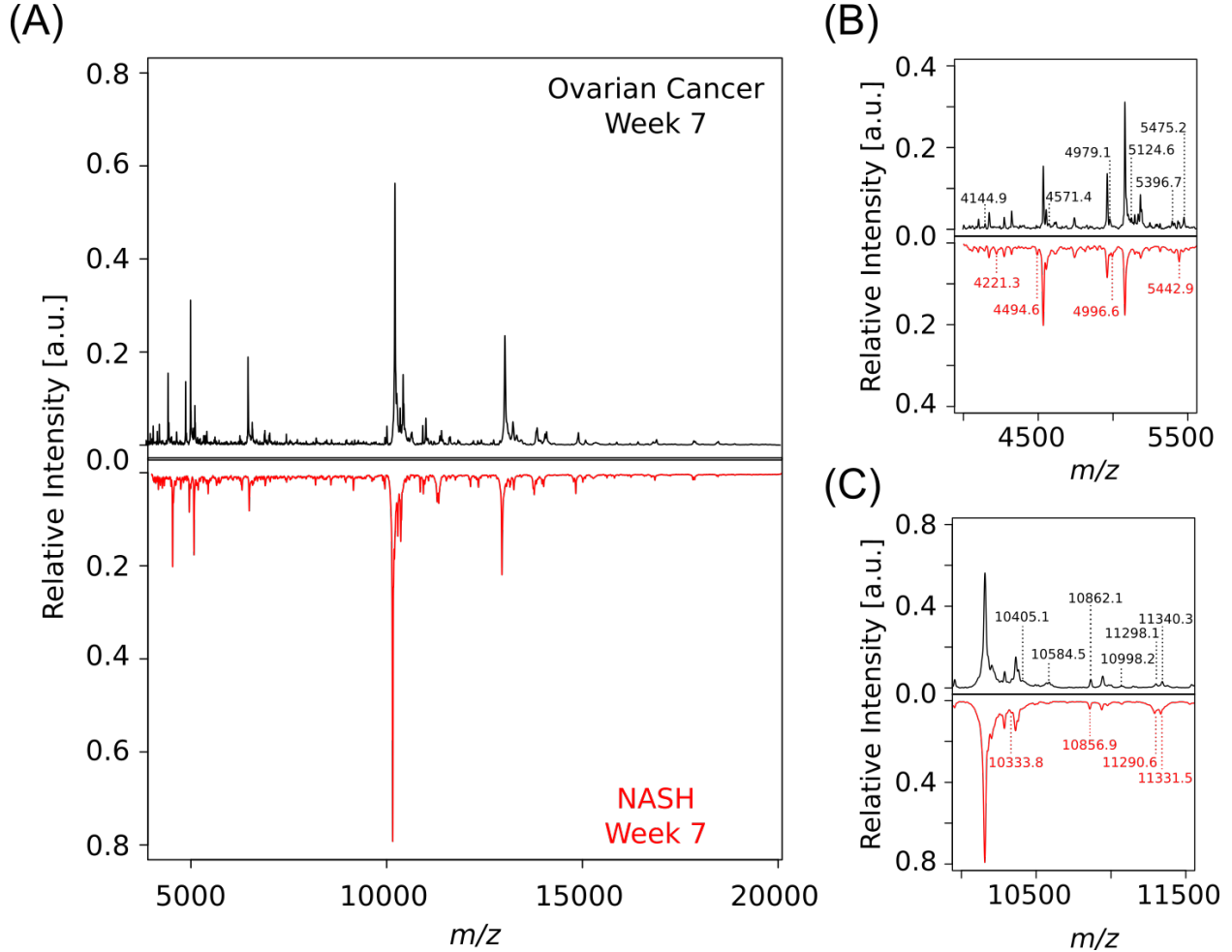
Figure 2.5. Mirror plot of average protein fingerprints of murine lavages comparing week seven in an ovarian cancer model and week seven in a NASH model (N=5, n=24 and N=9, n=24, respectively). Labeled peaks in the zoomed-in regions identify picked peaks that differ between conditions (A) Full spectra (*m/z* 4,000-20,000). (B) Spectral features in this region (*m/z* 4,000-5,500) differ between both disease states in terms of peaks and intensity. (C) Spectral features in this region (*m/z* 10,000-11,500) present another area in which peaks differ between both disease states in terms of appearance and intensity.

Additionally, while our study consisted of vaginal lavages on a weekly basis, we wanted to ensure that significant changes to the protein fingerprint are truly due to the progression of HGSOC and not inflammation of the vaginal cavity. Repetitive vaginal lavages were performed on healthy

athymic nude mice over a five day period and protein signatures were not significantly different

from day-to-day (**Figure 2.6**).
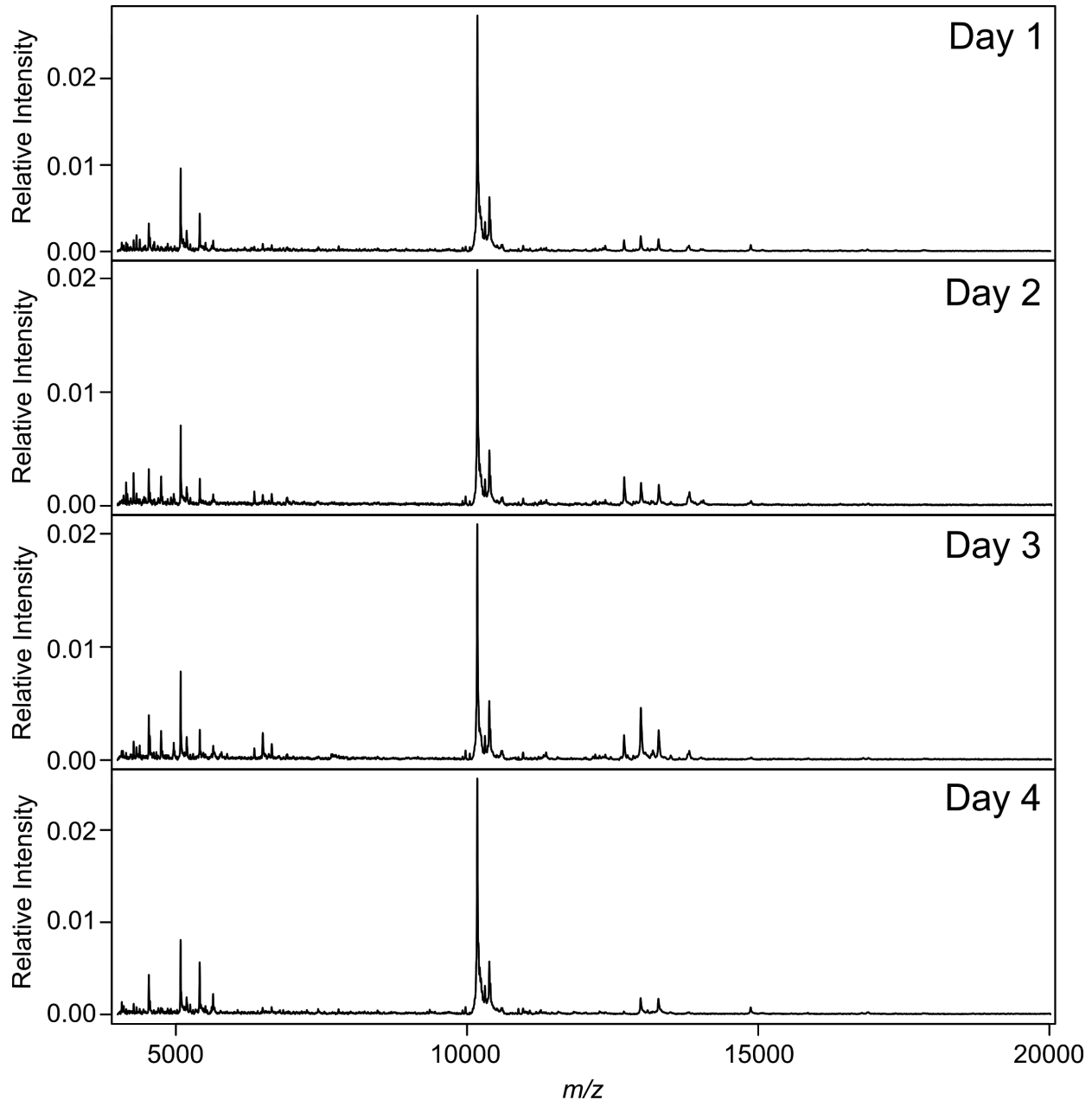
Figure 2.6. Consensus vaginal lavages from healthy athymic nude mice collected for a week on a daily basis (N=3, n=4). This was done to ensure that the signature detected at the conclusion of the study, when mice had heavy HGSOC tumor burden, was not due to inflammation of the vaginal cavity caused by repetitive sampling. It is also important to note that the murine estrous cycle spans a period of four to five days so slight changes could be attributed to this phenomenon.

2.2.4. Use of MALDI-TOF for Analysis of Vaginal Lavage Samples

MALDI-TOF MS had several advantages for this study such as being solvent-free, rapid data acquisition (milliseconds), minimal sample requirements and the availability of this technology in clinical laboratories.[15–18] MALDI-TOF MS also allows for rapid collection of a protein fingerprint over a large mass range, providing intact protein masses. Similar to how the Biotyper system (Bruker Daltonics) works for microbial identifications, the collection of a protein fingerprint allows for the comparison of different spectral patterns, in terms of the appearance and absence of features, to look for matches based on characteristic peaks.[18] This is advantageous to our study as we have the ability to statistically analyze and compare protein fingerprints collected at various time points throughout the study to detect changes in protein peaks during tumor progression.

Our lab had previously identified the small protein mass range (4-20 kDa) as having a higher number of characteristic peaks as well as the most distinctive when comparing cell types, particularly OVCAR and murine oviductal cell lines.[21] Therefore, protein fingerprints from this mass range were collected for murine vaginal lavages from weeks one through seven of the xenograft study, as they were most likely to yield the richest spectral fingerprint. During the collection of murine vaginal samples, a conscious choice was made to only analyze proteins coming from the cells isolated via centrifugation to measure spectral fingerprint changes from cells that could easily be extracted from a standard Pap smear procedure. To ensure that no critical spectral features were being missed by excluding the supernatant from statistical analysis, a small subset of supernatant samples that had been separated from the lavage cell pellets were analyzed via MALDI-TOF MS (**Figure 2.7**). These samples were found to have similar peaks but had much lower overall intensity and poorer ionization, likely caused by the PBS-induced suppression.[21]
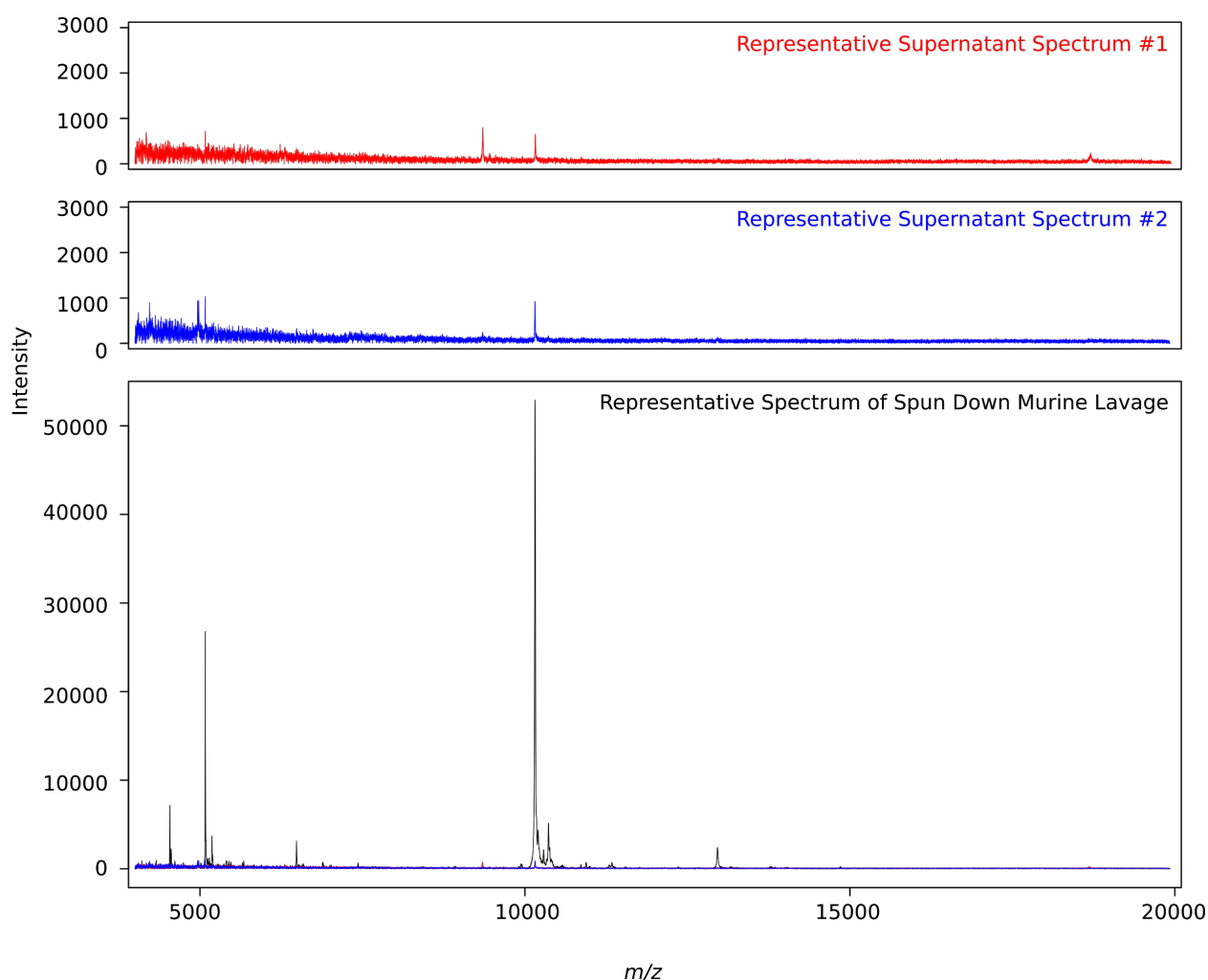
Figure 2.7. Representative spectra of supernatant and murine lavage samples illustrating intensity differences between sample types (n=24).

There were two important notes regarding this study with the first being that each mouse in the study acted as their own biological control prior to the IP injection of OVCAR-8-RFP. This not only reduced the overall number of animals necessary to complete the study but also facilitated as few biological variables as possible when comparing protein fingerprints from their respective lavages. The second being that the first week of the study was chosen as the first time point in our statistical analysis for comparative purposes due to irregularities in the samples taken at earlier time points including insufficient sample ionization. In addition to poor sample ionization, the mice were moved to a different facility just prior to the xenograft procedure which may have also added

undue stress that was not consistent with other sampling dates. Therefore, the samples from the seventh day of the study (Week 1) was used as the first time point in lieu of the true start date of the study for a more accurate comparison.

In order to begin to visualize the data, the cosine similarity of the murine vaginal lavages in the form of a dot product matrix was used (**Figure 2.8 A**). In this instance, cosine similarity is a measurement of how similar two groups of spectra are from each other with 0 being completely dissimilar and 1 being an exact match.[26] This allows for an easily accessible view of how the profiles may differ over time when compared to specific weeks in the study. Additionally, representative consensus spectra from each time point of all five mice was generated (**Figure 2.8 B**), with consensus spectra for each individual mouse in the study shown in **Figures 2.9-2.13**.

A)

B)
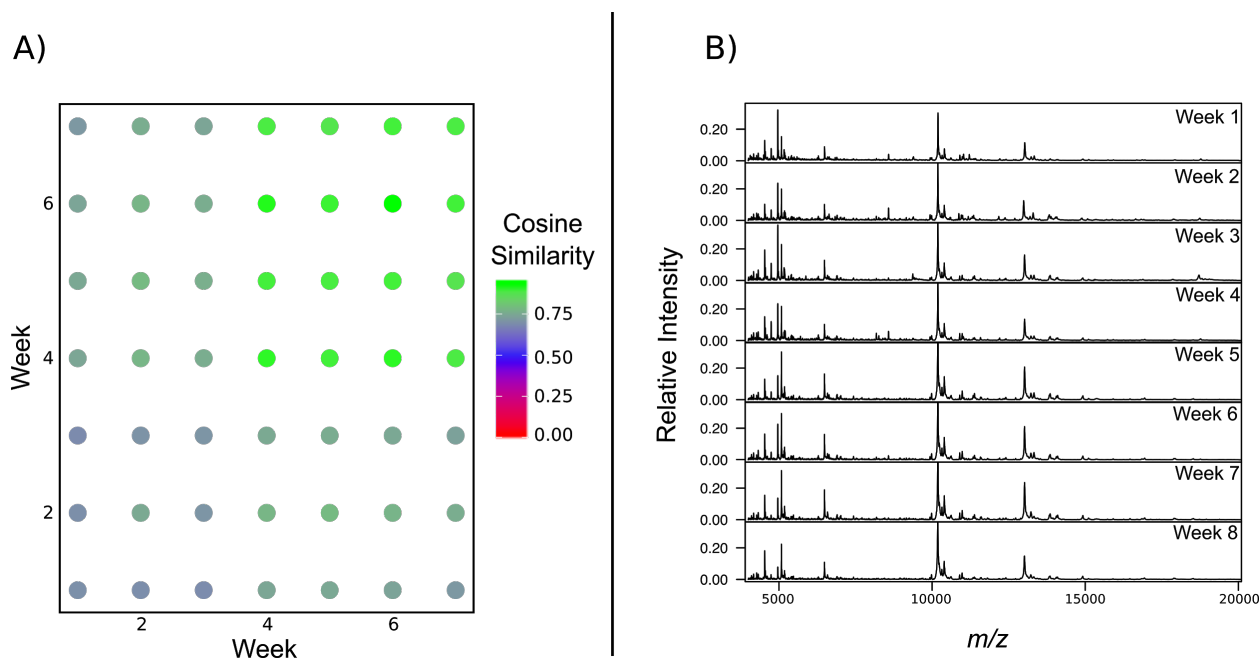
Figure 2.8. (A) Dot matrix plot comparing spectral similarity between time points. High cosine scores (green) indicates that the global profiles are highly similar between intersecting time point (i.e. weeks six and seven) while low cosine scores (red) indicates less similarity in features between the spectra of the respective time points. (B) Consensus spectra of vaginal lavages from all mice (N=5) throughout tumor progression for a total of eight weeks (n=24 for each mouse at each time point).
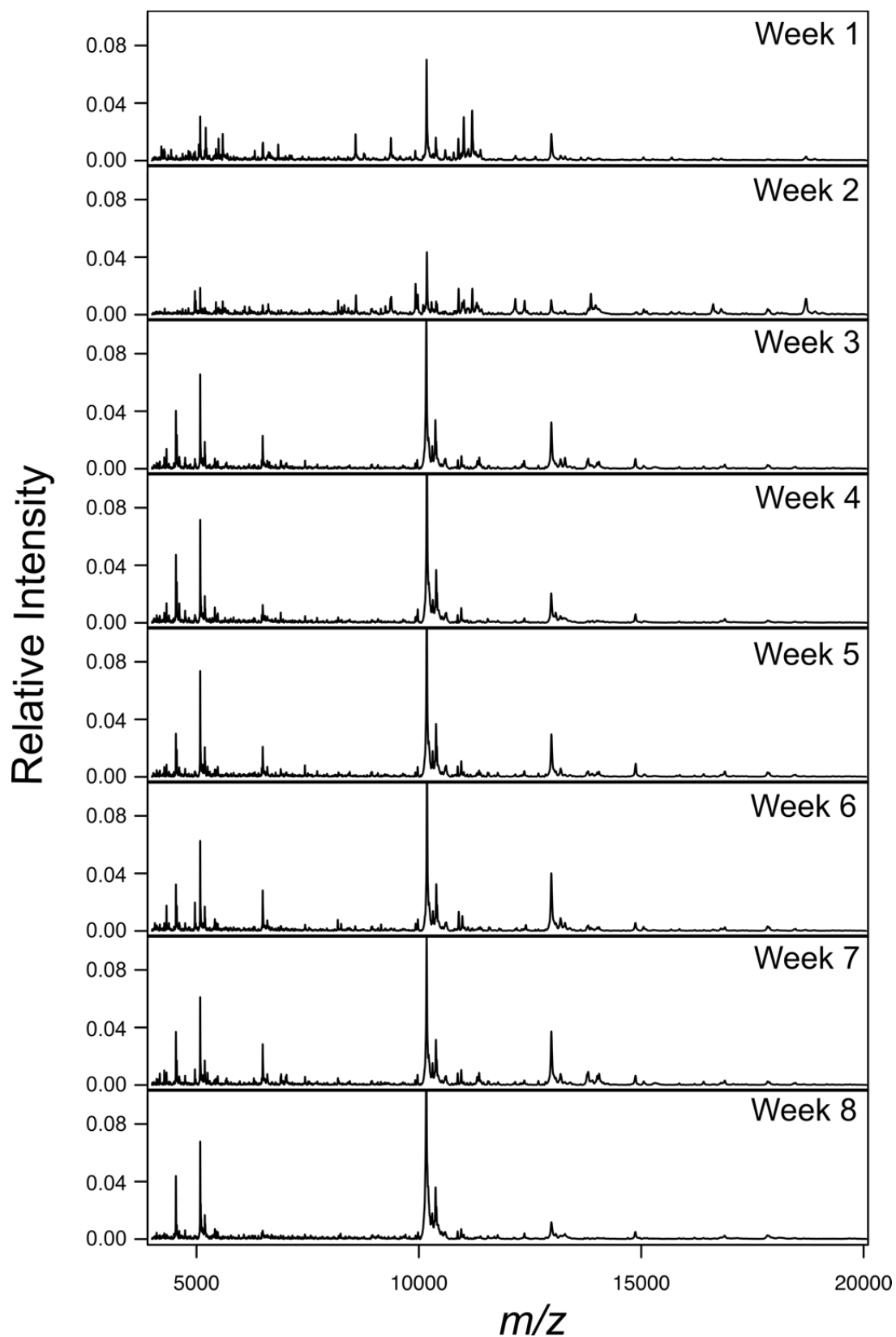
Figure 2.9. Consensus spectra of vaginal lavages from mouse 901 throughout tumor progression for a total of eight weeks (n=24 for each time point).
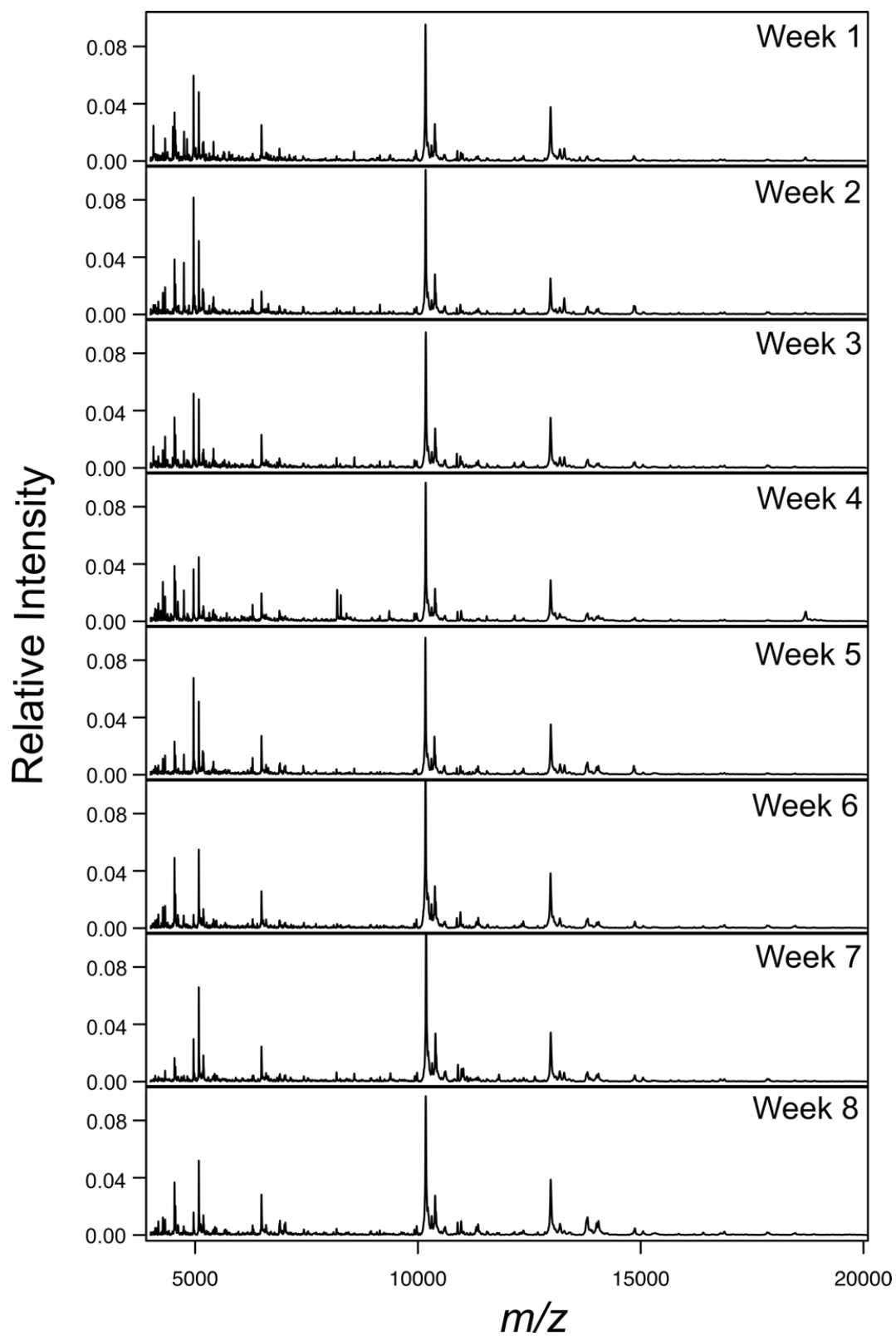
Figure 2.10. Consensus spectra of vaginal lavages from mouse 902 throughout tumor progression for a total of eight weeks (n=24 for each time point).
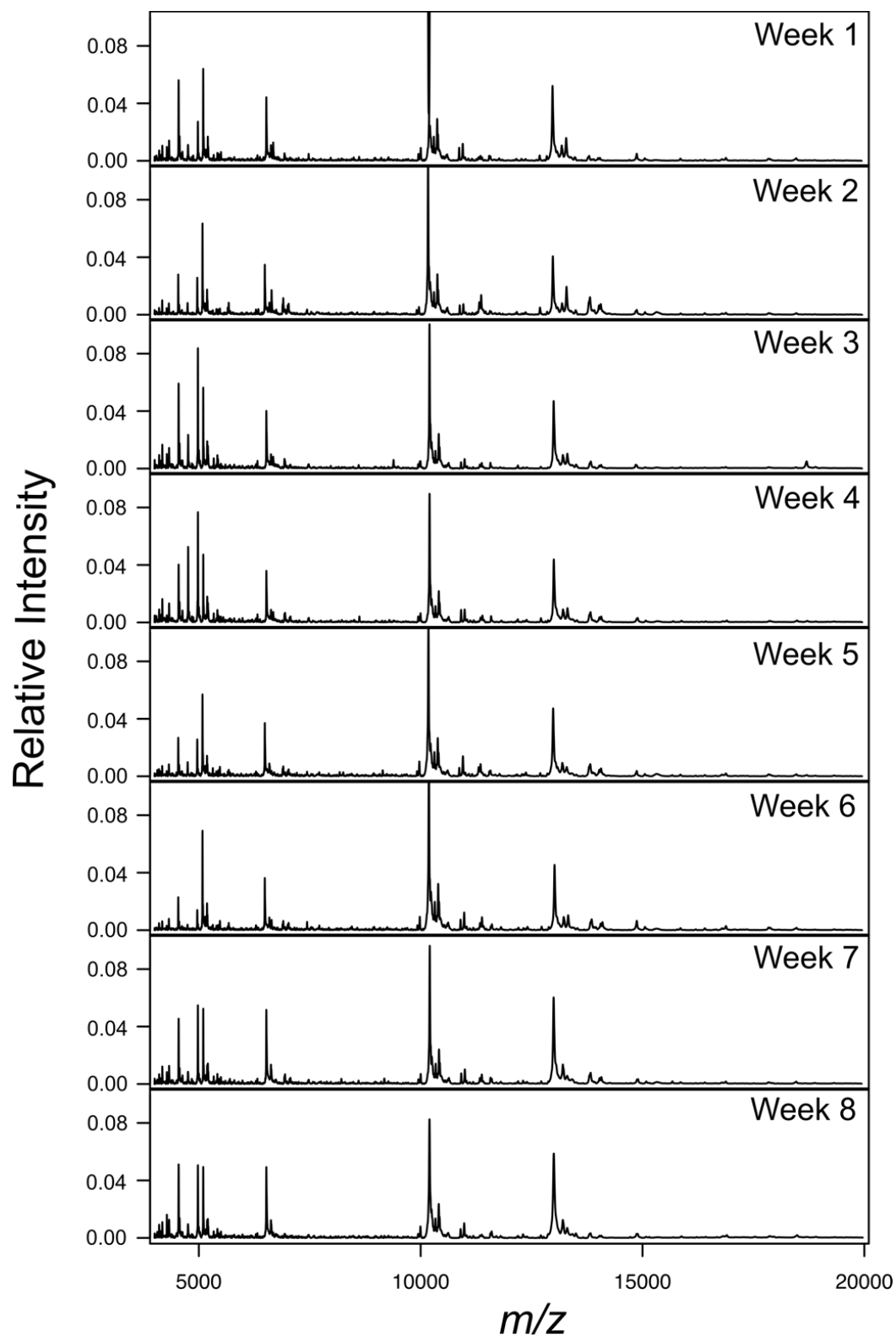
Figure 2.11. Consensus spectra of vaginal lavages from mouse 903 throughout tumor progression for a total of eight weeks (n=24 for each time point).
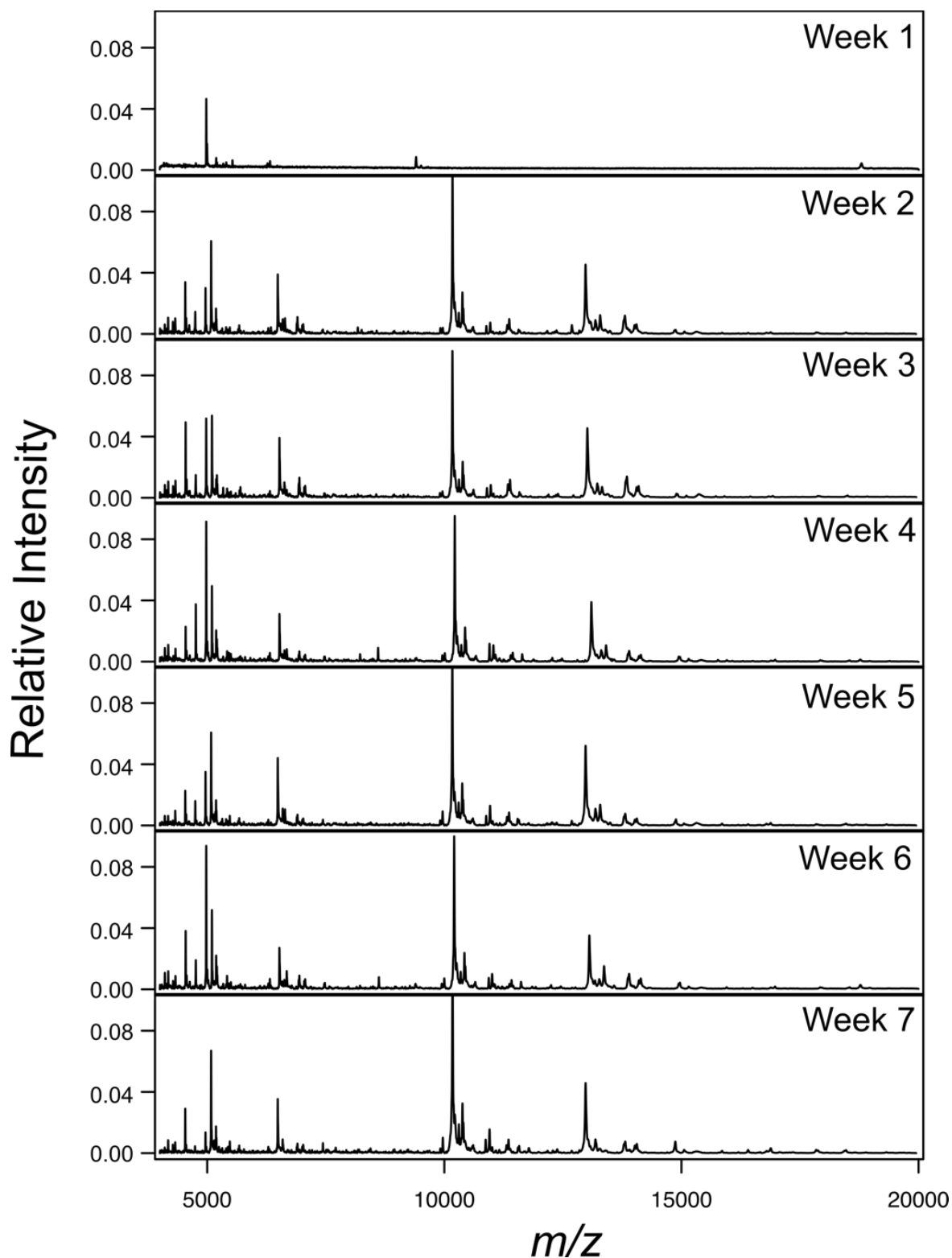
Figure 2.12. Consensus spectra of vaginal lavages from mouse 904 throughout tumor progression for a total of seven weeks (n=24 for each time point). This mouse expired prior to the conclusion of the study, which is why no lavage was obtained during the eighth week.
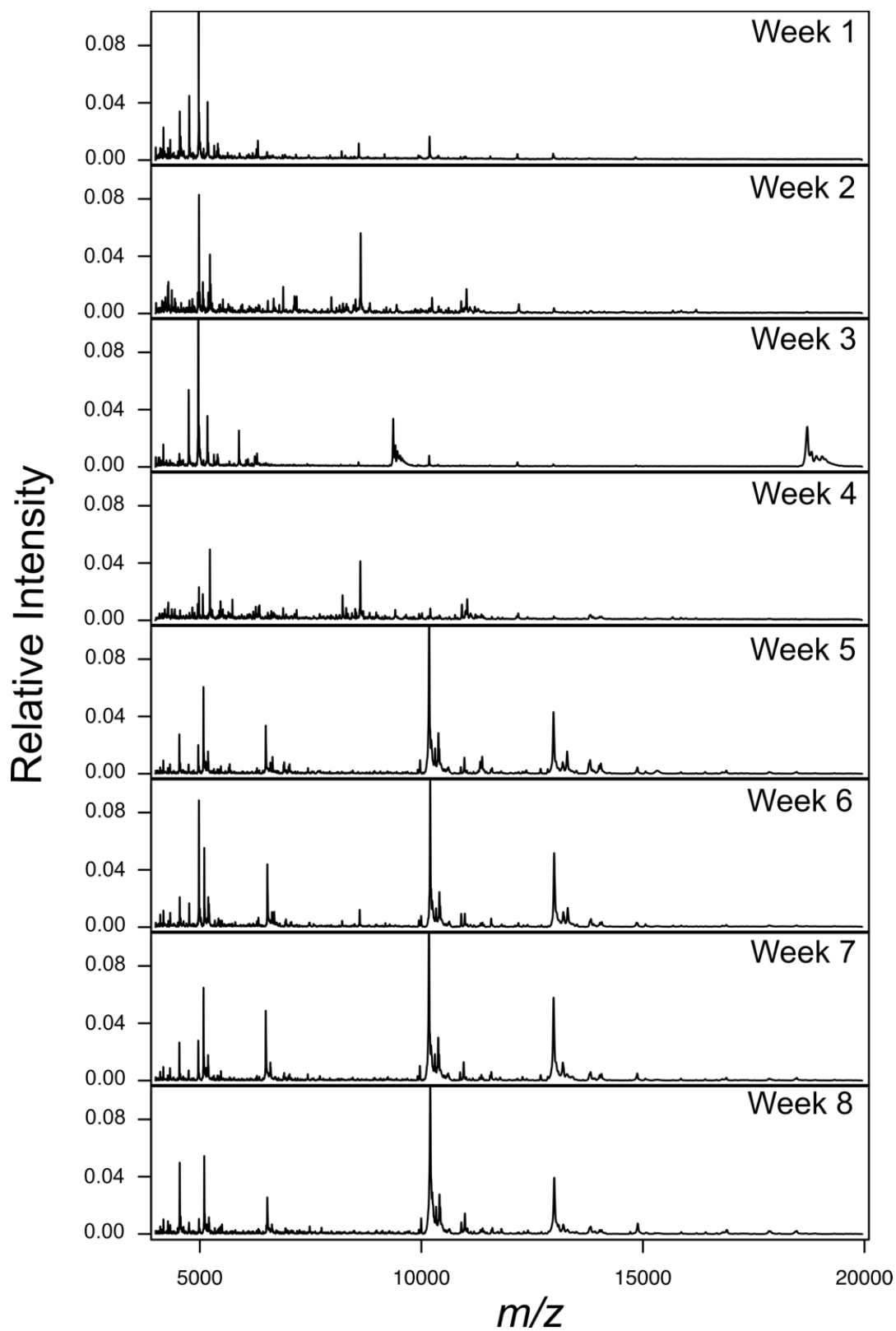
Figure 2.13. Consensus spectra of vaginal lavages from mouse 905 throughout tumor progression for a total of eight weeks (n=24 for each time point).

At the beginning of the study, each biological replicate (N=5) had a relatively unique profile when compared to others at or around the same time point with lower cosine score of around 0.7 being observed. However, one of the striking results was that at the end of the study (Week 7), the protein fingerprints from the vaginal lavages are largely conserved, which would indicate that all five mice have similar protein profiles once the tumor burden is representative of late stage ovarian cancer. This would imply that there are unique processes and/or cellular responses associated with the progression of HGSOC that can be captured in a spectral protein fingerprint. All detected peaks that were found to be differentially expressed across time points can be found in **Table 2.1**.

Table 2.1. PIVOT TABLES INDICATING SPECTRAL FEATURES THAT ARE DIFFERENTIALLY EXPRESSED ACROSS VARIOUS TIME POINTS THROUGHOUT THE STUDY. (A) UPREGULATED *M/Z* VALUES WITH A P-VALUE < 0.001 COMPARING WEEKS ONE THROUGH SEVEN. (B) DOWNREGULATED *M/Z* VALUES WITH A P-VALUE < 0.001 COMPARING WEEKS ONE THROUGH SEVEN.

(A) Upregulated Features Shared Across all Five Mice

	Week	**3**	**5**	**6**	**7**
		Unique Features			
	m/z	1	9	4	10
	4265.9	-	-	1	-
	4269.8	-	1	-	-
	4270.5	-	1	-	-
	4367.7	-	1	-	-
	4369.6	-	1	-	-
	4714.1	-	1	-	1
Week 1	4792.9	-	-	-	1
	4795.7	-	-	-	1
	4862.5	-	-	-	1
	5508.8	-	1	1	-
	5640.7	-	1	-	1
	5807.5	-	-	1	-
	5843.8	-	-	1	-
	6744.0	-	-	-	1

	m/z				
	6753.4	-	-	-	1
	6756.0	-	1	-	1
	6759.6	-	-	-	1
	7196.1	-	-	-	1
	12620.2	1	1	-	-
Week 2	*m/z*	0	0	0	6
	6634.8	-	-	-	1
	6661.3	-	-	-	1
	6744.0	-	-	-	1
	6749.6	-	-	-	1
	6753.4	-	-	-	1
	6759.6	-	-	-	1
Week 3	*m/z*	0	2	0	25
	4048.1	-	-	-	1
	4350.4	-	-	-	1
	4358.6	-	-	-	1
	4381.7	-	-	-	1
	4567.6	-	-	-	1
	4586.3	-	-	-	1
	4586.8	-	-	-	1
	4587.9	-	-	-	1
	4612.7	-	-	-	1
	4617.0	-	1	-	1
	4631.0	-	-	-	1
	4746.9	-	-	-	1
	4753.1	-	-	-	1
	4757.0	-	-	-	1
	4759.0	-	-	-	1
	4762.7	-	-	-	1
	4952.0	-	-	-	1
	5405.3	-	-	-	1
	5412.6	-	-	-	1
	5640.7	-	-	-	1
	5645.6	-	-	-	1
	6744.0	-	-	-	1
	6756.0	-	-	-	1
	6759.6	-	-	-	1
	6767.4	-	-	-	1
	9370.3	-	1	-	-

	m/z	0	12	2	25
	4139.5	-	1	-	-
	4140.7	-	1	1	1
	4198.4	-	-	-	1
	4226.2	-	-	-	1
	4230.0	-	-	-	1
	4269.8	-	1	-	-
	4358.6	-	1	-	-
	4381.7	-	1	-	-
	4545.4	-	1	-	-
	4566.7	-	-	-	1
	4567.6	-	1	-	1
	4617.0	-	-	-	1
	4627.5	-	-	-	1
	4631.0	-	-	-	1
	4636.2	-	-	-	1
	4757.0	-	1	-	1
Week 4	4834.7	-	1	-	-
	5412.6	-	-	-	1
	5528.8	-	1	-	-
	5640.7	-	-	-	1
	6041.4	-	1	-	1
	6233.9	-	-	-	1
	6236.0	-	-	-	1
	6653.0	-	-	-	1
	6661.3	-	-	-	1
	6759.6	-	-	-	1
	6767.4	-	-	-	1
	6838.4	-	1	-	-
	8261.0	-	-	1	-
	9354.6	-	-	-	1
	18704.5	-	-	-	1
	18716.8	-	-	-	1
	18720.6	-	-	-	1
	18767.5	-	-	-	1
Week 5	m/z	0	0	0	1
	9947.8	-	-	-	1

(B) Downregulated Features Shared Across all Five Mice

	Week	3	4	5	6	7
				Unique Features		
	m/z	0	3	12	42	19
	5110.5	-	-	-	1	-
	5127.1	-	-	-	1	-
	5129.8	-	-	-	1	-
	5147.2	-	-	-	1	-
	5149.1	-	-	-	1	-
	6574.9	-	-	-	-	1
	6904.0	-	-	1	1	1
	7024.0	-	-	1	-	1
	8179.0	-	1	-	-	-
	10105.1	-	-	-	1	-
	10108.1	-	-	-	1	-
	10111.1	-	-	-	1	-
	10118.3	-	-	-	1	-
	10126.6	-	-	-	1	-
	10141.9	-	-	-	1	-
	10226.2	-	-	-	1	-
Week 1	10296.2	-	-	-	1	-
	10344.0	-	-	-	1	-
	10388.4	-	-	-	1	-
	10430.1	-	-	-	1	-
	10440.8	-	-	-	1	-
	13770.4	-	-	1	1	1
	13777.6	-	-	1	1	1
	13786.8	-	-	1	1	1
	13805.6	-	-	1	1	1
	13851.0	-	-	-	1	-
	13853.6	-	-	-	1	-
	13861.8	-	-	-	1	1
	13870.8	-	-	-	1	-
	13887.0	-	-	-	1	1
	13888.7	-	-	-	-	1
	13889.8	-	-	-	1	1
	13891.4	-	-	-	1	1
	13892.9	-	-	-	1	1

m/z					
13907.1	-	-	-	1	-
13909.0	-	-	-	1	-
13910.5	-	-	-	1	-
13913.5	-	-	-	1	-
13997.2	-	1	1	1	1
14008.2	-	1	1	1	1
14016.7	-	-	1	1	1
14025.3	-	-	1	1	1
14048.3	-	-	1	1	1
14069.3	-	-	1	-	1
14869.0	-	-	-	1	-
15052.6	-	-	-	1	-
16879.2	-	-	-	1	-

Week 2

m/z	1	0	5	1	2
4065.3	1	-	-	-	-
6479.9	-	-	1	-	1
6600.4	-	-	1	-	-
10951.4	-	-	-	1	-
11774.8	-	-	-	-	1
12975.8	-	-	1	-	-
13201.2	-	-	1	-	-
13204.2	-	-	1	-	-

Week 3

m/z	0	3	2	2	4
5147.2	-	-	1	-	-
5436.7	-	-	-	-	1
5477.6	-	-	-	-	1
7713.0	-	-	1	-	-
8179.0	-	1	-	-	-
8183.9	-	1	-	-	-
8261.0	-	1	-	-	-
9962.3	-	-	-	1	1
10951.4	-	-	-	1	-
15052.6	-	-	-	-	1

Week 4

m/z	0	0	15	0	5
5147.2	-	-	1	-	-
5676.2	-	-	1	-	-
6488.6	-	-	-	-	1
6591.4	-	-	-	-	1
11296.9	-	-	1	-	-

	m/z					
	11308.0	-	-	1	-	-
	11334.3	-	-	1	-	-
	11349.8	-	-	1	-	-
	11384.4	-	-	1	-	-
	12278.0	-	-	-	-	1
	12284.1	-	-	-	-	1
	13181.8	-	-	-	-	1
	15302.8	-	-	1	-	-
	15309.2	-	-	1	-	-
	15319.2	-	-	1	-	-
	15329.3	-	-	1	-	-
	15330.8	-	-	1	-	-
	15334.7	-	-	1	-	-
	15346.5	-	-	1	-	-
	15359.2	-	-	1	-	-
Week 5	*m/z*	0	0	0	0	1
	8179.0	-	-	-	-	1
Week 6	*m/z*	0	0	0	0	1
	6581.4	-	-	-	-	1

This late stage similarity prompted us to search for the presence and absence of protein features across all mice across paired time points (i.e. week one versus week seven). We found that multiple proteins began to dominate the mass spectra throughout disease progression and that a number of proteins either appeared or became absent from the protein fingerprint over time. This led to the investigation of specific regions of the spectrum and the verification that specific peaks became either significantly up- or downregulated over time, which would suggest that tumor progression does, in fact, induce changes in specific processes in our murine model system. Several research groups have studied the proteome of cervical-vaginal fluid (CVF) obtained from healthy women. These clinical samples contained CVF-derived proteins that were measured within the mass range detailed in our study, including thioredoxin and profilin-1.[12,27–31] However, there is still not much known about the reproductive proteome between *m/z* 4,000-20,000 as many identified proteins are much larger. However, some studies have shown that proteins falling into

our targeted mass range can be detected via proteomic analysis of CVF, inclusive of proteins responsible for cell organization and immune response, such as thymosin beta-4annexin A1.[27–29] Scientists have speculated that this mass range contains an abundance of histones or ribosomal proteins based on previous whole-cell fingerprinting research and we hope to expand the knowledge of this area in the future through the identification of detected proteins using MS.[19]

The Wilcoxon-rank sum test was used for the normalized intensity values from each observed peak and ranks them in terms of value for comparison. This statistical test makes minimal assumptions about the data, which allows it to be used in cases of non-normal distributions. Following analysis, specific features shared between all mice were found to be significantly changed in intensity throughout the time course of the study (**Figure 2.14**). The determination of the test statistic in each comparison (week to week) allowed for the calculation of a p-value for significance. This analysis allowed for the identification of 118 upregulated and 97 downregulated spectral features when comparing data from different time points, implying that there were multiple significant changes over time in our mouse model. In particular, there are 19 and 10 features that are significantly up- and downregulated, respectively, in all mice (p <0.001).

(A)

Week

Week	2	3	4	5	6	7
1	-	-	3	12	42	19
2	-	1	-	5	1	2
3	-	-	3	2	2	4
4	-	-	-	15	-	5
5	-	-	-	-	-	1
6	-	-	-	-	-	1

(B)

Week

Week	2	3	4	5	6	7
1	-	1	-	9	4	10
2	-	-	-	-	-	6
3	-	-	-	2	-	25
4	-	-	-	12	2	25
5	-	-	-	-	-	1
6	-	-	-	-	-	-

(C)

	Peak	*m/z*	Avg. p-value
Upregulated	1	13770.4	6.20×10^{-14}
	2	13777.6	6.20×10^{-14}
	3	13786.8	6.20×10^{-14}
	4	13805.6	6.20×10^{-14}
	5	13997.2	6.20×10^{-14}
	6	14008.2	6.20×10^{-14}
	7	14016.7	6.20×10^{-14}
	8	14025.3	6.20×10^{-14}
	9	14048.4	6.20×10^{-14}
	10	14069.3	9.92×10^{-14}
Downregulated	1	5640.7	1.98×10^{-13}
	2	6753.3	9.45×10^{-11}
	3	6759.6	1.75×10^{-10}
	4	6756.0	1.83×10^{-10}
	5	4795.7	4.93×10^{-10}
	6	6744.0	5.43×10^{-10}
	7	4862.5	6.43×10^{-9}
	8	4792.9	9.09×10^{-9}
	9	4714.2	4.62×10^{-8}
	10	7196.1	3.14×10^{-7}

Figure 2.14. (A) Pivot table showing number of significantly upregulated signals observed across time points across all five mice. (B) Pivot table showing number of significantly downregulated signals observed across time points across all five mice. (C) Top ten *m/z* values according to average p-values when comparing weeks one and seven.

Interestingly, the significant features between the initial and final time points of the study are segregated into different subsets of the mass range (**Figure 2.15**). The majority of the signals that appear over time are approximately twice the mass as those observed to be downregulated. This

may point to a dysregulation in protease activity and requires further validation on the identity of these proteins to further test the possible mechanism by which these proteins accumulate in the disease state.
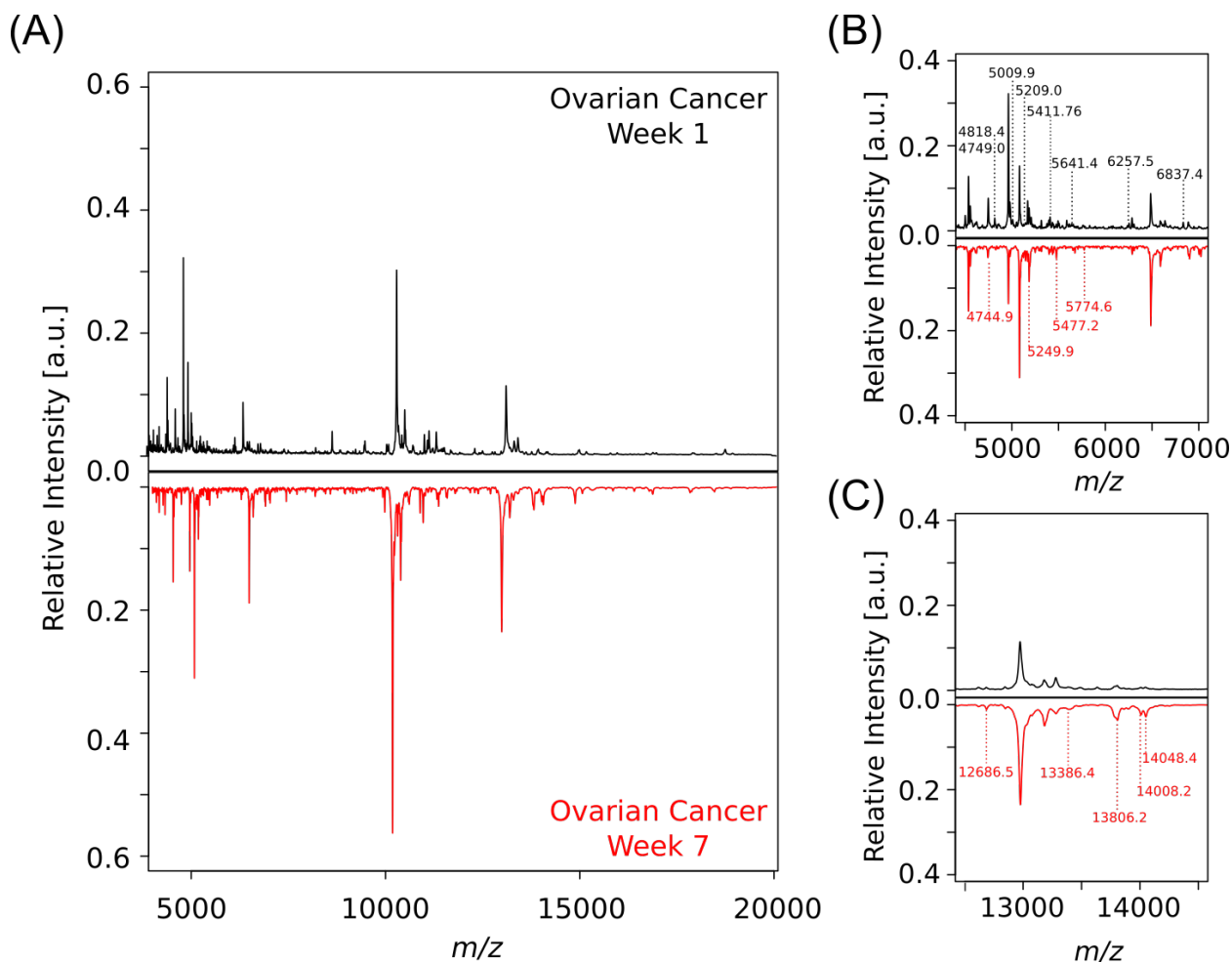
Figure 2.15. Mirror plot of average protein fingerprints of murine lavages comparing weeks one and seven (N=5, n=24). Labeled peaks in the zoomed-in regions identify picked peaks that differ between conditions (A) Full spectra (*m/z* 4,000-20,000). (B) Spectral features in this region (*m/z* 4,500-7,000) are downregulated between the two time points. (C) Spectral features in this region (*m/z* 12,500-14,500) are upregulated between the two time points.

A second murine xenograft study (N=3) was performed in an attempt to reproduce the results obtained from the first five mice with all of the same experimental conditions - the one difference being that IVIS images were not obtained. This was intentional as the goal of this study was to

determine if the onset of ovarian cancer could be detected without the aid of fluorescence imaging. At the finality of the study (seven weeks), two of the three mice had tumors on their reproductive organs and all had tumors throughout their peritoneal cavities.
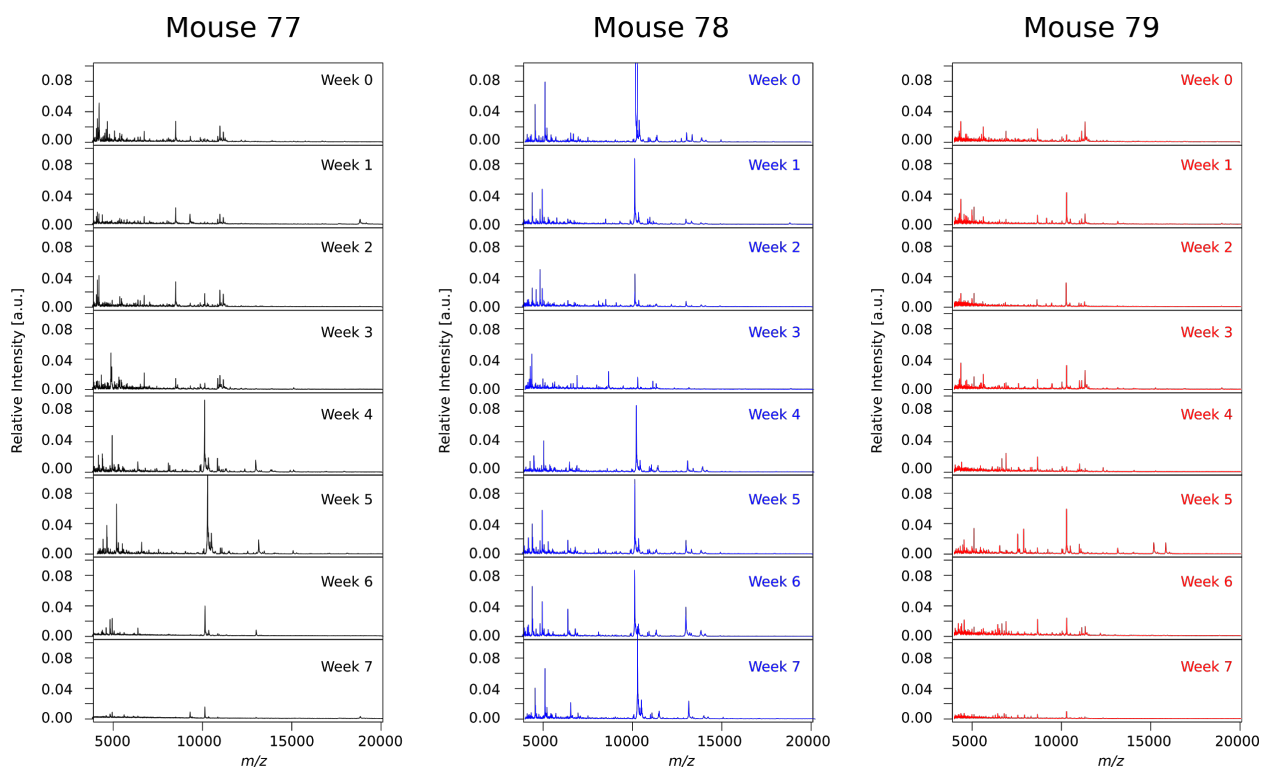
Figure 2.16. Consensus spectra of vaginal lavages from each mouse in the second xenograft study (n=24 for each time point) - Black: Mouse 77, Blue: Mouse 78, Red: Mouse 79

While the second murine study was successful in terms of the mice developing OVCAR-8-RFP tumors, there were significant issues observed in their respective protein fingerprints over time. When compared to the spectra from the first study, it was determined that there was a very low number of shared peaks between the second cohort of mice, meaning that some of the lavages were truly distinct from the remainder of the samples across mice and time points. This caused issues during spectral alignment as there were too few peaks for the alignment algorithm (Lowess Warping). Upon further investigation into the protein fingerprints of the three mice used in this second study, it is of note that the spectra vary greatly over time in terms of peaks and peak

intensity for each mouse as well as throughout the time series (**Figure 2.16**). It is plausible that this could be caused by factors such as environmental stressors or biological differences. Mice were housed in a different satellite facility than the first cohort and one of the mice in the second study (79) became extremely cachexic during the fourth week which may have altered the vaginal lavage make-up and subsequent protein fingerprint.

Due to issues in carrying out comparable statistical analyses as to what was done with the first cohort of mice, this data was not combined with that from the first cohort. However, all tumors and vaginal lavages were saved and stored for further analysis including mass spectrometry. The two studies provided a valuable lesson in the challenges of *in vivo* animal studies and foreshadow the challenges that we expect to see when progressing to human samples as no two patients will be alike in terms of their general health or protein fingerprints.

2.2.5. Bottom-Up Proteomics for Protein Identification

While the spectral fingerprint obtained from the murine vaginal lavages is a promising start to better understand the cellular processes that occur throughout the progression of ovarian cancer, it is of note that while MALDI-TOF mass spectrometers allow for the observance of intact protein masses, they do not have the mass resolving power in linear mode to provide an exact mass for the detected spectral features. Bottom-up proteomics, performed on a high-resolution instrument such as a hybrid quadrupole-orbitrap mass spectrometer, is required to definitively identify these proteins via analysis of peptide fragments. Bottom-up proteomics has its own limitations such as potentially not having enough cleavage sites for the digestion enzyme due to the small size of the proteins. However, using a combination of both MS methods to obtain an intact mass along with tandem fragmentation may allow us to identify these proteins.

In the process of developing and carrying out initial experiments for proteomics identification, a collaboration was formed with the Cologna lab at UIC due to their expertise in proteomics. To date, preliminary experiments with a healthy murine lavage has been performed using a ThermoFisher qExactive mass spectrometer and a total of 57 proteins were found in a pooled lavage sample. In order to further validate these protein hits, proteins that were observed using tandem mass spectrometry were compared to MALDI-TOF mass spectra that had been obtained on intact lavage proteins. Protein that were found to overlap in both data sets are shown in **Table 2.2** below. These proteins were also found to be present in the murine reproductive system based on alternate detection sources, which was further confirmation that proteins could be identified and correlated between different MS-based methods.[32]

Table 2.2. POTENTIAL PROTEIN IDENTIFICATIONS FROM HEALTHY MURINE LAVAGES USING BOTTOM-UP PROTEOMICS

Description	Coverage [%]	# Unique Peptides	MW [Da]	Biological Relevance
Thymosin beta-4	40.00	4	5679	Cell organization and biogenesis
Protein S100-A8	34.83	2	10295	Cell death; defense response; response to stimuli
Small Ubiquitin Related Modifier 2	25.26	3	10871	Metabolic process

Additionally, a single experiment has been performed with a murine lavage taken from a mouse with late stage ovarian cancer (seven weeks) using the same procedure as above. This sample was less rich than the healthy lavage, with only ten proteins being identified. When compared to a healthy lavage sample which was run concurrently, only two proteins were shown as being unique to the cancer condition: RIKEN cDNA 4932414N04 gene and zinc finger protein 346, which have both been shown to be present in the female reproductive organs. However, both had

low annotation scores in UniProt so it is necessary to get additional replicates and complete further experimentation on these late stage samples. It is also of interest to compare these proteomics datasets to the *Homo sapiens* (human) database in UniProt in addition to that of *Mus musculus* (mouse) in order to help determine the true origin of these proteins moving forward.

Efforts in the pursuit of further identifications is ongoing using reproductive tissues from previous murine studies with a collaboration between the Sanchez and Cologna labs. Identifying these proteins remains of high interest as this would help to determine if they play any role in tumor formation or elsewhere in the reproductive tract such as in the form of a stress response.

2.2.6. Future Directions

Moving forward with this project, there are a number of to consider in terms of what we can use previously acquired data for and what additional data is needed to get a better understanding of changes to the local microenvironment due to HGSOC progression. Due to the fact that we have been able to see up- and downregulated signals shared across an entire cohort of mice (N=5) throughout the progression of HGSOC, it would interesting to take a close look at some of the time points to determine if we could find markers for early detection that are shared between median and final time points. While this was not focused on in this chapter, it would be extremely useful moving forward and would not necessarily require any subsequent *in vivo* xenograft experiments. In terms of additional experiments, I believe that it would be beneficial to repeat the OVCAR-8-RFP xenograft study using an intrabursal injection as that would introduce the tumor cells directly to the organs of interest. While an IP injection was found to result in tumors on the reproductive organs in almost all the mice used in our study, it was not definitive that the OVCAR-8 cells would repeatedly make their way into the bursa. This type of experiment would ensure that the cells were placed in very close proximity to the tissue of interest and we would hopefully be able to ensure that the mice would all develop HGSOC tumors. An additional animal study that

may be worth pursuing is one using a transgenic mouse model, in which the mice are susceptible to developing ovarian tumors without external pressures. This would likely represent the most natural state of disease progression in terms of tumor formation but the overall timeline of the study would need to be greatly extended and we would lose the ability to track tumor burden over time through in vivo imaging as there would be no fluorescence.

2.3. Conclusions

Based on statistical analysis with the Wilcoxon rank-sum test, we have been able to identify intact *m/z* values of small proteins obtained from murine vaginal lavages. We conclude that the protein fingerprint region obtained from our MALDI-TOF MS technique can be used to detect the presence of ovarian cancer. By sourcing samples from a local microenvironment, such as the vaginal cavity or cervix, we have shown that significant changes in protein signatures can be observed over time in the progression of ovarian cancer in a murine model. Our next step will be to further investigate and identify these proteins of interest using tandem MS to gain a better understanding of their role in disease progression in our *in vivo* model.

Additionally, we have recently obtained tampon samples from the University of Kansas from women with either benign, endometrial, ovarian or uterine tumors prior to surgical resection. Upon full optimization of sample preparation, protein fingerprints will be acquired alongside other analysis types such as deep sequencing and bottom-up proteomics, for comparison between the different tumor types. Through a deeper understanding of the signature proteins from both the murine and human samples, we may be able to further enhance our ability to design a diagnostic test for ovarian or other reproductive cancers in the future.

2.4. Experimental Section

2.4.1. General Experimental Procedures

OVCAR-8, a human-derived ovarian cancer cell line, expressing RFP was a gift from M. Sharon Stack at the University of Notre Dame.[33,34]

2.4.2. Cell Culture

OVCAR-8-RFP were grown in DMEM with an addition of 10% FBS and 1% penicillin/streptomycin. A humidified incubator (37°C) was used to maintain the cultured cells at in 5% CO_2. Cells used in this study were passaged no more than 20 times. Validation of cell lines occurred using short tandem repeat analysis and were found to be mycoplasma-free in 2017.

2.4.3. Limit of Detection Studies

2.4.3.1 Cell Counting

OVCAR-8-RFP cells as well as cells sourced from murine vaginal lavages were separately counted using a K2 Cellometer (Nexcelom, Lawrence, MA) and concentrated to a final concentration of 10,000 cells/μL in deionized water. RFP-tagged cells were spiked into healthy cell mixtures at 1% and 10% for detection. Fluorescent images were taken using a 660 nm filter to quantify the number of OVCAR-8-RFP cells present in the lavage samples.

2.4.3.2 Fluorescence-activated cell sorting (FACS)

Cells obtained from murine vaginal lavages of healthy mice were obtained and counted using a Cellometer K2 cell counter (Nexcelom, Lawrence, MA) to obtain quantitative values for observed leukocytes and cornified epithelial cells. Standard solutions containing 1×10^6 cells for each condition were prepared in PBS. Additionally, OVCAR-8-RFP cells were trypsinized, resuspended in medium and subsequently counted using a Cellometer K2 cell counter. Spiked lavage samples containing 0%, 0.1%, 1%, 10% and 100% OVCAR-8-RFP cells were prepared in PBS with a final

volume of 500 µL. Flow cytometry was used to measure the percentage of OVCAR-8-RFP (Cytoflex, Brea, CA). Samples comprised of 100% murine lavage cells (negative control) and 100% OVCAR-8-RFP cells (positive control) were used to set up the gates.

2.4.4. *In Vivo* Murine Xenograft Study

$5x10^6$ OVCAR-8-RFP cells suspended in PBS were injected intraperitoneally into NCr *nu/nu* athymic female mice (N=5) aged 10 to 12 weeks (Taconic, Rensselaer, NY). Tumor burden was monitored on a weekly basis using a Xenogen IVIS® Spectrum *In Vivo* Imaging System (PerkinElmer, Waltham, MA). Mice were also given weekly vaginal lavages using 200 µL of sterile PBS throughout the study to collect cells from the local microenvironment of the reproductive organs as described by McLean *et. al*.[35] Cells sourced from murine vaginal lavages were counted using a K2 Cellometer (Nexcelom, Lawrence, MA) by pipetting 20 µL of the sample into disposable counting chambers for imaging. Brightfield images were taken of each sample for accurate counts of leukocytes and epithelial cornified cells present which were used to calculate the concentration of the lavage samples using FCS Express software (De Novo). Fluorescent images were also taken using a 660 nm filter to determine if OVCAR-8-RFP cells were present in murine samples. All lavages were spun down at 150 rcf for five minutes to remove PBS as it has been shown to suppress MALDI-TOF MS ionization.[21] This initial centrifugation step also removes mucous and mucus-associated proteins, such as mucin. Cells were then normalized to 10,000 cells/µL using DI water and stored at -80°C following collection. Upon addition of DI water, cells underwent osmotic stress and lysed, which removes the need for a wash step as all remaining proteins will be in solution. This lysing step prior to analysis also allows for proteins or other similarly sized molecules to be detected via MALDI-TOF MS. A second murine study was completed with N=3 with identical conditions that ended in its seventh week, with the only exception being the lack of weekly IVIS imaging.

Tumor burden was monitored using a Xenogen IVIS® Spectrum *In Vivo* Imaging System (PerkinElmer, Waltham, MA) as described by Lewellen *et al.* Imaging was done using an exposure time of one second, an Fstop of two, and an excitation and emission wavelength of 535 and 620 nm, respectively.[36]

Mice were housed in facilities managed by the Biological Resources Laboratory at UIC and were provided food and water *ad libitum*. All animals were humanely treated in accordance with the Animal Care and Use Committee guidelines at UIC using Protocol #17-174. After two months of tumor progression, all animals were humanely sacrificed followed by collection of tumors and reproductive organs.

Vaginal lavage samples were also collected using 200 µL of sterile PBS of Black 6 age-matched mice (N=9) with NASH for comparative purposes to our ovarian cancer study.

2.4.5. MALDI-TOF MS of Murine Vaginal Lavage Samples

Frozen lavage suspensions were thawed on ice and diluted to 5,000 cells/µL using deionized water. Equal volumes of lavage samples and a 20 mg/mL sinapic acid matrix solution (Sigma Aldrich, St. Louis, MO) in 30/70 ACN/H_2O with 0.1% TFA were mixed together for a final concentration of 2,500 cells/µL. Samples were placed on ice for ten minutes and 1.5 µL of each sample was spotted onto a 384- well ground steel MALDI target plate with 24 technical replicates per lavage with Protein Standard I (Bruker Daltonics, Billerica, MA) used as a calibrant. This procedure was previously optimized and described in depth in Petukhova *et. al.*[21] An Autoflex Speed LRF MALDI-TOF mass spectrometer (Bruker Daltonics, Billerica, MA) was used to acquire mass spectra of murine vaginal lavages samples in positive linear mode with a mass range of 4 to 20 kDa using a laser power of 75%, a laser width of 3 (medium) and a gain of 18.1x. Protein spectra was acquired using AutoXecute, an automated run function of FlexControl v.3.4 software

(Bruker Daltonics, Billerica, MA). 4,000 laser shots were accumulated in fifty shot increments for each sample using the random walk option. All mass spectra were externally calibrated using Protein Standard I (Bruker Daltonics, Billerica, MA), which had been spotted directly adjacent to each sample spot in a square pattern.

Spectra were pre-processed using FlexAnalysis v. 3.4 (Bruker Daltonics, Billerica, MA) with baseline subtraction (TopHat algorithm) and smoothing (SavitzkyGolay algorithm, width of *m/z* 5 over five cycles). Peak picking was performed using a signal-to-noise threshold of four following processing. Mass spectra were converted to a mzML format and further pre-processed using MALDIquant, an open-source R package, using a standard workflow consisting of steps such as baseline correction and spectra alignment; resulting in a feature matrix comprised of intensity and *m/z* values shown in **Figure 2.17**.[37] Spectral data are publicly available online (ftp://MSV000083628@massive.ucsd.edu).

Import mzML files

↓

Square Root Transformation and
Savitzky-Golay Smoothing

↓

SNIP Baseline Correction and
Total-Ion-Current Calibration

↓

Align Spectra Using
Lowess Warping Method

↓

Peak Detection Using
MAD Algorithm and SNR of 4

↓

Peak Binning and Filtering

↓

Feature Intensity Matrix
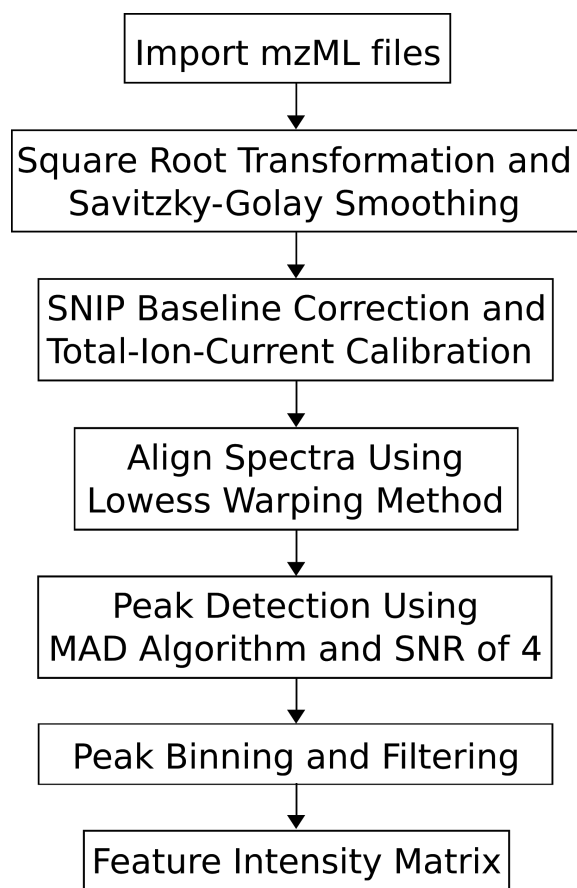
Figure 2.17. Pre-processing workflow using the MALDIquant package in R. All mzML files were uploaded using the MALDIquant package and batch processed using the outlined parameters with a signal-to-noise ratio (SNR) of 4, resulting in a feature matrix that consists of feature peaks and their corresponding intensity values.

2.4.6. Statistical Analysis

In order to search for features that were differentially expressed throughout the longitudinal sampling points in every mouse, a Wilcoxon rank-sum test was applied, using the abundances of each feature, to assess whether the abundance differences between all pairs of days within one mouse were statistically significant. The Wilcoxon rank-sum test was used due to the fact that very few assumptions are made regarding the distribution of the data. To account for multiple hypothesis testing, a Bonferroni-correction was also applied to the p-value of each test followed by the application of threshold of 0.01 to the corrected p-value of each test. Source code is available online (https://github.com/mwang87/ometa_mousemaldi).

2.4.7. Bottom-Up Proteomics

A Bradford assay was performed on a pooled murine lavage to ascertain protein concentration and was found to be 97 µg/mL. Due to relatively low sample volume of all murine lavage samples, it was determined that this value would be a good approximation concentration for all lavages. Samples were centrifuged using an Amicon Ultra-0.5 Centrifugal Filter Unit (MilliporeSigma, Burlington, MA) to collect only proteins under 30 kDa for analysis. Samples were then digested with Lys-C, an enzyme that cleaves at the C-terminus of lysine residues. Following digestion, samples were desalted and cleaned up with a C_{18} ZipTip (MilliporeSigma, Burlington, MA) followed by analysis with a qExactive mass spectrometer (Thermo Fisher Scientific, Waltham, MA) coupled with an Agilent 1260 Infinity nanoLC (Agilent Technologies, Santa Clara, CA). Peptide fragments were separated over a 60 minute gradient (5-25% B over 40 minutes and 25-60% B over 20 minutes) with solvent A being 0.1% formic acid and solvent B being acetonitrile with 0.1% formic acid. This was originally done and optimized with a healthy murine lavage. Most recently, a murine lavage from a mouse with late-stage ovarian cancer was run using the same procedure. Proteins were identified based on at least two unique fragments using Proteome Discoverer 2.2 and the UniProt *Mus musculus* (house mouse) database.

2.4.8. Human Sample Optimization

A total of 54 tampon samples were obtained from the Godwin Lab at the University of Kansas and stored at -70°C; all sample details are outlined in **Table 2.3**. A series of optimization experiments were performed to ensure proper analysis of these samples. A control tampon, previously streaked with murine blood and frozen at -80°C, was cut using scissors, razor blades and scalpels. The latter two were most effective but it was decided to move forward with the scalpel due to additional user control of the blade. In an attempt to most efficiently extract the biological samples from the cotton tampon matrix, both manual and centrifugal compression was attempted. Centrifugation was found to have the best overall average recovery and reproducibility. A

centrifuge speed of 2,000 rcf for 30 minutes was chosen in order to recover the liquid from the matrix without lysing the red blood cells. In order to properly filter out any cotton fibers or larger biological particles (i.e. clots or mucus) from the proteins, a variety of cell strainers and filters were used throughout the centrifugation steps. Amicon Ultra 30k centrifugal filter units were the most effective and were able to trap blood within the filter.

Table 2.3. INVENTORY OF HUMAN TAMPON SAMPLES OBTAINED FROM FEMALE PATIENTS PRIOR TO DEBULKING SURGERY, WHICH INCLUDED EIGHT SAMPLES FROM WOMEN DIAGNOSED WITH OVARIAN CANCER (BOLDED)

Sample #	Primary Cancer	Diagnosis
1	Endometrial	Endometrial adenocarcinoma, FIGO II
2	Benign	Adenomyosis and leiomyoma
3	Benign	Leiomyomata and adenomyosis
4	Benign	Leiomyoma, Multiple large, hemorrhagic, cystic corpora lutea bilaterally
5	Endometrial	Endometrial adenocarcinoma, FIGO II
6	Uterine	Squamous cell carcinoma
7	Benign	Leiomyomas
8	Endometrial	Endometrioid adenocarcinoma, FIGO I
9	Endometrial	Endometrioid adenocarcinoma, FIGO I
10	Benign	Disordered proliferative endometrium, Bilateral endosalpingiosis
11	Endometrial	Stage IVB endometrioid adenocarcinoma of the uterus
12	Endometrial	FIGO I endometrial adenocarcinoma
13	Benign	Cervix: Multiple small Nabothian cysts, Endometrium: Atrophy and endometrial polyp, Myometrium: Multiple leiomyomata
14	Benign	Ovary: Mucinous cystadenoma, Endometrium: Early proliferative phase; negative for hyperplasia or malignancy
15	**Ovarian**	Stage IIIC bilateral high grade serous ovarian carcinoma
16	**Ovarian**	Stage IIIC high grade serous carcinoma of the R ovary
17	Endometrial	Clear cell high grade endometrial carcinoma
18	Endometrial	Microscopic foci of endometrioid adenocarcinoma, Stage IA, endometrial cancer, FIGO I
19	Endometrial	Endometrioid adenocarcinoma, FIGO I
20	Endometrial	Stage IA endometrioid adenocarcinoma of the uterus, FIGO I
21	**Ovarian**	Granulosa cell tumor of the left ovary, grade 2, Stage Ia
22	Endometrial	Stage IA endometrioid adenocarcinoma of the uterus, FIGO I

23	Uterine	Stage IIIC2 Serous adenocarcinoma of the uterus
24	Endometrial	Stage IA endometrioid adenocarcinoma of the uterus, FIGO I
25	Benign	Endometrium: Disordered proliferative endometrium; Myometrium: Leiomyomata and focal adenomyosis.
26	Endometrial	Endometrioid adenosquamous carcinoma, arising in the lower uterine segment
27	Benign	Large thick walled cystic adnexal mass
28	**Ovarian**	Both ovaries: Serous tumor, borderline type | Endometrium: Early proliferative phase endometrium
29	Endometrial	Endometrioid adenocarcinoma, FIGO II, myometrial invasion
30	Endometrial	Endometrial adenocarcinoma, FIGO II, myometrial invasion | Myometrium: Leiomyomata
31	Benign	Inactive endometrium, Endosalpingiosis involving serosa, Endometriotic cyst
32	Benign	Inactive endometrium | Myometrium: Leiomyomata including a cellular leiomyoma and focal adenomyosis | Peritubal cyst in left fallopian tube
33	Endometrial	Endometrium: Poorly differentiated endometrial carcinoma, endometrioid type, FIGO III, nuclear grade 3 | Myometrium: Superficial involvement by endometrioid adenocarcinoma, vascular invasion | Parametrium: right side vascular invasion
34	Endometrial	Uterus: Endometrial adenocarcinoma, FIGO I, myometrial invasion | Leiomyoma, serosa endometriosis | Right Ovary: Adult granulosa cell tumor
35	**Ovarian**	Ovary: Clear cell carcinoma | Myometrium: Leiomyomata | Parametrium: Endometriosis | Cul-de-sac peritoneum: metastatic clear cell carcinoma
36	Benign	Left sided paratubal cyst: Benign multiloculated cyst | Endometrium: Atrophic endometrium | Myometrium: Leiomyomata, with focal calcification and hyalinization | Fallopian tubes: Small paratubal cysts
37	Uterine	Uterosacral nodule: Metastatic adenocarcinoma | Right Ovary: Sex cord-stromal tumor | Myometrium, right parametrium: Involvement by adenocarcinoma, FIGO I, nuclear grade 2
38	Benign	Both ovaries: Benign ovarian cyst | Left Fallopian tube: Paratubal cysts | Endometrium: Endometrial polyp
39	Endometrial	Endometrium and myometrium: Endometrioid adenocarcinoma, FIGO III, myometrial invasion | Leiomyomata with focal involvement by endometrial adenocarcinoma | Left ovary: Benign serous inclusion cysts
40	Uterine	Uterus: Endometrioid adenocarcinoma, FIGO I | Benign endometrial polyp | Leiomyomata
41	Endometrial	Endomyometrium: Endometrioid adenocarcinoma, FIGO II, focal III,

		myometrial and lymphovascular invasion
42	Benign	Cervix: Acute and chronic cervicitis | Myometrium: Leiomyoma | Endometrium: Secretory phase endometrium
43	Endometrial	Endometrium and myometrium: Endometrial adenocarcinoma, FIGO grade 2, myometrial invasion
44	Endometrial	Endometrium: Small focus of residual endometrioid adenocarcinoma, FIGO I | Myometrium: Adenomyosis
45	Benign	Atrophic endometrium | Small leiomyoma | Left Ovary: Serous cystadenoma | Right Ovary: Surface inclusion cysts
46	Endometrial	Endometrium: Endometrioid adenocarcinoma, FIGO II | Myometrium: Hyalinized leiomyoma with calcifications
47	Uterine	Uterine adenosarcoma with sarcomatous overgrowth and heterologous elements including chondrosarcoma and osteosarcoma
48	**Ovarian**	Left Ovary: Surface and stromal involvement by low-grade serous carcinoma | Uterus: Myometrial involvement by low-grade serous carcinoma
49	**Ovarian**	Right ovary: Carcinosarcoma | Uterus: Serosal involvement by carcinosarcoma | Myometrium: Leiomyomata
50	**Ovarian**	Ovaries: Bilateral high grade papillary serous carcinoma | Myometrium: Metastatic serous carcinoma involving the myometrium and serosal surface of the uterus, lymphovascular invasion
51	Benign	Ovary: Massive edema | Endometrium: Inactive endometrium | Myometrium: Leiomyoma
52	Benign	Endometrium: Benign proliferative endometrium | Myometrium: Leiomyoma | Ovaries: Follicular cyst
53	Uterine	Uterus: Endometrioid adenocarcinoma, FIGO III, Adenomyosis
54	Unidentified Tampon and Cytobrush	Dx Unknown

2.5. References

1. Siegel, R. L., Miller, K. D. & Jemal, A. Cancer statistics, 2019. *CA Cancer J. Clin.* **69**, 7–34 (2019).

2. Noone, A. M. *et al.* SEER Cancer Statistics Review, 1975-2015, National Cancer Institute. Bethesda, MD. (2018).

3. Torre, L. A. *et al.* Ovarian cancer statistics, 2018. *CA Cancer J. Clin.* **68**, 284–296 (2018).

4. Klinkebiel, D., Zhang, W., Akers, S. N., Odunsi, K. & Karpf, A. R. DNA Methylome Analyses Implicate Fallopian Tube Epithelia as the Origin for High-Grade Serous Ovarian Cancer. *Mol. Cancer Res.* **14**, 787–794 (2016).

5. Labidi-Galy, S. I. *et al.* High grade serous ovarian carcinomas originate in the fallopian tube. *Nat. Commun.* **8**, 1093 (2017).

6. van Nagell, J. R., Jr *et al.* The efficacy of transvaginal sonographic screening in asymptomatic women at risk for ovarian cancer. *Gynecol. Oncol.* **77**, 350–356 (2000).

7. Buys, S. S. *et al.* Effect of screening on ovarian cancer mortality: the Prostate, Lung, Colorectal and Ovarian (PLCO) Cancer Screening Randomized Controlled Trial. *JAMA* **305**, 2295–2303 (2011).

8. Kinde, I. *et al.* Evaluation of DNA from the Papanicolaou test to detect ovarian and endometrial cancers. *Sci. Transl. Med.* **5**, 167ra4 (2013).

9. Bakkum-Gamez, J. N. *et al.* Detection of endometrial cancer via molecular analysis of DNA collected with vaginal tampons. *Gynecol. Oncol.* **137**, 14–22 (2015).

10. Erickson, B. K. *et al.* Detection of somatic TP53 mutations in tampons of patients with high-grade serous ovarian cancer. *Obstet. Gynecol.* **124**, 881–885 (2014).

11. Shintaku, M., Taniguchi, H., Yamamoto, Y., Kono, F. & Sumitomo, M. Detection of tumor cells of serous tubal intraepithelial carcinoma (STIC) in cervical smears and rapid development of the ovarian involvement: A case report. *Diagn. Cytopathol.* **46**, 945–949

(2018).

12. Boylan, K. L. *et al.* A feasibility study to identify proteins in the residual Pap test fluid of women with normal cytology by mass spectrometry-based proteomics. *Clin. Proteomics* **11**, 30 (2014).

13. Balog, J. *et al.* Intraoperative tissue identification using rapid evaporative ionization mass spectrometry. *Sci. Transl. Med.* **5**, 194ra93 (2013).

14. Zhang, J. *et al.* Nondestructive tissue analysis for ex vivo and in vivo cancer diagnosis using a handheld mass spectrometry system. *Sci. Transl. Med.* **9**, (2017).

15. Fenselau, C. & Demirev, P. A. Characterization of intact microorganisms by MALDI mass spectrometry. *Mass Spectrom. Rev.* **20**, 157–171 (2001).

16. Croxatto, A., Prod'hom, G. & Greub, G. Applications of MALDI-TOF mass spectrometry in clinical diagnostic microbiology. *FEMS Microbiol. Rev.* **36**, 380–407 (2012).

17. Rodrigo, M. A. M. *et al.* MALDI-TOF MS as evolving cancer diagnostic tool: a review. *J. Pharm. Biomed. Anal.* **95**, 245–255 (2014).

18. Maier, T. & Kostrzewa, M. Spectrophotometric identification of microbe subspecies. *US Patent* (2011).

19. Munteanu, B. & Hopf, C. Emergence of whole-cell MALDI-MS biotyping for high-throughput bioanalysis of mammalian cells? *Bioanalysis* **5**, 885–893 (2013).

20. Munteanu, B. & Hopf, C. Whole/Intact Cell MALDI MS Biotyping in Mammalian Cell Analysis. in *Advances in MALDI and Laser-Induced Soft Ionization Mass Spectrometry* (ed. Cramer, R.) 249–262 (Springer International Publishing, 2016).

21. Petukhova, V. Z. *et al.* Whole Cell MALDI Fingerprinting Is a Robust Tool for Differential Profiling of Two-Component Mammalian Cell Mixtures. *J. Am. Soc. Mass Spectrom.* **30**, 344–354 (2019).

22. Domcke, S., Sinha, R., Levine, D. A., Sander, C. & Schultz, N. Evaluating cell lines as tumour models by comparison of genomic profiles. *Nat. Commun.* **4**, 2126 (2013).

23. Olive, K. P. *et al.* Mutant p53 gain of function in two mouse models of Li-Fraumeni syndrome. *Cell* **119**, 847–860 (2004).

24. Quartuccio, S. M. *et al.* Mutant p53 expression in fallopian tube epithelium drives cell migration. *Int. J. Cancer* **137**, 1528–1538 (2015).

25. Ahmed, N. & Stenvers, K. L. Getting to know ovarian cancer ascites: opportunities for targeted therapy-based translational research. *Front. Oncol.* **3**, 256 (2013).

26. Wan, K. X., Vidavsky, I. & Gross, M. L. Comparing similar spectra: from similarity index to spectral contrast angle. *J. Am. Soc. Mass Spectrom.* **13**, 85–88 (2002).

27. Dasari, S. *et al.* Comprehensive Proteomic Analysis of Human Cervical−Vaginal Fluid. *Journal of Proteome Research* **6**, 1258–1268 (2007).

28. Tang, L.-J. *et al.* Proteomic analysis of human cervical-vaginal fluids. *J. Proteome Res.* **6**, 2874–2883 (2007).

29. Shaw, J. L. V., Smith, C. R. & Diamandis, E. P. Proteomic analysis of human cervico-vaginal fluid. *J. Proteome Res.* **6**, 2859–2865 (2007).

30. Panicker, G., Ye, Y., Wang, D. & Unger, E. R. Characterization of the Human Cervical Mucous Proteome. *Clin. Proteomics* **6**, 18–28 (2010).

31. Soleilhavoup, C. *et al.* Proteomes of the Female Genital Tract During the Oestrous Cycle. *Mol. Cell. Proteomics* **15**, 93–108 (2016).

32. UniProt Consortium. UniProt: a worldwide hub of protein knowledge. *Nucleic Acids Res.* **47**, D506–D515 (2019).

33. Russo, A. *et al.* PTEN loss in the fallopian tube induces hyperplasia and ovarian tumor formation. *Oncogene* **37**, 1976–1990 (2018).

34. Hardy, L. R. *et al.* Proteomic analysis reveals a role for PAX8 in peritoneal colonization of high grade serous ovarian cancer that can be targeted with micelle encapsulated thiostrepton. *Oncogene* **38**, 6003–6016 (2019).

35. McLean, A. C., Valenzuela, N., Fai, S. & Bennett, S. A. L. Performing vaginal lavage,

crystal violet staining, and vaginal cytological evaluation for mouse estrous cycle staging identification. *J. Vis. Exp.* e4389 (2012).

36. Lewellen, K. A., Metzinger, M. N., Liu, Y. & Stack, M. S. Quantitation of Intra-peritoneal Ovarian Cancer Metastasis. *J. Vis. Exp.* (2016). doi:10.3791/53316

37. Gibb, S. & Strimmer, K. MALDIquant: a versatile R package for the analysis of mass spectrometry data. *Bioinformatics* **28**, 2270–2271 (2012).

Chapter 3

Small Molecule Interactions from the Cheese Microbiota: Exploration of Bacterial and

Fungal-Derived Antimicrobials

3.1. Introduction

3.1.1. Importance of Antimicrobial Research

Microorganisms, such as bacteria and fungi, are implicated in a wide variety of ailments ranging from food-borne illnesses to blood-borne infections.[1,2] Treatment of these diseases is often complicated by antimicrobial resistance (AMR), such as is the case with infections like methicillin-resistant *Staphylococcus aureus* (MRSA) and tuberculosis. AMR infections result in poorer patient prognosis, even when following prescribed courses of antibiotic or antifungal medications.[3,4] There are several contributing factors to AMR; the primary component being the overuse and prescription of antimicrobials that aren't necessary to combat infections. This over prescription creates a selective pressure for the microorganisms to mutate and become resistant (**Figure 3.1**).[5]

Over-Prescription of Antimicrobials **Unnecessary Use of Antimicrobials in Agriculture** **Poor Sanitation Practices**
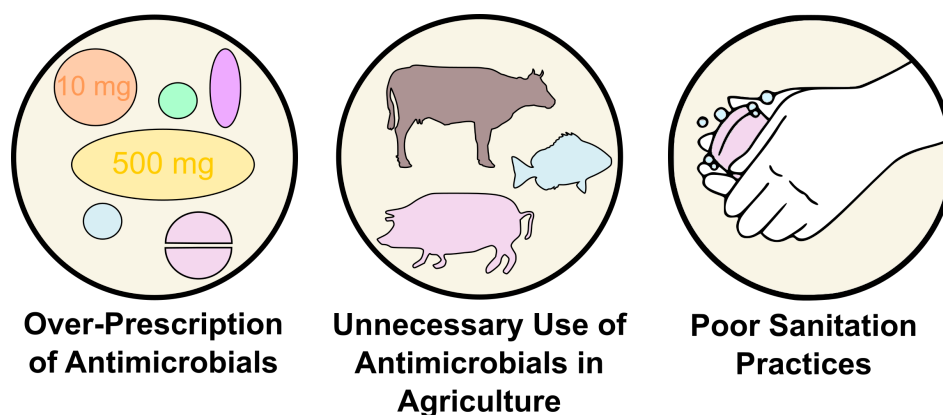
Figure 3.1. Common causes for antimicrobial resistance including over-prescription of antimicrobials for infections, poor sanitary conditions including the unnecessary use of antibiotics in feedstock as well as hand-washing and general hygiene. *Figure adapted from the CDC.[6]

Additionally, AMR can be caused by patients not complying with the prescribed regimen of antimicrobials as well as lack of efficient laboratory diagnostic tests, which could lead to the prescription of a broad-spectrum antimicrobials in lieu of species-targeted medications. AMR is one of the most pressing public health issues with close to two million infections and an expected 23,000 deaths, in the US alone, attributed to antimicrobial-resistant microorganisms each year.[7]

In 2018 alone, the Center for Disease Control (CDC) invested 241 million dollars in the United States and over 11 million dollars internationally to address AMR, which includes research in areas such as detection, prevention and containment.[8] Additionally, hospitals have begun implementing oversight programs to those prescribing antimicrobials, specifically antibiotics, with built-in checkpoints including preauthorization requirements to combat AMR.[9]

Increasing public education and decreasing prescription rates for antimicrobials, while important, are only a part of a larger strategy to guarantee that antimicrobials remain an effective lifesaving tool. The development of novel antibiotics and antifungals to help combat these increasingly resistant microorganisms is very important. Privately owned companies, including Merck and Pfizer, have made significant contributions to actively combating AMR by continuing to invest funds in the development of new antimicrobials such as Noxafil (antifungal) and Zithromax (antibiotic). However, with the ability of pathogenic microorganisms to rapidly become resistant to approved therapeutics, the need for antimicrobial research in academia and the private sector is greater now more than ever.

3.1.2. The Rise of Antibiotic-Resistant Bacteria

The golden age of antibiotic drug discovery was initially kick-started by the accidental discovery of penicillin in 1928 when Sir Alexander Fleming noted that mold contamination on culture plates of *Staphylococcus aureus* had elicited growth inhibition during co-culture.[10] Penicillin, a β-lactam SM produced by certain *Penicillium* species, was first used in World War II to treat soldiers with bacterial infections but the success of this was short-lived as penicillin-resistant strains began to emerge in the 1940s.[11] As with penicillin, this is the case with many antibiotics, such as tetracycline and vancomycin; resistant strains are observed to appear shortly after discovery (**Figure 3.2**).
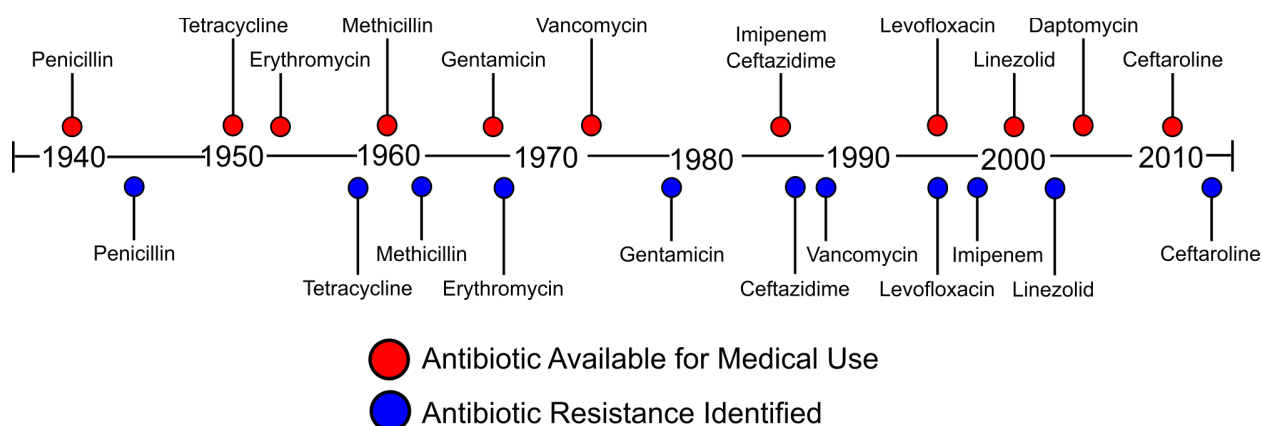
Figure 3.2. Timeline of antibiotic introduction to the medical community compared to when antibiotic resistance was observed *Figure adapted from the CDC.[12]

Bacteria are able to overcome these barriers and become resistant through evolution and horizontal gene transfer, employing mechanisms such as efflux pumps and specialized metabolite degradation, ultimately escaping death.[13] This is quickly becoming a critical issue with many bacteria, such as the ESKAPE pathogens and *Mycobacterium tuberculosis* (tuberculosis), acquiring multidrug resistance which further complicates treatment.

3.1.3. The Need for Novel Antifungal Metabolites

In addition to antibiotics, there is also a pressing need for the discovery of novel antifungal metabolites considering that fungal infections are becoming increasingly present in today's society. These infections have been associated with high rates of mortality as well as other health complications. This is the case with candidiasis caused by *Candida auris*, which is becoming resistant to modern antifungal agents.[2,14] Research of novel antifungal agents from natural sources got off to a promising start in the 1950s with the discovery of nystatin and amphotericin B, both from bacterial origins, and into the late twentieth century with the discovery of the triazoles and echinocandins but has since slowed down due to developmental challenges (**Figure 3.3**).[15] This stagnation in the discovery of novel antifungals and the uptick in antifungal resistance among

invasive fungal infections like candidiasis indicates that there is a significant need for looking more closely at nature for potential drug candidates.
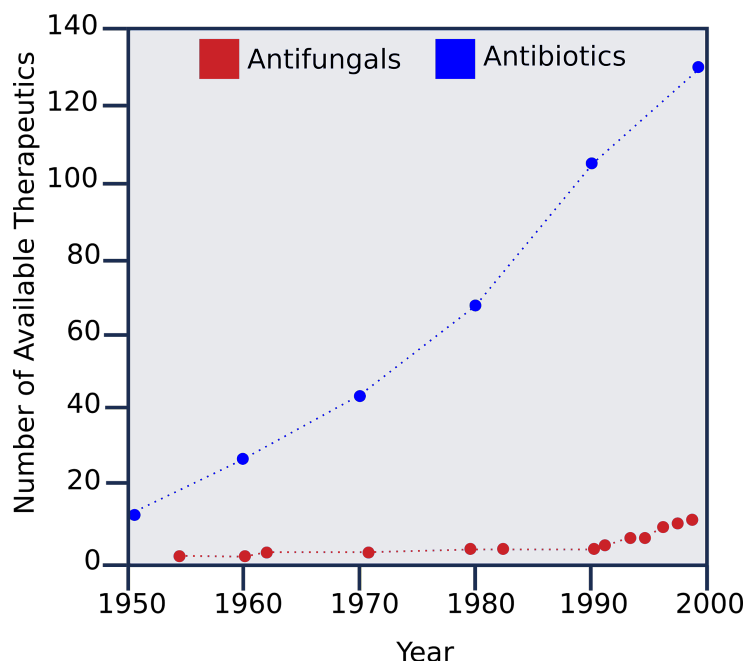

Figure 3.3. Number of FDA-Approved Antimicrobial Agents in the USA in the 20th century. Figure adapted from Ostrosky-Zeichner *et al*.[15]

3.1.4. Looking to the Cheese Microbiome for Novel Antimicrobials

In addition to the synthesis of metabolites that are responsible for the flavor or aroma, the cheese rind microbiota has also been implicated in the production of antimicrobials.[16–18] Based on the ability of this microbial community to synthesize metabolites that can potentially have a significant impact on human health, it is important to further study these chemical interactions *in situ*. Previous research from the Dutton and Wolfe labs have explored the diverse microbial landscape present on cheese rinds and found that cheese rinds are composed of relatively simplified microbial community populations with about ten to twelve microbial species on any given rind.[19,20] This allows for the study of interactions between specific species in a controlled environment, in which the strains are easily cultivated due to their ability to grow on cheese. In particular, the combination of phenotypic screens and analytical chemistry techniques, such as mass

spectrometry (MS) can be used to further probe these interactions between microbial species to better understand their chemistry. This chapter focuses on three separate narratives of antimicrobial research from bacteria and fungi isolated from cheese rinds - one of which focuses on an antifungal metabolite while the other two center on the isolation of antibacterial compounds.

3.2. Results and Discussion

3.2.1. Detection of Antifungal Metabolites from a *Pseudomonas - Candida* Interaction

Phenotypic screens completed in the Dutton Lab at UCSD identified a specific microbial interaction between *Pseudomonas psychrophilia* sp. JB418 and *Candida catenulata sp.* 135E, both isolated from natural cheese rinds. When the two species were grown in co-culture, growth inhibition of the fungus was observed (**Figure 3.4**) which could be due to an antifungal metabolite produced by *Pseudomonas psychrophilia* sp. JB418. In addition to this phenotype, it was also observed that this interaction is species-specific as the bacteria does not inhibit growth of other fungal species including *Geotrichum candidum*, *Penicillium* JBC and *Scopulariopsis* JB370 as shown in **Figure 3.4**. After seeing the specificity in the growth inhibition phenotypic screen, we hypothesized that *Pseudomonas psychrophilia* sp. JB418 was excreting a selective antifungal metabolite, which was contributing to the adverse effects as seen with the growth of *Candida catenulata* 135E when the two were grown in co-culture. Therefore, we chose to isolate the metabolite of interest for structure determination and characterization.
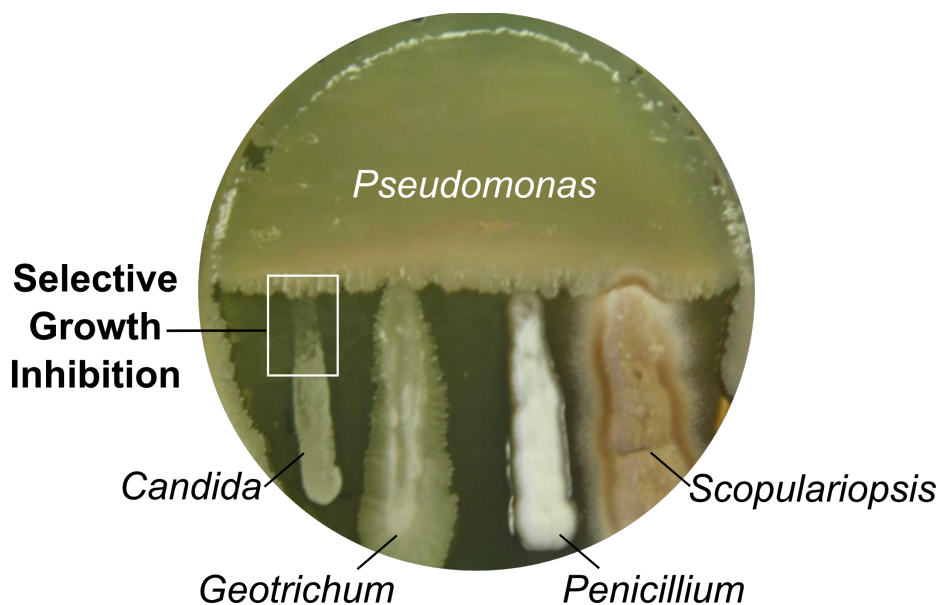
Figure 3.4. Interaction plate between *Pseudomonas psychrophila* sp. JB418 and four fungal species (left to right: *Candida catenulata sp.* 135E, *Geotrichum candidum*, *Penicillium* sp. JBC, *Scopulariopsis* sp. JB370) showing growth inhibition in the interaction between *Pseudomonas* and *Candida*.

3.2.1.1. Use of MALDI-TOF IMS to Visualize Metabolite Distribution

The development of matrix-assisted laser desorption/ionization time-of-flight (MALDI-TOF) imaging mass spectrometry (IMS) in the late 1990s was revolutionary as it allowed for the direct detection of biomolecules, such as proteins and small molecules, on a biological surface.[21] Since its original development in the Caprioli lab, MALDI-TOF IMS has been used for a wide range of applications such as drug distribution and metabolism in mammalian tissue samples to biomolecule distribution in plant tissues.[22,23] Due to the growth inhibition that was previously observed, MALDI-TOF IMS was proposed as the first investigatory technique to determine if any metabolites were shown to be upregulated or highly distributed in the observed zones of inhibition. MALDI-TOF IMS experiments were originally done by a previous undergraduate student in the Sanchez lab to test our hypothesis that *Pseudomonas psychrophila* sp. JB418 excreted an antifungal metabolite in the presence of *Candida catenulata* sp. 135E. Those original experiments identified some potential *m/z* leads, so to test the reproducibility of those signals we performed

additional IMS experiments. All experiments were done using interaction plates between *Pseudomonas psychrophila* sp. JB418 and *Candida catenulata* sp. 135E along with individual controls for both (**Figure 3.5 A**). Experiments were set up in a cross-like formation in an attempt to visualize upregulation of the excreted antifungal metabolite in multiple locations in the interaction zone.
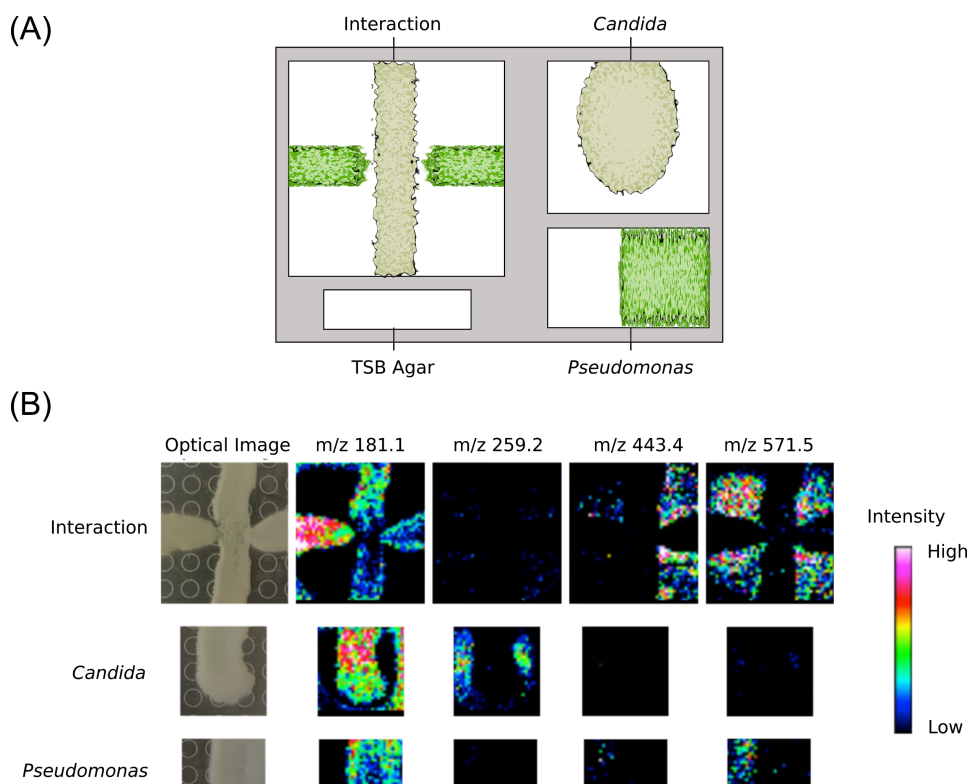

Figure 3.5. MALDI-TOF IMS was performed to visualize spatial distribution of specialized metabolites identified as *m/z* values. (A) Layout of interaction of *Pseudomonas psychrophila* sp. JB418 and *Candida catenulata* sp. 135E and controls on MALDI target plate. (B) Imaging data of *Pseudomonas psychrophila* sp. JB418, *Candida catenulata* sp. 135E and their interaction showing unique *m/z* values for each condition.

While subsequent attempts at MALDI-TOF imaging did not replicate the initial findings in terms of *m/z* values and their distributions, a multitude of signals were found to be specific to the fungus, bacteria or a paired co-culture (**Figure 3.5 B**). These experiments showed that *Pseudomonas psychrophilia* sp. JB418 is capable of producing many metabolites which can be further

investigated for antifungal capabilities. However, the observed signals, including those that are specific to the interaction and *Pseudomonas psychrophilia* sp. JB418 were not shown to colocalize with the zone of inhibition; therefore, it was decided to move towards a bioactivity-guided extraction approach.

3.2.1.2. Bioactivity Guided Fractionation of Specialized Metabolites Produced by *Pseudomonas psychrophila* sp. JB418
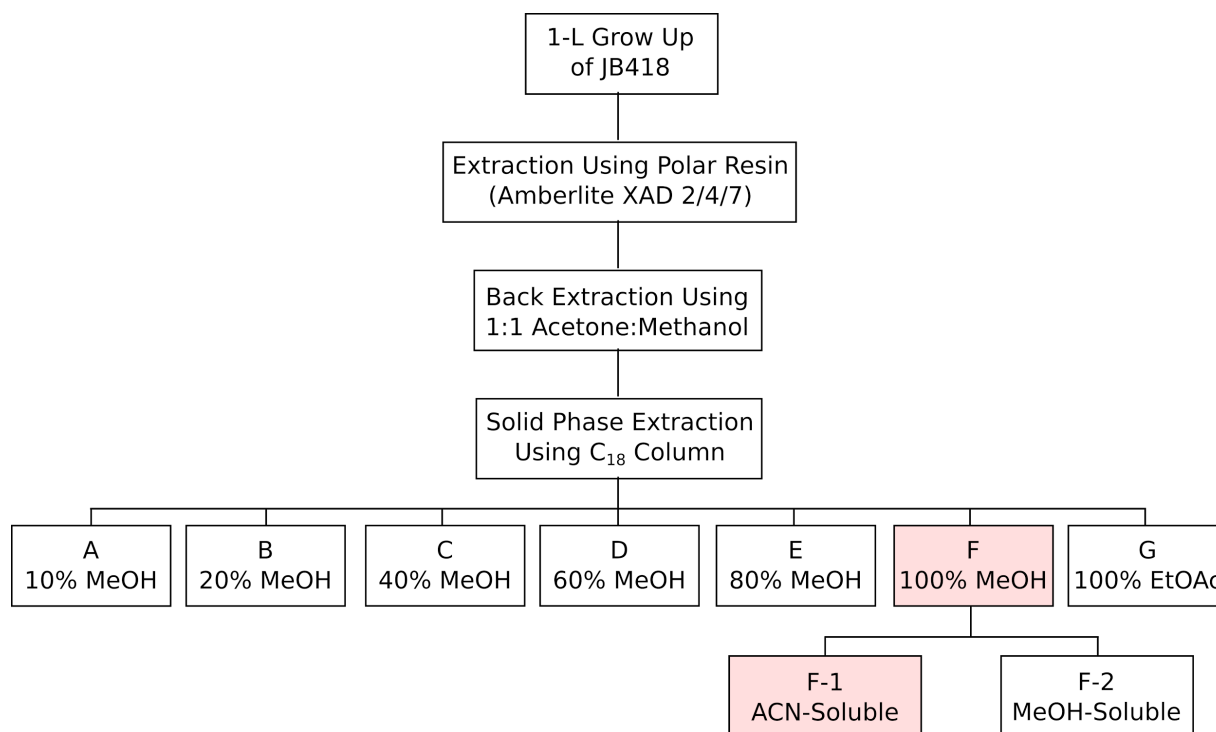

Figure 3.6. Isolation scheme for the antifungal metabolite produced by *Pseudomonas psychrophilia* sp. JB418

In order to further investigate the metabolites produced by *Pseudomonas psychrophilia* sp. JB418 with the use of bioassays, large 1-L fermentation of the bacteria were extracted using polar resin and further separated into seven fractions using solid phase extraction (SPE) (**Figure 3.6**). Additionally, the sample was purified through trituration, a solvent-based separatory process in which certain metabolites are either soluble or insoluble, using acetonitrile (ACN) - a purification

step which was serendipitously discovered while performing sample preparation for NMR experiments.
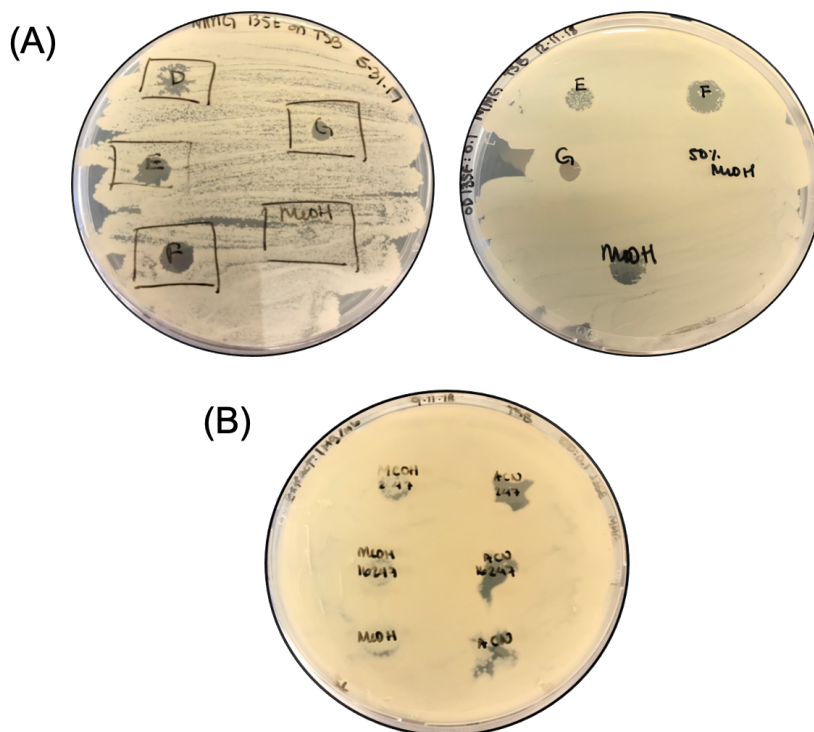

Figure 3.7. Bioactivity plates of *Candida catenulata* sp. 135E. (A) Reproducible bioactivity in Fraction F across multiple bacterial extractions. (B) Bioactivity shown in the subfraction of Fraction F that was found to be soluble in ACN following trituration.

Throughout the separation process, bioactivity plates were made by plating *Candida catenulata* sp. 135E at an optical density of 0.1 and directly spotting small volumes of extracts onto the fungus. Bioactivity plates were repeated to show that Fraction F was reproducibly bioactive and had the largest zone of growth inhibition of any SPE fraction (**Figure 3.7 A**). Additionally, once it was determined that trituration with ACN was able to serve as a purification step, bioactivity plates were generated using the same procedure with the subfractions, which showed that the ACN-soluble subfraction yielded reproducible bioactivity against *Candida catenulata* sp. 135E (**Fraction 3.7 B**).

In further attempts to isolate the compound, a well plate assay was performed in which Fraction F was further separated into 74 subfractions using high-performance liquid chromatography (HPLC), with time-based fraction collection, to form a peak library.[24] Upon further investigation of the UV-vis chromatogram many peaks were observed, which leads to the conclusion that Fraction F is comprised of multiple specialized metabolites from *Pseudomonas psychrophila* sp. JB418 (**Figure 3.8 A-B**). However, due to the fact that metabolites can co-elute, it is plausible that each peak could represent multiple bacterial compounds. Fractions were then spotted onto a 96-well agar plate which had been previously inoculated with *Candida catenulata* sp. 135E. After 24 hours, it was shown that four subfractions had the ability to inhibit the growth of *Candida catenulata* sp. 135E (**Figure 3.8 C**).

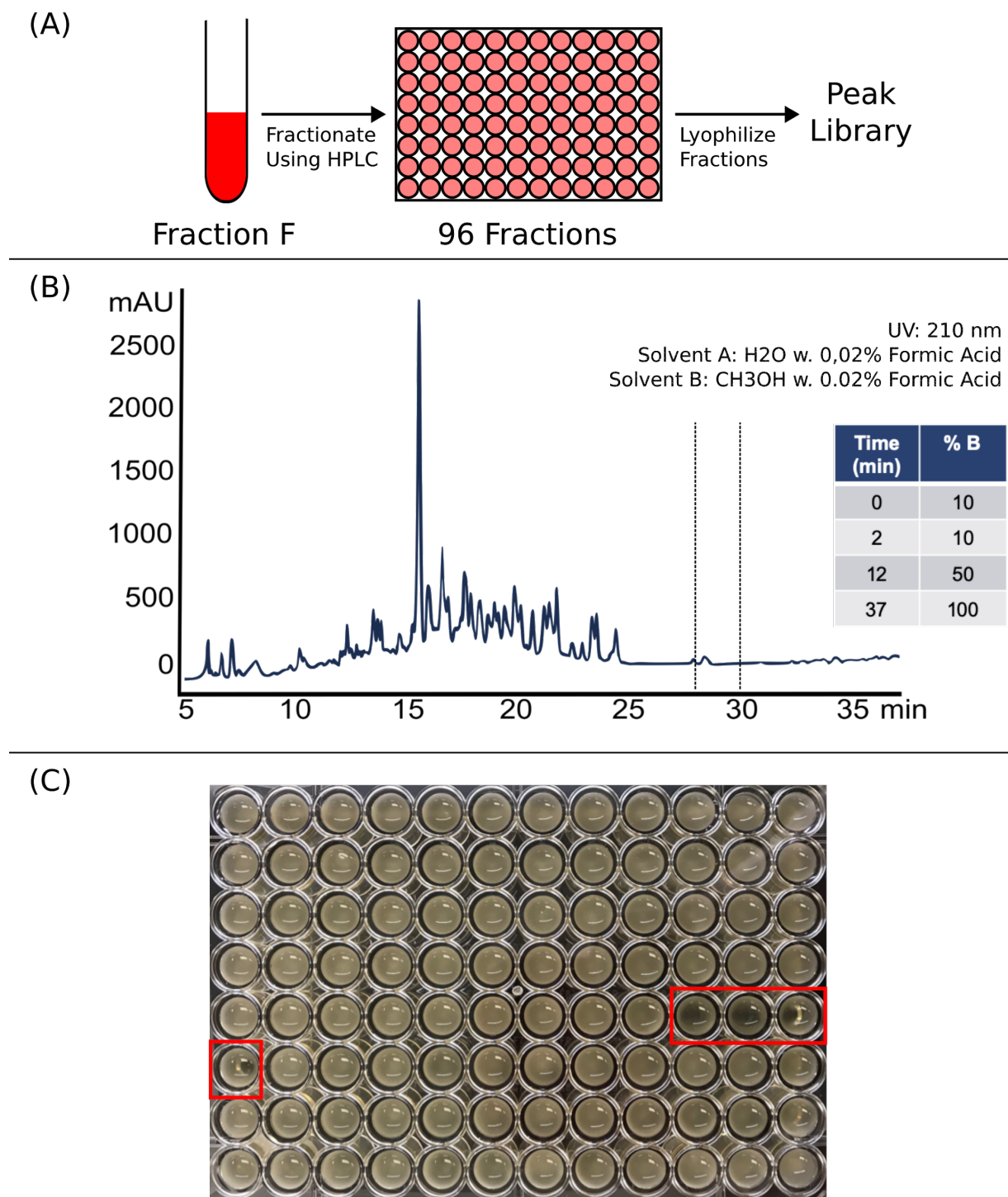**Figure 3.8.** (A) Well plate assay workflow to acquire peak library (B) HPLC chromatogram of polar metabolites extracted from *Pseudomonas psychrophila* sp. JB418 in which fractions were collected every 30 seconds along the gradient with bioactive fractions shown within dotted lines. (C) Bioactivity results from well plate assay showing four fractions with growth inhibition against *Candida catenulata* sp. 135E.

3.2.1.3. Mass Spectrometry Analysis of Bioactive Subfractions

In the UV-vis chromatogram obtained during the HPLC run, the four bioactive fractions showed very little absorbance at 210 nm or any other measured wavelength, including 254 and 600 nm, indicating that the compound(s) does not have high levels of conjugation or any other discernible features that are normally detected by UV-vis spectroscopy (**Figure 3.9 A**). MALDI-TOF MS dried droplet analysis was used to take a closer look at the subfractions found to be bioactive from the well plate assay. After subtraction of the matrix peaks, *m/z* 300.2 and 695.6 were found to be shared between the bioactive samples - *m/z* 693.6 was also present in the fourth sample which is likely to be an analog of 695.6 due to the difference of two Daltons (**Figure 3.9 B**). While the MALDI-TOF MS provided an idea of masses that would be worth investigating, it was still necessary to gather additional analytical data to determine the structure and identity of the antifungal metabolite produced by *Pseudomonas psychrophila* sp. JB418.
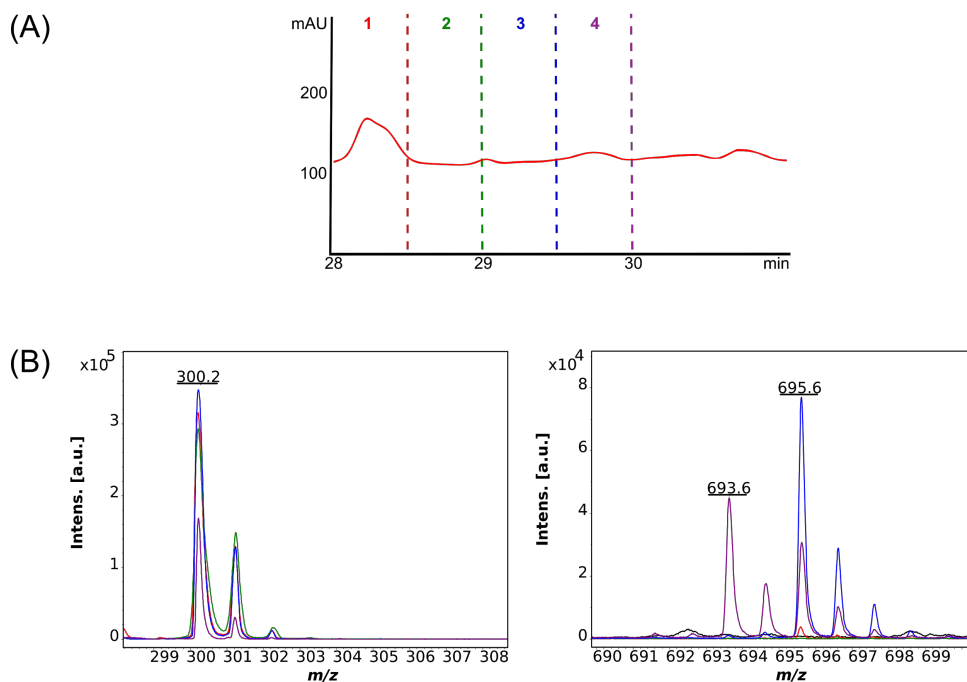

Figure 3.9. (A) UV-vis chromatogram trace of bioactive subfractions from well plate assay at 210 nm (B) *m/z* peaks shared between the four fractions using MALDI-TOF MS

Following MALDI-TOF MS analysis, samples were submitted for tandem MS analysis using an electrospray ionization (ESI) quadrupole time-of flight (qTOF) MS instrument. This type of analysis allows for fragmentation data to be obtained, which can help piece together the molecular structure through common ion losses. Fragmentation data was obtained from two of the bioactive subfractions (F1 and F3) following separation by an ACN gradient using a data dependent acquisition (DDA) method with the top three *m/z* values being fragmented per MS[1] spectrum at three different collision energies. While fragmentation data was obtained, values were not consistent between the two instruments (MALDI-TOF MS and ESI-qTOF MS). Upon closer investigation of the total ion chromatogram (TIC) and extracted ion chromatograms (EIC) for each sample, the *m/z* values observed in the MALDI-TOF spectra were not present, inclusive of the protonated and sodiated forms (**Figure 3.10**). We hypothesize that this could be caused by the molecule(s) of interest not ionizing well using either of the two ionization methods or differentially ionizing between sources.
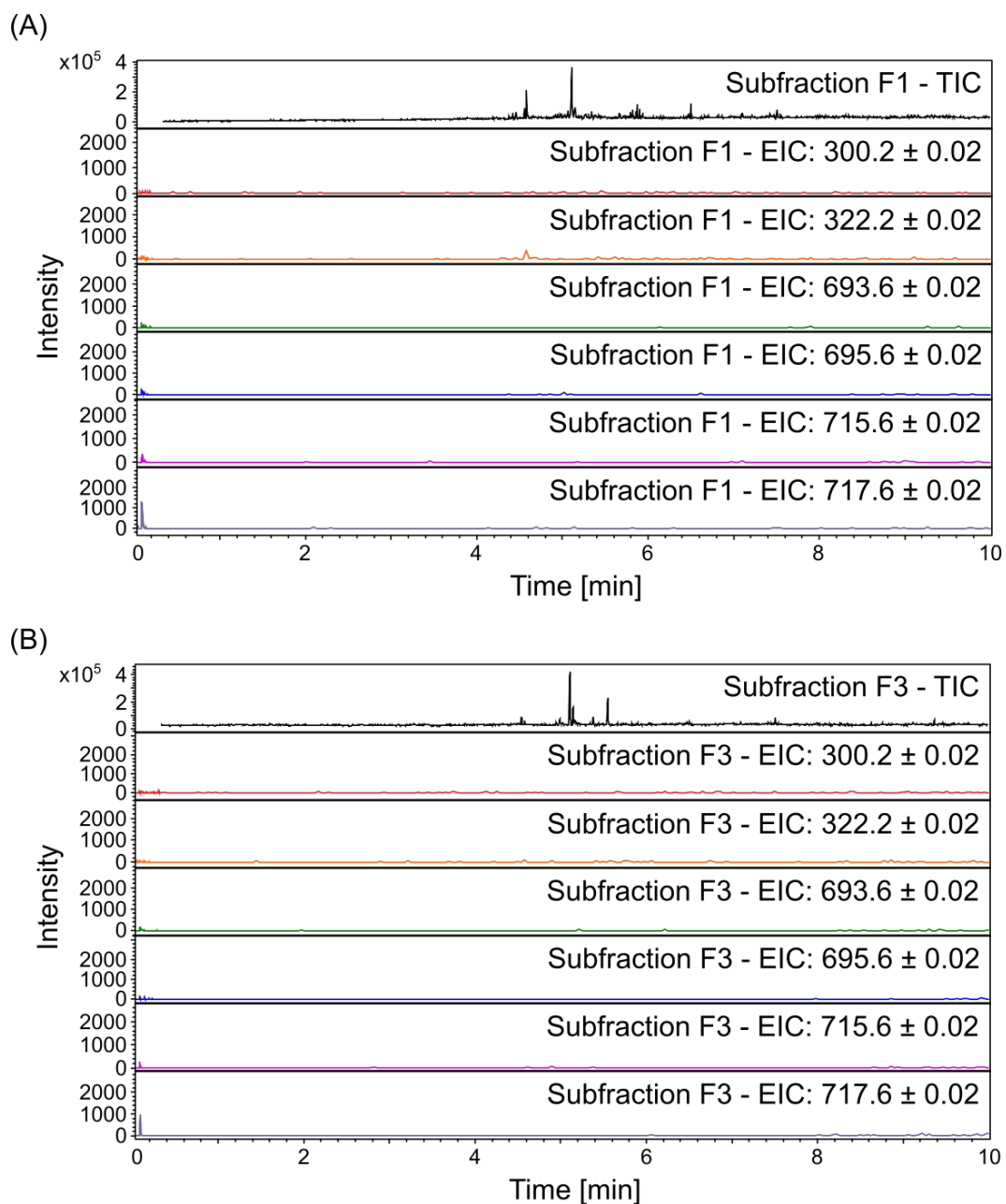
Figure 3.10. Fragmentation data from bioactive subfractions from the well plate assay containing TIC and EIC spectra for protonated and sodiated *m/z* values from MALDI-TOF analysis for (A) Subfraction F1 and (B) Subfraction F3.

3.2.1.4. NMR Analysis of Bioactive Subfraction Purified Via Trituration

In addition to MS analysis, the bioactive subfraction of Fraction F that was found to be soluble in

ACN was further investigated using NMR to gain more information about the molecule's structure.

A full 2D data set of NMR spectra was collected with assistance from the Structural Biology Core Facility at UIC, in which the sample appeared to be relatively pure (**Figures 3.11 - 3.15**). Based on the proton spectrum, no aromatic peaks were observed with evidence supporting the presence of methyl groups as well as oxygen and nitrogen atoms within the structure (**Figure 3.11**). However, upon looking at the heteronuclear experiments such as HSQC and HMBC, which provides information regarding the direct connection of a hydrogen and carbon atom or a three to four bond correlation, respectively, there were very few correlations observed (**Figures 3.14 - 3.15**). This would indicate that there are a significant number of quaternary carbons in the structure and that the lack of multiple bond correlations would make this molecule extremely difficult to assign via NMR. However, the spectra are able to provide clues as to what compound classes can be excluded from analysis including peptides, which are also known to ionize well, and alkaloids.

Figure 3.11. ^{1}H NMR spectrum of antifungal metabolite, 900 MHz, CDCl$_3$

Figure 3.12. ^{13}C NMR spectrum of antifungal metabolite, 900 MHz, CDCl$_3$

Figure 3.13. COSY NMR spectrum of antifungal metabolite, 900 MHz, CDCl$_3$
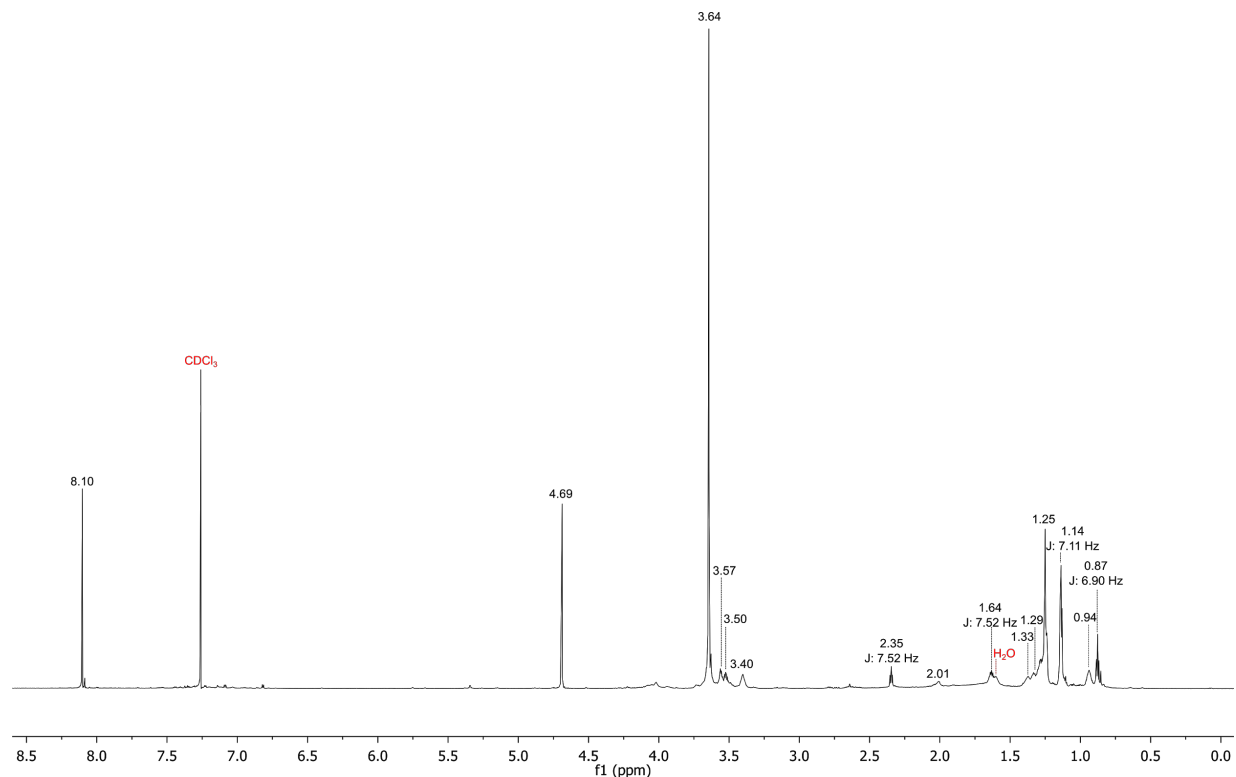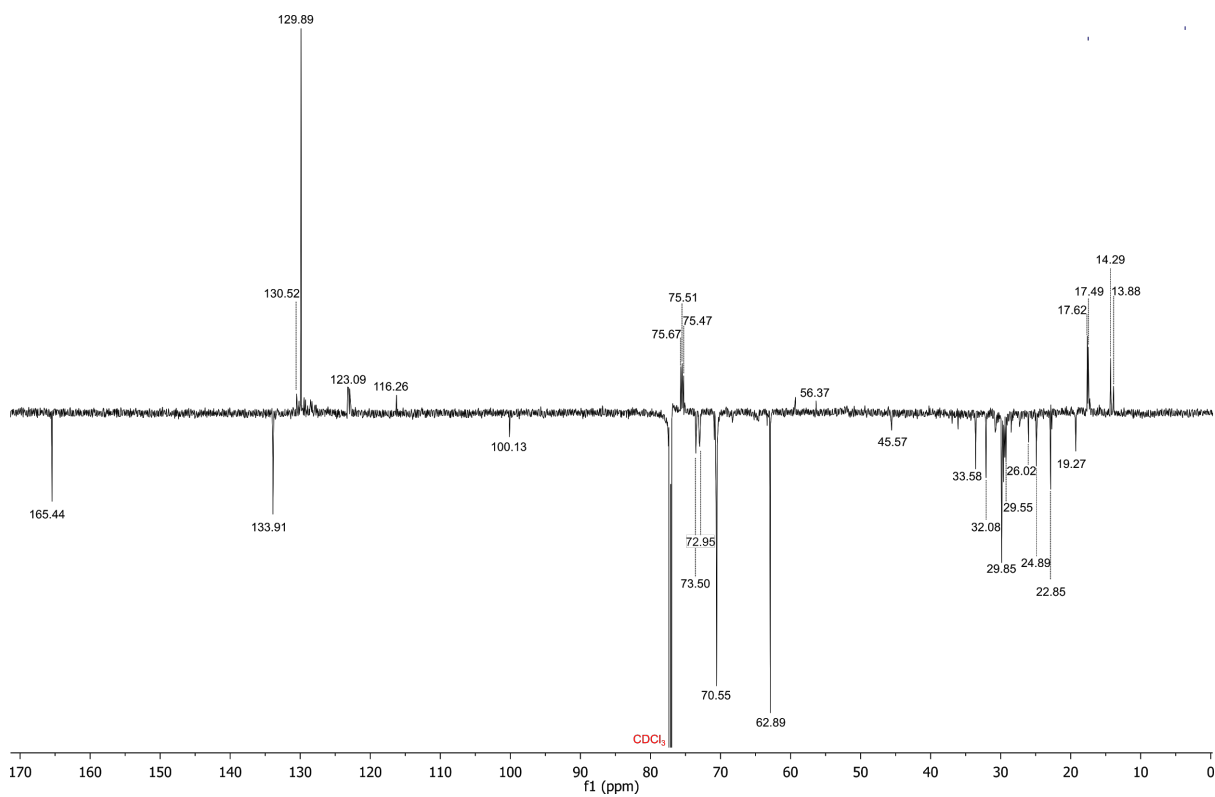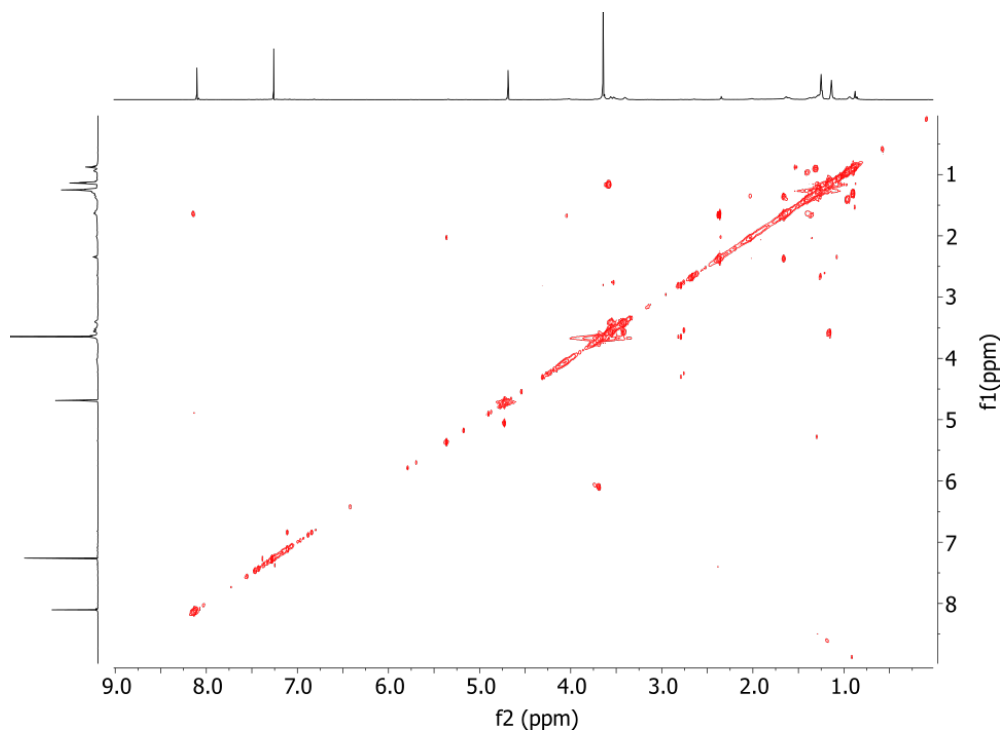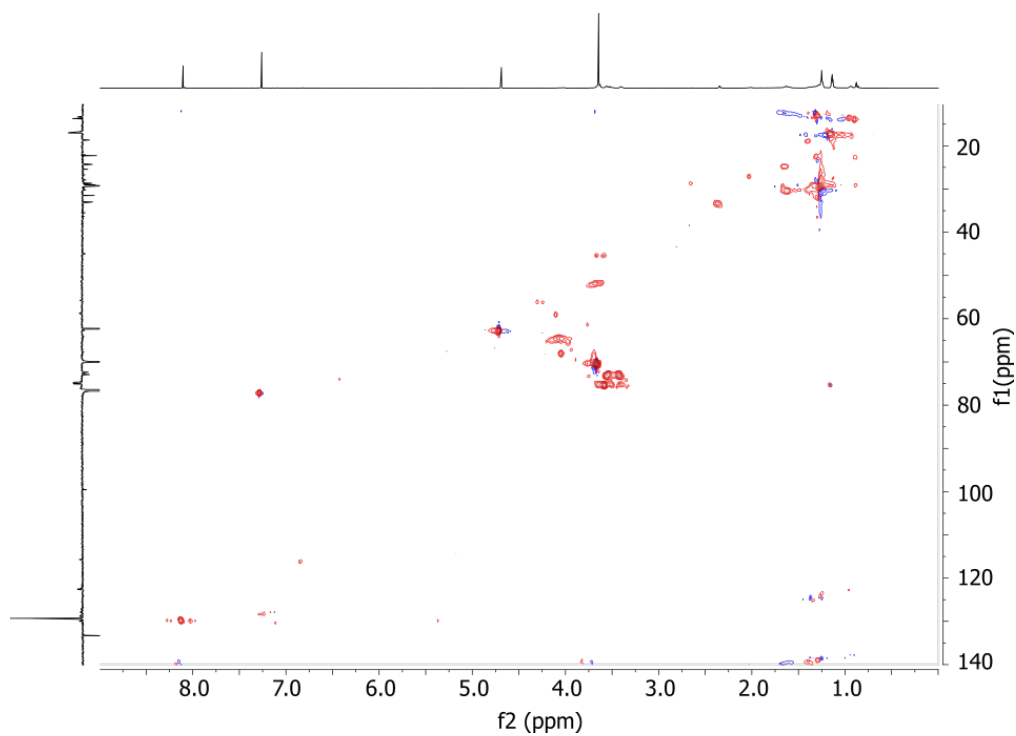
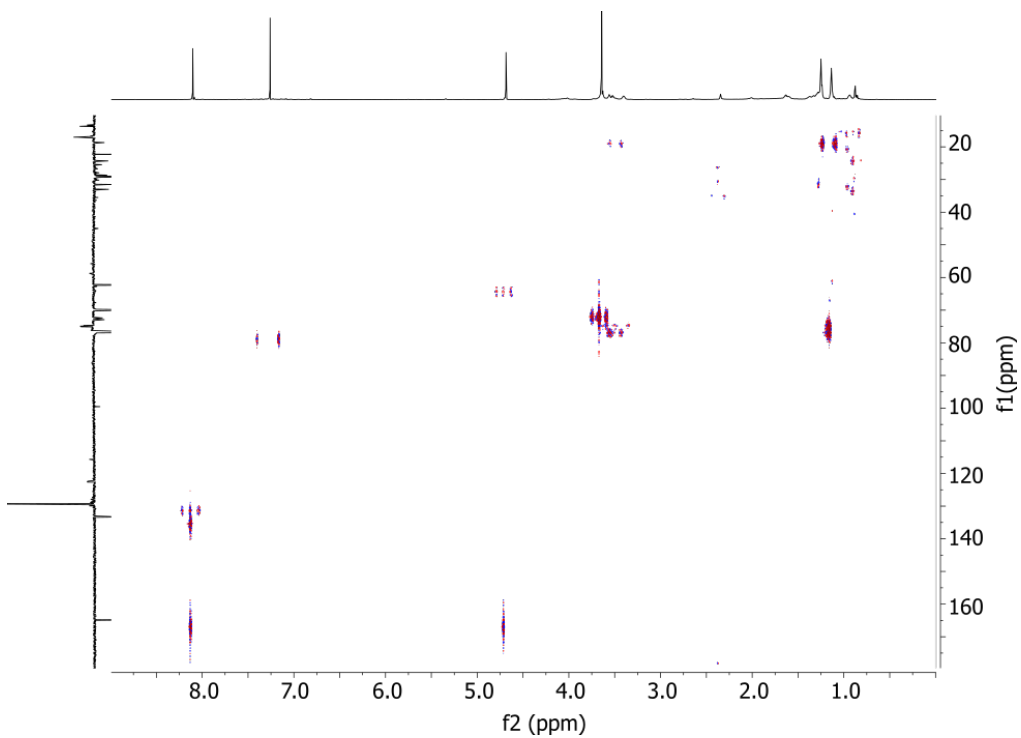**Figure 3.14.** HSQC NMR spectrum of antifungal metabolite, 900 MHz, CDCl$_3$

Figure 3.15. HMBC NMR spectrum of antifungal metabolite, 900 MHz, CDCl$_3$

3.2.1.5. Future Directions

With the difficulties encountered in solving the structure of the metabolite responsible for the selective growth inhibition observed in *Candida catenulata* sp. 135E, it was decided to enlist the help of the Nelson lab at UCLA that specializes in the use of microcrystal electron diffraction (MicroED), a cryo-electron microscopy (CryoEM) derived structure elucidation method.[25,26] The Nelson lab just obtained a new transmission electron microscope and it is hopeful that the sample will be able to produce microcrystals as well as electron diffraction patterns to obtain the overall molecular structure. One milligram of the purified sample was sent to their lab and analysis is currently pending.

3.2.2. Antibiotic Metabolites from a *Staphylococcus - Scopulariopsis* Interaction

A second antimicrobial project, which originated from the Wolfe lab at Tufts University, revolves around the observation of growth inhibition of *Staphylococcus* spp. when grown alongside *Scopulariopsis.* As with the *Pseudomonas - Candida* interaction, this negative growth phenotype appears to be species specific as other fungal species do not elicit the same effect (**Figure 3.16**). The approach used by the Wolfe lab was a plug-on-lawn approach, in which a sporulating fungal plug, around 2 cm in diameter, is placed directly onto a bacterial lawn. In particular, this negative growth phenotype is most prominent when *Scopulariopsis* is paired with *Staphylococcus saprophyticus*, a bacterium known to cause urinary tract infections.[27,28] This specific species of *Staphylococcus* is becoming increasingly resistant to commonly used antibiotics such as methicillin, which makes pursuit of the potential antibiotic metabolite from *Scopulariopsis* extremely attractive.*[29]*

Figure 3.16. Interaction of *Staphylococcus* strains with various fungal species. (A) Plate map of bioactivity plates containing a *Staphylococcus* lawn and four fungal plugs. (B) Bioactivity plates with lawns of four different *Staphylococcus* and fungal strains using PCAMS agar.

3.2.2.1. Bioactivity Guided Isolation of Specialized Metabolites Produced by *Scopulariopsis*

Attempts to recreate the growth phenotype observed by the Wolfe lab were unsuccessful using plug-on-lawn bioactivity plates, leading to the transition towards a bioactivity-guided fractionation approach in order to isolate the metabolite responsible for the bacterial growth inhibition. Sporulating colonies of *Scopulariopsis* sp. JB370 and sp. 165.5 were grown on agar plates and underwent small molecule extractions using a 50:50 mixture of ACN and H_2O. Further separation of the metabolites was performed via SPE. Bioactivity plates showed reproducible growth inhibition of Fraction F in *Scopulariopsis* sp. JB370 against *Staphylococcus equorum* (BC9) and of Fraction F in *Scopulariopsis* sp. 165.5 against *Staphylococcus succinus* (BC15) (**Figure 3.17**).
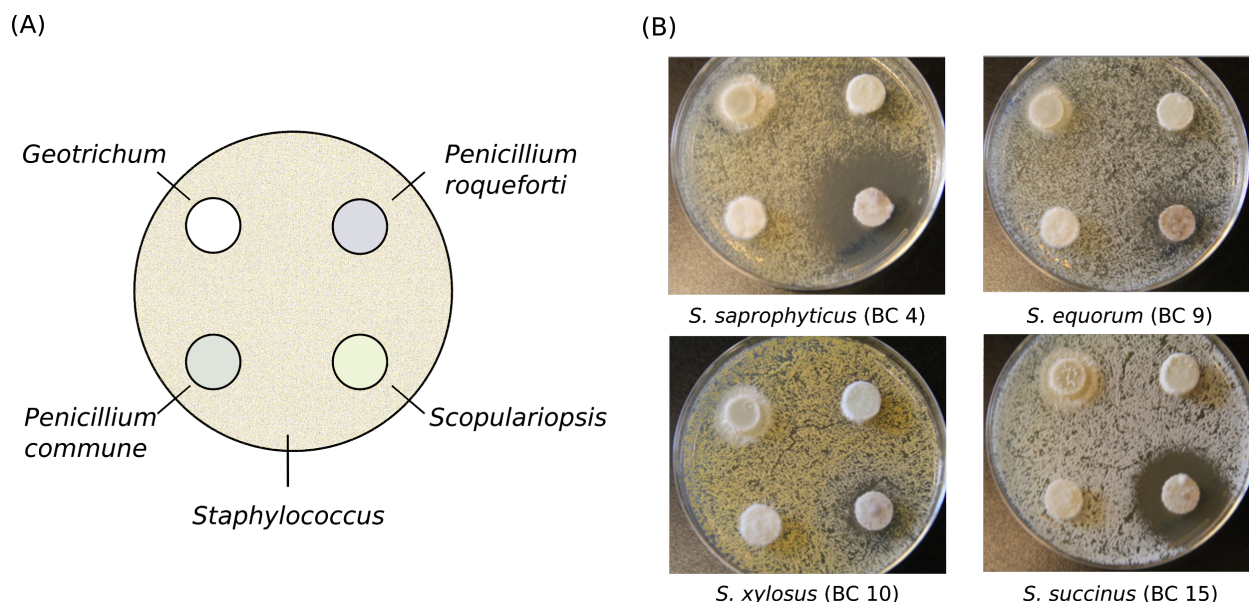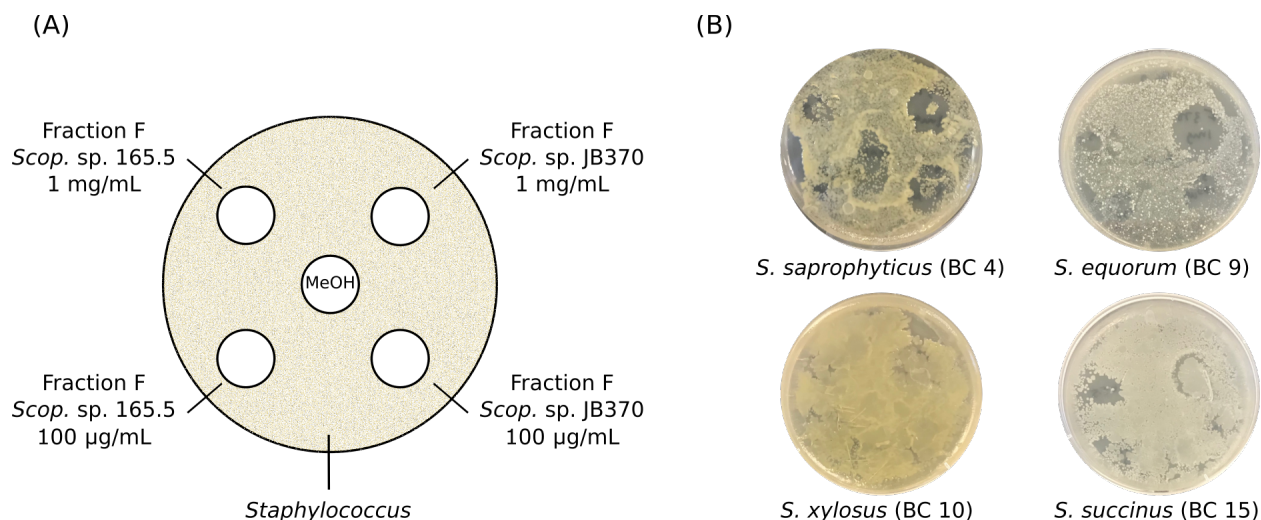
Figure 3.17. Interaction of *Staphylococcus* strains with Fraction F from two fungal extracts. (A) Plate map of bioactivity plates containing a *Staphylococcus* lawn and two extracts at varying concentrations (B) Bioactivity plates showing growth inhibition of Fraction F fungal extracts of *Scopulariopsis* sp. JB370 and sp. 165.5 against *Staphylococcus saprophyticus* (BC4), *Staphylococcus equorum* (BC9), *Staphylococcus xylosus* (BC10) and *Staphylococcus succinus* (BC15)

3.2.2.2. Future Directions

In order to investigate the growth inhibition of *Staphylococcus* species, additional work is needed to further fractionate the bioactive fractions obtained from both fungal species. A larger-scale fungal fermentation and extraction is in progress and a well-plate assay will be performed with the bioactive fractions against *Staphylococcus saprophyticus* (BC4). It is hopeful that this assay will lead to a specific peak that is bioactive that can be further investigated using MS and NMR to fully elucidate the structure of the antibiotic metabolite.

3.2.3. Antibiotic Metabolites from Interactions between *Penicillium* and Cheese-Isolated Bacterial Species

The final antimicrobial project, which also originated from the Wolfe lab at Tufts University, focuses on the investigation of the secondary metabolism of *Penicillium* sp. MB. This was initiated by the observation of growth inhibition of four separate bacterial species when grown in co-culture

83

with *Penicillium* sp. MB. In an effort to further explore this chemical space, the lab chose to investigate a Δ*laeA* strain, which knocks out a gene found to regulate secondary metabolism in fungi, to determine its effects on metabolite production and in the process, identify the molecule responsible for this antibiotic activity.[30,31] Upon knock out of *laeA*, bacterial growth inhibition no longer occurs in the *Penicillium* sp. MB Δ*laeA* strain, leading to the hypothesis that this phenotype is due to a secondary metabolite produced by the fungus (**Figure 3.18**). Upon further investigation, they also found that the transcription of gene clusters which may produce pseurotin A and fumagillin, both known to have antibiotic capabilities, was downregulated in the *laeA* knockout, which provided a lead to what may be causing the observed phenotype.[32,33]

(A)

(B)
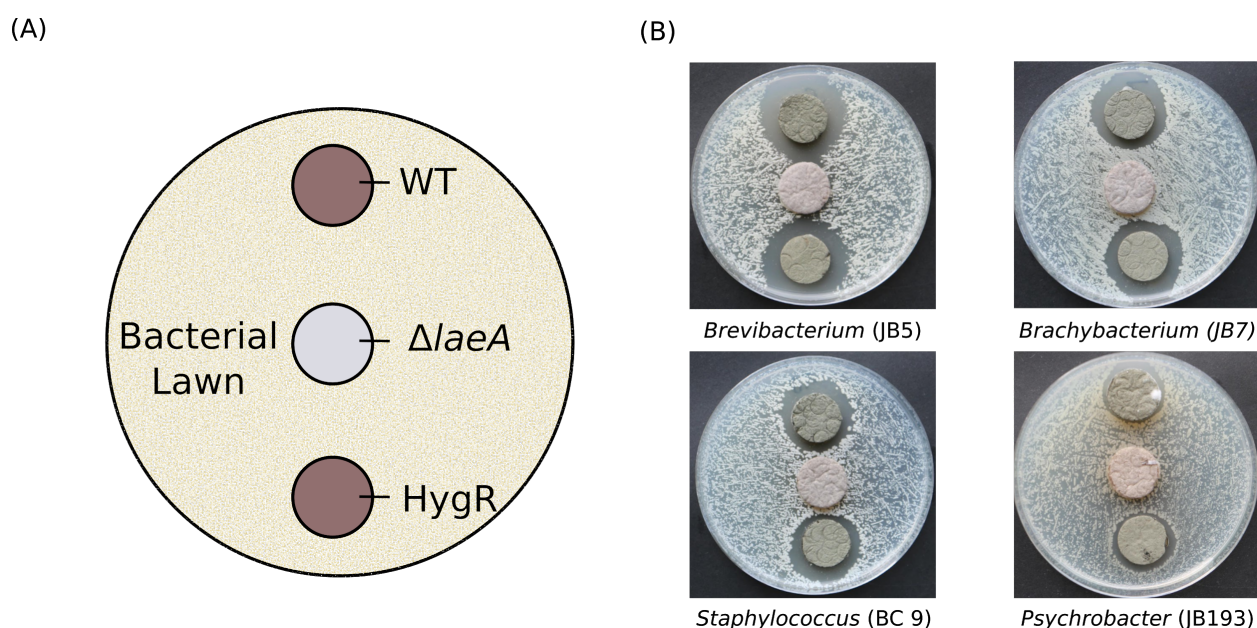
Figure 3.18. Interaction of four species of cheese-derived bacteria with plugs of *Penicillium* sp. MB. (A) Plate map of bioactivity plates containing a bacterial lawn and three fungal plugs. (B) Bioactivity plates with lawns of four different bacterial species with plugs of *Penicillium* sp. MB and two mutants using PCAMS agar.

3.2.3.1. Investigation of Bioactivity of *Penicillium* sp. MB Fungal Strains Against Cheese-Isolated Bacterial Species

To replicate the negative growth phenotype observed by the Wolfe lab, a plug-on-lawn approach was taken using four strains of *Penicillium* sp. MB including a wild-type (WT), Δ*laeA*, a Δ*laeA* complement mutant and a HygR (hygromycin) control. While they were able to observe growth inhibition in four bacterial species, *Staphylococcus equorum* sp. BC9*, Brevibacterium auranticum* sp. JB5, *Brachybacterium alimentarium* sp. JB7*, and Psychrobacter* sp. JB193, this was not fully reproducible across labs. To date, attempts to recreate this phenotype have only been successful with *Staphylococcus equorum* sp. BC9 (**Figure 3.19**).

WT   ΔlaeA
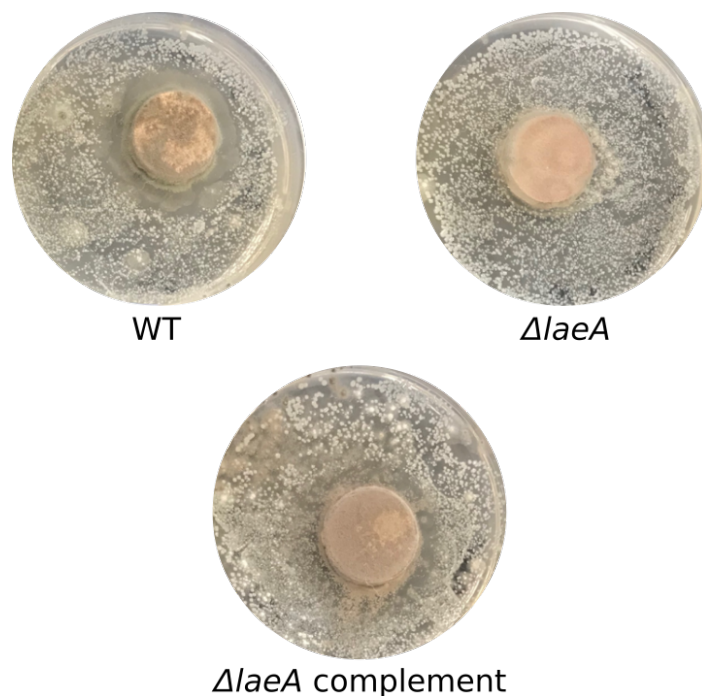
ΔlaeA complement

Figure 3.19. Bioactivity plates showing growth inhibition of *Staphylococcus equorum* (BC9) against a wild-type *Penicillium* sp. MB strain, Δ*laeA* and a Δ*laeA* complement mutant

3.2.3.2 Future Directions

In order to further investigate the growth inhibition of *Staphylococcus equorum* sp. BC9, additional work is needed to determine if pseurotin A or fumagillin is the responsible antibiotic agent. Plug-on-lawn bioactivity plates are currently in progress on thin agar plates for MALDI-TOF IMS analysis in the hopes that these two molecules can be detected in the inhibition zone. Additionally, extracts of the interactions between *Staphylococcus equorum* sp. BC9 and *Penicillium* sp. MB wild-type and mutant strains will be tested using liquid chromatography tandem mass spectrometry (LC-MS/MS) with commercial standards of pseurotin A and fumagillin to determine if the presence of these molecules can be confirmed in these strains.

3.3. Conclusions

The cheese microbiome serves as a largely untapped source of microbial and chemical diversity in which bacteria and fungi have been shown to produce a wide variety of secondary metabolites, some implicated in antimicrobial activity. Based on phenotypic screens, it has been observed that three specific interactions between bacteria and fungi isolated from cheese rinds have yielded the production of either antibiotic or antifungal metabolites. Growth inhibition observed when two microbial species are within close proximity to one another provides opportunities for scientists to probe their interactions *in situ* - opening the door for exploration of chemical communication and undiscovered secondary metabolites. While continued investigation is needed in each case to successfully isolate and elucidate the metabolites responsible for the antimicrobial activity, Overall, this research suggests that the cheese microbiome, as well as that of any fermented food, could be a viable source of novel drug candidates moving forward.

3.4. Experimental Section

3.4.1. General Experimental Procedures

Solvents used for HPLC experiments were all HPLC grade and were used directly from the vendor. Optical densities were measured using a Thermo Scientific Genesys 20 visible spectrophotometer at 600 nm (Thermo Fisher Scientific, Waltham, MA). pH measurements were made using a Jenco VisionPlus pH6175 (Jenco, San Diego, CA). NMR spectra were acquired on a Bruker AVANCE 900 MHz spectrometer with a 5mm TCI cryogenic probe (Bruker Daltonics, Billerica, MA) using $CDCl_3$ (δ_H 7.26, δ_C 77.16) a deuterated solvent (Cambridge Isotope Laboratories, Tewksbury, MA).

3.4.2. Interaction of *Pseudomonas psychrophila* sp. JB418 and *Candida catenulata* sp. 135E

3.4.2.1. Phenotypic Screen

Pseudomonas psychrophilia sp. JB418 was grown on tryptone soya broth (TSB) agar at room temperature (RT) under static conditions and single colonies were chosen for liquid cultures. A liquid culture was made in 5 mL of brain heart infusion (BHI) media and were grown for 24 hours at RT on an orbital shaker at 225 revolutions per minute (RPM). The overnight culture was spread across the top half of a TSB plate and allowed to grown at RT for two days. Fungal glycerol stocks of *Candida catenulata* 135E, *Geotrichum candidum*, *Penicillium* sp. JBC and *Scopulariopsis* JB370 were streaked out perpendicular to the bacterium and were allowed to grow at RT for observation of growth inhibition phenotypes.

3.4.2.2. Imaging Mass Spectrometry

Pseudomonas psychrophilia sp. JB418 and *Candida catenulata* 135E were grown on TSB agar at RT under static conditions and single colonies were chosen for liquid cultures. A liquid culture was made in 5 mL of BHI media and were grown for 24 hours at RT on an orbital shaker at 225

RPM. *Pseudomonas psychrophilia* sp. JB418 was plated at an OD_{600} of 0.9 and *Candida catenulata* 135E at an OD_{600} of 0.1. Ten μL of the fungus was spread in a thin line across the thin TSB plate and ten μL of the bacteria was spread in a thin line perpendicular to the fungus without touching it - creating a cross.

After three days of growth, regions of interest along with appropriate controls (bacteria, fungus and agar) were excised and plated onto a steel MALDI plate using the outline provided in **Figure 3.5 A**. A general IMS sample preparation procedure was used in which the plate was homogeneously coated in matrix comprised of 50:50 α-cyano-4-hydroxycinnamic acid:dihydroxybenzoic acid via a 53 micron stainless steel sieve, followed by drying in a 30°C oven for four hours.[34] Once dry, the plate was placed in the MALDI-TOF mass spectrometer for analysis. Analysis was performed in positive, reflectron mode with a medium laser size, frequency of 500 Hz and a spatial resolution of 500 microns. Data analysis was performed using Bruker Flex Imaging v.4.1 and total ion current normalization (Bruker Daltonics, Billerica, MA).

3.4.2.3. Bacterial Grow-up & Extraction Procedures

Pseudomonas psychrophila sp. JB418 was grown on TSB agar at RT under static conditions and single colonies were chosen for liquid cultures. These cultures were made in 5 mL of BHI media and were grown for 24 hours at RT on an orbital shaker at 225 rpm. All cultures were grown under the same temperature and shaker conditions unless otherwise specified. Each small-scale liquid culture was normalized to an OD_{600} of 0.1 prior to inoculation into 50 mL of TSB media, which was then grown for 24 hours. This culture was subsequently used to inoculate 1 L of TSB media, which was grown for 5 days with the addition of 20 g of an equal mixture (w/w) of Amberlite XAD-2, -4 and -7.

Bacterial cultures were adjusted to a pH of 4.00 using 12M HCl acid and then the resin, along with bacterial cells, was collected via vacuum-filtration. The resulting solids were back-extracted with 250 mL of a 1:1 acetone:MeOH solution for one hour at 225 rpm and vacuum-filtered to isolate the filtrate.[35] The resulting solution was dried in vacuo, resulting in a crude bacterial extract. In order to fractionate the crude extract, SPE was performed using a Discovery DSC$_{18}$ SPE cartridge with a bed weight of 5 grams. Seven fractions were generated using elution solvents of varying polarity (10% MeOH, 20 - 100% MeOH, in 20% increments and 100% EtOAc. Each fraction was then dried in vacuo.

3.4.2.4. Bioassay Guided Fractionation

Candida catenulata 135E was grown on TSB agar at RT under static conditions and single colonies were chosen for liquid cultures. A liquid culture was made in 5 mL of BHI media and grown for 24 hours at RT at 225 RPM. The fungal liquid culture was normalized to an OD$_{600}$ of 0.1 and 0.01 and uniformly spread out on TSB agar plates in duplicate, respectively. SPE fractions (5 µL) was spotted on the fungal plates and allowed to grow at RT in static conditions for up to a week to observe fraction bioactivity.

The fraction of interest (100% methanol) was separated further via HPLC using a Kinetex C$_{18}$ column (5 µm, 100 Å, 150 x 4.6 mm) (Phenomenex, Torrance, CA) at an isocratic gradient of 77% ACN with 0.01% formic acid at 2 mL/min. Fractions were collected every thirty seconds and dried in vacuo. A liquid culture of *C. catenulata* 135E was normalized to an OD$_{600}$ of 0.01 and spread onto TSB agar set in 96-well plates. HPLC fractions were resuspended in 15 µL of 77% ACN and 5 µL of each was spotted on the fungal wells, in duplicate, and remaining sample was dried down in vacuo. Well plates were allowed to grow at RT in static conditions for up to a week to observe fraction bioactivity.

3.4.2.5. qTOF MS Analysis of Bioactive Fraction from *Pseudomonas psychrophila* sp. JB418

Two fractions of interest at a concentration of 100 µg/mL from the well plate assay were subjected to LC-MS/MS analysis using a Bruker Impact II qTOF mass spectrometer (Bruker Daltonics, Billerica, MA). Five µL of the samples were injected onto a Cortecs C_{18} column (2.7 µm, 90 Å, 100 x 3.0 mm) (Waters Corporation, Milford, MA) with a column temperature of 40°C and separated along a gradient of 10 to 100% ACN with 0.1 % formic acid over a ten minute time period. Spectra were collected in positive mode using a detection window of 50 to 1500 *m/z*, collision energies of 12, 48 and 60 kV and an isolation width of 3 *m/z*.

3.4.3. Interaction of *Staphylococcus* and *Scopulariopsis*

3.4.3.1. Phenotypic Screen

Scopulariopsis sp. JB370 and 165.5 were grown on plate count agar supplemented with 0.1% milk and 1% salt (PCAMS) at RT for ten days, at which point, sporulation had occurred. *Staphylococcus saprophyticus* sp. BC4, *Staphylococcus equorum* sp. BC9, *Staphylococcus xylosus* sp. BC10 and *Staphylococcus succinus* sp. BC15 were grown on PCAMS agar at RT under static conditions and single colonies were chosen for liquid cultures. A liquid culture was made in 5 mL of BHI media and were grown for 24 hours at RT on an orbital shaker at 225 RPM. The overnight cultures were spread across PCAMS plates at an OD_{600} of 0.1 and 0.01 and fungal plugs were added onto the bacteria lawns. This was also done on cheese curd agar (CCA) to determine if this growth phenotype observed by the Wolfe lab could be replicated on an environment that more closely mimicked a cheese rind.

3.4.3.4. Bioassay Guided Fractionation

Scopulariopsis sp. JB370 and 165.5 were grown on PCAMS agar at RT until the occurrence of sporulation. The PCAMS agar plates containing the fungal strains were extracted into a 50:50

(v/v) solution of ACN:H_2O and was sonicated for one hour. The resulting solution was dried in vacuo, resulting in a crude fungal extract. In order to fractionate the crude extract, fractionation was performed using a Discovery DSC$_{18}$ SPE cartridge with a bed weight of 5 grams. Seven fractions were generated using elution solvents of varying polarity (10% MeOH, 20 - 100% MeOH, in 20% increments and 100% EtOAc. Each fraction was then dried in vacuo.

A liquid culture of each *Staphylococcus* strain was made in 5 mL of BHI media and grown for 24 hours at RT at 225 RPM. The bacterial liquid cultures were normalized to an OD$_{600}$ of 0.01 and 0.001 and uniformly spread out on PCAMS agar plates. SPE fractions (3 µL) were spotted on the bacterial plates along with a vehicle control, which allowed to grow at RT in static conditions for up to a week to observe fraction bioactivity.

3.4.4. Interaction of *Penicillium* and Cheese-Isolated Bacterial Species

3.4.4.1. Phenotypic Screen

Four strains of *Penicillium* sp. MB (WT, *ΔlaeA*, comp and HygR) were grown on PCAMS agar at RT until sporulation had occurred (seven to ten days). Concurrently, *Staphylococcus equorum* sp. BC9*, Psychrobacter* sp. JB193 and *Brevibacterium auranticum* sp. JB5 were grown on PCAMS agar at RT under static conditions and single colonies were chosen for liquid cultures. Cultures were made in 5 mL of BHI media and were grown for 24 hours at RT on an orbital shaker at 225 RPM. The overnight cultures were spread across PCAMS plates at an OD$_{600}$ of 0.01 and 0.001 and fungal plugs were added onto the bacteria lawns.

3.4.4.2. LC-MS/MS Analysis of Standards and Extracts

Pseurotin A (Biovitica, The Netherlands) and fumagillin (BioVision, Milpitas, CA) standards were diluted to 10 µg/mL. Tandem mass analysis was performed using a Thermo Finnigan LCQ Advantage Max mass spectrometer (Thermo Fisher Scientific, Waltham, MA) via direct infusion

or LC-MS/MS . Samples were fragmented via direct infusion in positive mode using a detection window of 200 to 2,000 *m/z*, a collision energy of 20 kV and an isolation width of 5 *m/z*. Extract samples were diluted to 10 mg/mL using methanol and 20 µL were injected onto a Kinetex C$_{18}$ column (5 µm, 100 Å, 150 x 4.6 mm) (Phenomenex, Torrance, CA) and separated along a gradient of 10 to 100% MeOH with 0.02% formic acid over forty minutes prior to introduction to the mass spectrometer.

3.5. References

1. Newell, D. G. *et al.* Food-borne diseases — The challenges of 20years ago still persist while new ones continue to emerge. *International Journal of Food Microbiology* **139**, S3–S15 (2010).

2. Chowdhary, A., Sharma, C. & Meis, J. F. Candida auris: A rapidly emerging cause of hospital-acquired multidrug-resistant fungal infections globally. *PLoS Pathog.* **13**, e1006290 (2017).

3. Lowy, F. D. Antimicrobial resistance: the example of Staphylococcus aureus. *J. Clin. Invest.* **111**, 1265–1273 (2003).

4. Seung, K. J., Keshavjee, S. & Rich, M. L. Multidrug-Resistant Tuberculosis and Extensively Drug-Resistant Tuberculosis. *Cold Spring Harb. Perspect. Med.* **5**, a017863 (2015).

5. Holmes, A. H. *et al.* Understanding the mechanisms and drivers of antimicrobial resistance. *Lancet* **387**, 176–187 (2016).

6. CGH - Newsletter - Feb. 16, 2016: The Challenge of Antibiotic Resistance. Available at: https://www.cdc.gov/globalhealth/newsletter/2016/feb_16_2016.html. (Accessed: 1st October 2019)

7. CDC. Antibiotic Resistance. *Centers for Disease Control and Prevention* (2019). Available at: https://www.cdc.gov/features/antibiotic-resistance-global/index.html. (Accessed: 1st October 2019)

8. Antibiotic Resistance Investments. Available at: https://wwwn.cdc.gov/arinvestments. (Accessed: 30th September 2019)

9. Marston, H. D., Dixon, D. M., Knisely, J. M., Palmore, T. N. & Fauci, A. S. Antimicrobial Resistance. *JAMA* **316**, 1193–1204 (2016).

10. Kardos, N. & Demain, A. L. Penicillin: the medicine with the greatest impact on therapeutic outcomes. *Appl. Microbiol. Biotechnol.* **92**, 677–687 (2011).

11. Sengupta, S., Chattopadhyay, M. K. & Grossart, H.-P. The multifaceted roles of antibiotics and antibiotic resistance in nature. *Front. Microbiol.* **4**, 47 (2013).

12. CDC. What Exactly is Antibiotic Resistance? *Centers for Disease Control and Prevention* (2019). Available at: https://www.cdc.gov/drugresistance/about.html. (Accessed: 7th October 2019)

13. Rossiter, S. E., Fletcher, M. H. & Wuest, W. M. Natural Products as Platforms To Overcome Antibiotic Resistance. *Chem. Rev.* **117**, 12415–12474 (2017).

14. Pfaller, M. A. & Diekema, D. J. Epidemiology of invasive candidiasis: a persistent public health problem. *Clin. Microbiol. Rev.* **20**, 133–163 (2007).

15. Ostrosky-Zeichner, L., Casadevall, A., Galgiani, J. N., Odds, F. C. & Rex, J. H. An insight into the antifungal pipeline: selected new molecules and beyond. *Nat. Rev. Drug Discov.* **9**, 719–727 (2010).

16. Izquierdo, E., Wagner, C., Marchioni, E., Aoude-Werner, D. & Ennahar, S. Enterocin 96, a novel class II bacteriocin produced by Enterococcus faecalis WHE 96, isolated from Munster cheese. *Appl. Environ. Microbiol.* **75**, 4273–4276 (2009).

17. Dal Bello, B. *et al.* Microbial ecology of artisanal products from North West of Italy and antimicrobial activity of the autochthonous populations. *LWT - Food Science and Technology* **43**, 1151–1159 (2010).

18. Kastman, E. K. *et al.* Biotic Interactions Shape the Ecological Distributions of Staphylococcus Species. *MBio* **7**, (2016).

19. Wolfe, B. E., Button, J. E., Santarelli, M. & Dutton, R. J. Cheese rind communities provide tractable systems for in situ and in vitro studies of microbial diversity. *Cell* **158**, 422–433 (2014).

20. Bonham, K. S., Wolfe, B. E. & Dutton, R. J. Extensive horizontal gene transfer in cheese-associated bacteria. *Elife* **6**, e22144 (2017).

21. Caprioli, R. M., Farmer, T. B. & Gile, J. Molecular imaging of biological samples:

localization of peptides and proteins using MALDI-TOF MS. *Anal. Chem.* **69**, 4751–4760 (1997).

22. Schulz, S., Becker, M., Groseclose, M. R., Schadt, S. & Hopf, C. Advanced MALDI mass spectrometry imaging in pharmaceutical research and drug development. *Curr. Opin. Biotechnol.* **55**, 51–59 (2019).

23. Kaspar, S., Peukert, M., Svatos, A., Matros, A. & Mock, H.-P. MALDI-imaging mass spectrometry--an emerging technique in plant biology. *Proteomics* **11**, 1840–1850 (2011).

24. Johnson, T. A. *et al.* Natural product libraries to accelerate the high-throughput discovery of therapeutic leads. *J. Nat. Prod.* **74**, 2545–2555 (2011).

25. Shi, D., Nannenga, B. L., Iadanza, M. G. & Gonen, T. Three-dimensional electron crystallography of protein microcrystals. *Elife* **2**, e01345 (2013).

26. Jones, C. G. *et al.* The CryoEM Method MicroED as a Powerful Tool for Small Molecule Structure Determination. *ACS Cent Sci* **4**, 1587–1592 (2018).

27. Raz, R., Colodner, R. & Kunin, C. M. Who Are You—Staphylococcus saprophyticus? *Clin. Infect. Dis.* **40**, 896–898 (2005).

28. Flores-Mireles, A. L., Walker, J. N., Caparon, M. & Hultgren, S. J. Urinary tract infections: epidemiology, mechanisms of infection and treatment options. *Nature Reviews Microbiology* **13**, 269–284 (2015).

29. Higashide, M. *et al.* Methicillin-Resistant Staphylococcus saprophyticus Isolates Carrying Staphylococcal Cassette Chromosome mec Have Emerged in Urogenital Tract Infections. *Antimicrobial Agents and Chemotherapy* **52**, 2061–2068 (2008).

30. Bok, J. W. & Keller, N. P. LaeA, a regulator of secondary metabolism in Aspergillus spp. *Eukaryot. Cell* **3**, 527–535 (2004).

31. Bayram, O. *et al.* VelB/VeA/LaeA complex coordinates light signal with fungal development and secondary metabolism. *Science* **320**, 1504–1506 (2008).

32. Mehedi, M. A. U. *et al.* Pseurotin A: an antibacterial secondary metabolite from Aspergillus

fumigatus. *Asian J. Chem.* **22**, 2611–2614 (2010).

33. Pinheiro, E. A. A. *et al.* Antibacterial activity of alkaloids produced by endophytic fungus Aspergillus sp. EJC08 isolated from medical plant Bauhinia guianensis. *Nat. Prod. Res.* **27**, 1633–1638 (2013).

34. Yang, J. Y. *et al.* Primer on agar-based microbial imaging mass spectrometry. *J. Bacteriol.* **194**, 6023–6028 (2012).

35. Berlinck, R. Chromatographic Approach to Polar Compounds: Isolation Of The Hydrophylic Constituents Of The Marine Sponge Crambe. *Química Nova* **17**, 167–171 (1994).

APPENDICES

Appendix A: ASM Statement of Author Rights

Statement of Author Rights

[ASM Author Center](#) / [Preparing Your Manuscript](#)

Authors may post their articles to their institutional repositories

ASM grants authors the right to post their accepted manuscripts in publicly accessible electronic repositories maintained by funding agencies, as well as appropriate institutional or subject-based open repositories established by a government or non-commercial entity.

In preparation for the REF 2021, ASM would like to remind Authors that the [current author fee structure](#), along with the policy outlined above, allows authors to comply with the [HEFCE deposition requirements](#). If authors have paid a fee to make their article "gold" open access then there is no need to worry about these deposition requirements (See section 38 of the "Policy for open access in Research Excellence Framework 2021" document).

Please note that ASM makes the final, typeset articles from its primary-research journals available free of charge on the ASM Journals and PMC websites 6 months after final publication.

Authors may post their articles in full on personal or employer websites

ASM grants the author the right to post his/her article (after publication by ASM) on the author's personal or university-hosted website, but not on any corporate, government, or similar website, without ASM's prior permission, provided that proper credit is given to the original ASM publication.

Once ASM grants permission to the author, ASM requests that the posting release date for the content be no earlier than 6 months after the final publication of the typeset article by ASM.

Authors may make copies of their articles in full

Corresponding authors are entitled to 10 free downloads of their papers. Additionally, all authors may make up to 99 copies of his/her own work for personal or professional use (including teaching packs that are distributed free of charge within your own institution). For orders of 100 or more copies, you should seek ASM's permission or purchase access through Highwire's Pay-Per-View option, available on the ASM online journal sites.

Authors may republish/adapt portions of their articles

ASM also grants the author the right to republish discrete portions of his/her article in any other publication (including print, CD-ROM, and other electronic formats) of which he or she is author or editor, provided that proper credit is given to the original ASM publication. An ASM author also retains the right to reuse the full article in his/her dissertation or thesis. "Proper credit" means either the copyright lines shown on the top of the first page of the PDF version, or "Copyright © American Society for Microbiology, [insert journal name, volume number, year, page numbers and DOI]" of the HTML version. For technical questions about using Rightslink, please contact Customer Support via phone at (877) 622-5543 (toll free) or (978) 777-9929, or e-mail Rightslink customer care at customercare@copyright.com.
Please note that the ASM is in full compliance with NIH Policy.

Appendix B: BioRxiv Statement of Author Rights

Copyright

VITA

Melissa Marie Galey

Education

B.S., Biochemistry, Rose-Hulman Institute of Technology, Terre Haute, Indiana   2012

M.S., Pharmacognosy, University of Illinois at Chicago, Chicago, Illinois   2019

Research Experience

Graduate Research Assistant   Aug. 2016 - Dec. 2019
Advisor: Dr. Laura M. Sanchez
University of Illinois at Chicago

Intern, Discovery Chemistry Department   June 2019 – Aug. 2019
Supervisor: Dr. Sarah J. Robinson
Genentech

Research Scientist   June 2012 - July 2016
Supervisors: Drs. Christopher P. Nicholas & Benjamin D. Yuhas
UOP, A Honeywell Company

Interdisciplinary Research Collaborative Scholar   June 2011 – Aug. 2011
Advisor: Dr. Mark E. Brandt
Rose-Hulman Institute of Technology

Interdisciplinary Research Collaborative Scholar   June 2010 – Aug. 2010
Advisor: Dr. Mark E. Brandt
Rose-Hulman Institute of Technology

Awards and Honors

US Young Investigator Educational Grant, MSACL   2019

First Place Poster Award for Clinical, Social and Applied   2019
Sciences Division, Research Day, University of Illinois at
Chicago

Al R. Langerman Memorial Scholarship HSC, University of Illinois at Chicago	2019
Graduate College Provost's Graduate Research Award, University of Illinois at Chicago	2018
Graduate College Student Presenter's Award, University of Illinois at Chicago	2018
Travel Fellowship, May Institute, Northeastern University	2018
Frank A. Guthrie Memorial Scholarship, Rose-Hulman Institute of Technology	2010 - 2012

Peer Reviewed Publications

1. Li, F. *et al.* Chemically Transformed Monolayers on Acene Thin Films for Improved Metal/Organic Interfaces. *ChemComm.* (2019, Accepted).

2. Van Santen, J. *et al.* The Natural Products Atlas: An Open Access Knowledge Base for Microbial Natural Products Discovery. *ACS Cent. Sci.* (2019, Accepted).

3. Mowat, J.P.S. *et al.* A Complex Zeolite Containing Multiple Ring Sizes in a Single Channel: One-Dimensional Zeolite UZM-55. *Chem. Eur. J.* 24, 17779-17787 (2018).

4. **Galey, M. M.** & Sanchez, L.M. Spatial Analyses of Specialized Metabolites: The Key to Studying Function in Hosts. *mSystems* 3, e00148–17 (2018).

5. Miller, M.A. *et al.* Synthesis, characterization and structure solution of ULS-1 |ETMA$_8$(H$_2$O)$_{20}$|[S$_{i24}$O$_{48}$(OH)$_8$], a layered silicate composed of half-sodalite cages. *Microporous Mesoporous Mater.* 202, 250–258 (2015).

Research Publications

1. **Galey, M.M.** *et al.,* Detection of Ovarian Cancer Using Samples Sourced from the Vaginal Microenvironment. *BioRxiv* (2019).

2. **Galey, M. M.** & Sanchez, L. M. Review of Oceanography and Marine Biology. *J. Nat. Prod.* 80, 2591–2592 (2017).

Patents

1. Lobo, R.J., Nicholas, C.P., Miller, M.A., **Galey, M.M.**, Composition of Matter and Structure of Zeolite UZM-55 and Use in Isomerization of Aromatic Molecules, U.S. Patent No. 10,384,989 B2 (2019)

2. Miller, M.A., Nicholas, C.P., **Galey, M.M.**, Mowat, J.P.S., Sinkler, W., Composition of Matter and Structure of Zeolite UZM-55, U.S. Patent No. 10,272,420 B2 (2019)

3. Nicholas, C.P., Miller, M.A., **Galey, M.M.**, Zeolites using an Organo-1-oxa-4-azonium Cyclohexane Compound, U.S. Patent No. 9,815,706 B2 (2017)

4. Yuhas, B.D., Nicholas, C.P., Miller, M.A., **Galey, M.M.**, Aluminophosphate Molecular Sieves using an Organo-1-oxa-4-azonium Cyclohexane Compound, U.S. Patent No. 9,751,772 B2 (2017)

5. Nicholas, C.P., Miller, M.A., **Galey, M.M.**, Yuhas, B.D., Prabhakar, S., Organo-1-oxa-4-azonium Cyclohexane Compounds, U.S. Patent No. 9,522,896 B2 (2016)

Published Patent Applications

1. Nicholas, C.P., Mowat, J.P.S., Nicholas, C.L., Miller, M.A., **Galey, M.M.**, Hydrocarbon Conversion Using UZM-50, Application Number 15/857,458 (December 2018)

2. Yuhas, B.D., **Galey, M.M.**, Miller, M.A., Crystalline Metallophosphates, Their Method of Preparation and Use, Application Number 16/036,745 (July 2018)

3. Yuhas, B.D., **Galey, M.M.**, Miller, M.A., Mowat, J.P.S., Sinkler, W., Crystalline Metallophosphates, Their Method of Preparation and Use, Application Number 16/036,709 (July 2018)

4. Yuhas, B.D., **Galey, M.M.**, Miller, M.A., Mowat, J.P.S., Sinkler, W., Lewis, G.L., Knight, L.M., Crystalline Metallophosphates, Their Method of Preparation and Use, Application Number 16/036,572 (July 2018)

5. Nicholas, C.P., Mowat, J.P.S., Nicholas, C.L., Miller, M.A., **Galey, M.M.,** Hydrocarbon Conversion Using UZM-50, Application Number 15/857,458 (December 2017)

6. Miller, M.A., Nicholas, C.P., **Galey, M.M.**, Sylejmani, M., Mowat, J.P.S., Nicholas, C.L., Aluminosilicate Zeolite UZM-50, Application Number 15/857,184 (December 2017)

7. Mowat, J.P.S., Sinkler, W., Nicholas, C.P., Miller, M.A., **Galey, M.M.**, Zeolites having a One-Dimensional Channel System, 10-Membered Rings and 12-Membered Rings, Application Number 15/658,825 (October 2016)

8. Nicholas, C.P., Miller, M.A., **Galey, M.M.**, Yuhas, B.D., Prabhakar, S., Organo-1-oxa-4-azonium Cyclohexane compounds, Application Number 15/981,435 (December 2014)

9. Nicholas, C.P., Miller, M.A., **Galey, M.M.**, Yuhas, B.D., Prabhakar, S., Organo-1-oxa-4-azonium Cyclohexane compounds, Application Number 15/981,148 (December 2014)

10. Nicholas, C.P., Miller, M.A., **Galey, M.M.**, Yuhas, B.D., Prabhakar, S., Organo-1-oxa-4-azonium cyclohexane compounds, Application Number 15/981,084 (December 2014)

Oral Presentations

1. **Galey, M.M**., Young, A.N., Petukhova, V., Wang, M., Wang, J., Burdette, J.E., Sanchez, L.M., "Utilizing Protein Signatures from Heterogeneous Cell Populations in a Murine Model for Diagnosis of Ovarian Cancer", MSACL Annual Conference, Palm Springs, California, April 2019

2. **Galey, M.M.,** Pierce, E.C., Dutton, R.J., Sanchez, L.M., "Small Molecule Interactions from the Cheese Microbiota: *Pseudomonas* vs. *Candida*", ASMS Annual Conference, San Diego, California, June 2018

3. **Galey, M.M.**, Pierce, E.C., Dutton, R.J., Sanchez, L.M., "Small Molecule Interactions from the Cheese Microbiota: *Pseudomonas* vs. *Candida* ", Specialized Metabolite Community, Chicago, Illinois, May 2018

4. **Galey, M.M.**, Brandt, M.E., "Cloning and Expression of the Ligand Binding Domain of the Estrogen Receptor Beta" IRC Symposium, Terre Haute, Indiana, October 2011

5. **Galey, M.M.**, Brandt, M.E., "Molecular Docking Simulations for Organic Compounds to the Estrogen Receptor Alpha", IRC Symposium, Terre Haute, Indiana, October 2010

Poster Presentations

1. **Galey, M.M.**, Sanchez, L.M., Lui, Y., Robinson, S.J., "Configuration Analysis of Small Molecules Using Residual Dipole Coupling (RDC) NMR Measurements", Genentech, University Talent Acquisition and Strategy (UTAS) Poster Day, South San Francisco, California, July 2019

2. **Galey, M.M.**, Young, A.N, Petukhova, V., Wang, M., Wang, J., Burdette, J.E., Sanchez, L.M., "Utilizing Protein Signatures from Heterogeneous Cell Populations in a Murine Model for Diagnosis of Ovarian Cancer", UIC Research Day, Chicago, Illinois, February 2019

3. **Galey, M.M.**, Kolachina, S., Dutton, R.J., Sanchez, L.M., "Small Molecule Interactions from the Cheese Microbiota: *Pseudomonas* vs. *Candida* ", Perlman Symposium, Madison, Wisconsin, April 2018

4. **Galey, M.M.**, Kolachina, S., Dutton, R.J., Sanchez, L.M., "Small Molecule Interactions from the Cheese Microbiota: *Pseudomonas* vs. *Candida* ", MIKI Medicinal Chemistry Meeting, Chicago, Illinois, April 2018

5. **Galey, M.M.**, Kolachina, S., Dutton, R.J., Sanchez, L.M., "Small Molecule Interactions from the Cheese Microbiota: *Pseudomonas* vs. *Candida* ", UIC Research Day, Chicago, Illinois, February 2018

6. **Galey, M.M.**, Miller, M.A., Nicholas, C.P., "Zeolitic Materials Made Using Novel Organoammonium Cations", UOP, Technical Community Organization (TCO) Symposium, Chicago, Illinois, May 2014

7. **Galey, M.M.**, Miller, M.A., Nicholas, C.P., "Matrix Materials and their Effect on Catalytic Performance", UOP, TCO Symposium, Chicago, Illinois, May 2013

Professional Society Memberships

American Society for Mass Spectrometry	2018 - Present
American Association for the Advancement of Science	2016 - Present

Teaching Experience

Department of Pharmacy Practice, University of Illinois at Chicago: Principles of Drug Action and Therapeutics VII	2018
Department of Pharmacy Practice, University of Illinois at Chicago: Introductory Pharmacy Practice	2017
Department of Pharmacy Practice, University of Illinois at Chicago: Principles of Drug Action and Therapeutics IV	2017
Department of Pharmacy Practice, University of Illinois at Chicago: Experiential Practice	2016

Undergraduate Mentoring

Leslie Martinez, L@s GANAS Scholar, University of Illinois at Chicago	2019

Outreach and Volunteer Activities

The Anti-Cruelty Society, Volunteer, Chicago, IL	2018 - Present
Chicago Cares at Marillac Social Center, Workshop Leader, Chicago, IL	2019
Science Club, Science Fair Judge, Chicago, IL	2018
Chicago Mass Spec Day, Program Chair, Chicago, IL	2018
Expanding Your Horizons, Workshop Leader, Chicago, IL	2017 - 2018
Summer Research miniSymposium, Poster Judge, Chicago, IL	2017 – 2018
Explorer's Post, Group Leader, Chicago, IL	2015-2016
Illinois Chemical Education Foundation, Volunteer, Chicago, IL	2013-2016
Chemistry on Wheels, Volunteer, Terre Haute, IN	2010-2012
Chemistry Demonstrations, Organizer & Guest Demonstrator, The Woodlands, TX	2010-2012